

# Sustainable Direct Recycling of Spent Lithium-Ion Batteries: Closed-Loop Regeneration and AI-Optimized Systems Toward Next-Generation Battery Circular Economy

Tianran Liang, Yi Chen, Jing Xu,\* and Yang Jin\*

The surging demand for electric vehicles and energy storage technologies drives an unprecedented accumulation of spent batteries, which leads to severe environmental burdens and critical resource wastage. Traditional recycling technologies rely on high-temperature calcination or acid/base leaching, and the final products in the form of alloys or salts can only be used as precursors. In contrast, advanced direct recycling regenerates spent cathode and anode into materials that can be directly used in battery production, simplifying the recycling process and improving economic benefits, which is expected to become a shortcut for lithium-ion battery recycling in the future. This review analyzes

the state-of-the-art direct recycling methods based on the failure mechanisms for anodes and cathodes, divides them into solid-state recycling, hydrothermal repair, and others according to different recycling conditions, and summarizes separately the advancements and limitations of each method, to guide the scale-up and sustainability of recycling. Furthermore, this review systematically introduces artificial intelligence (AI) assisted direct recycling strategies, emphasizing the role of AI in optimizing the pretreatment and recycling processes. Finally, the practical challenges and future opportunities for direct recycling are discussed, providing important reference for further development.

## 1. Introduction

Developing alternative, clean, and renewable energy sources, as well as energy storage devices, are consistent with the sustainable development goals.<sup>[1]</sup> Due to high energy density, long cycle life, no memory effect, and low self-discharge rate, lithium-ion batteries (LIBs) have gradually expanded from computer, communication and consumer electronics (3C electronic products) to electric vehicles (EVs) and grid-scale energy storage.<sup>[2,3]</sup> The rapid development and widespread use of LIBs have led to a sharp increase in the number of decommissioned batteries.<sup>[4]</sup> According to the International Energy Agency (IEA) report “Global EV Outlook 2024,” global registrations of new EVs grew by 35% in 2023 compared to the previous year. The growth in EVs will continue to drive up global battery demand, with projected demand reaching 4200 GWh by 2030. Meanwhile, global battery recycling capacity exceeded 300 GWh in 2023.<sup>[5]</sup> However, the current recycling rate of spent LIBs is less than 5% because of the technical and economic limitations.<sup>[6]</sup> The sharp growth in battery demand and the limitations of current recycling capacity will result in a large number of spent batteries

lacking proper recycling solutions (Figure 1a). Therefore, the recycling of spent batteries has been attracting increasing attention from researchers (Figure 1b).

The main components of LIBs consist of the cathode, anode, electrolyte, and separator.<sup>[7,8]</sup> Among these, the cathode materials account for ≈30% of the battery cost and contain a significant amount of expensive metals such as Li, Co, and Ni (Figure 1c).<sup>[9]</sup> Projections indicate that by 2029, global lithium supply will fail to meet market demand (Figure 1d).<sup>[10]</sup> Moreover, resources of expensive metals like cobalt are limited, and the uneven distribution of cobalt exacerbates the instability of the supply chain (Figure 1e,f).<sup>[11,12]</sup> Compared with mining and extracting lithium from low-quality brines, spent LIBs present a tremendous resource potential (Figure 1c).<sup>[13–15]</sup> That is because the valuable metal content in LIBs is much higher than that in ores, and the recovery methods require lower demands in terms of geography, climate, technological maturity, and cost. Therefore, the efficient recycling of spent LIBs is currently the best solution to the resource crisis.<sup>[16–18]</sup> Furthermore, improper disposal of spent batteries may induce risks of self-ignition and explosion.<sup>[19]</sup> Traditional treatment methods (such as incineration and landfilling) may lead to the release of toxic metals into the environment, accumulating through the food chain and harming human health.<sup>[20,21]</sup> Proper disposal of spent LIBs will significantly reduce the safety risks of recycling. Consequently, large-scale recycling is urgently needed.<sup>[22]</sup>

Currently, pyrometallurgical and hydrometallurgical recycling are widely used in industry, while direct recycling is still in the experimental development stage.<sup>[23–25]</sup> Pyrometallurgical recycling breaks down the cathode structure through a high-temperature environment to decompose the cathode into

T. Liang, J. Xu, Y. Jin  
Research Center of Grid Energy Storage and Battery Application  
School of Electrical and Information Engineering  
Zhengzhou University  
Zhengzhou 450001, China  
E-mail: xu.jing@zzu.edu.cn  
yangjin@zzu.edu.cn

Y. Chen  
School of New Energy and Electrical Engineering  
Hubei University  
Wuhan 430062, China

various metal compounds for element separation.<sup>[26,27]</sup> The recycling process is simple to operate, suitable for large-scale production, and highly adaptable. However, the process involves high energy consumption and emissions, causing secondary environmental pollution.<sup>[28,29]</sup> In comparison to it, hydrometallurgical recycling offers higher recovery rates of metal extraction and higher purity than pyrometallurgical recycling. The recycling process dissolves the cathode materials using leaching agents and precipitates metal ions for recovery.<sup>[30]</sup> However, the process generates large amounts of wastewater, inevitably increasing environmental pressure.<sup>[31,32]</sup>

Direct recycling is considered an effective recycling method that can replace traditional recycling methods. It is well-known that spent LIBs still contain 80% of the original capacity and the failed cathode materials retain a relatively high structural integrity.<sup>[33,34]</sup> Traditional recycling processes achieve recycling purposes by completely breaking down the cathode structure, which is inefficient and complex. In contrast, direct recycling abandons the traditional recycling principle, focusing on "decomposition and extraction," choosing to preserve the original structure of the failed cathode material.<sup>[35]</sup> Through "repairing," which is specifically shown in external supplementation of lithium and

internal reconstruction of lattice structure, the failed cathode material can be directly regenerated. The resulting material can be directly used in battery production, eliminating the cumbersome processes of multi-element extraction, precipitation, separation, purification, and resynthesis involved in traditional recycling. Therefore, direct recycling not only alleviates supply shortages of raw materials but also avoids high-energy processes and toxic chemical treatments. Meanwhile, reducing energy consumption and greenhouse gas emissions makes the process more environmentally friendly and efficient.

Moreover, to meet market demand and control management, LIBs are developed toward high-nickel, low-cobalt, or cobalt-free designs.<sup>[36,37]</sup> Since traditional recycling focuses on extracting valuable metals such as cobalt and nickel from recovered metal oxides or alloys, the developing trend of LIBs will eventually lead to a profit crisis in the traditional recycling industry. In contrast, direct recycling follows the trend of the LIBs market. Even as new cathode materials are developed in the near future, the flexible direct recycling methods can also ensure a sustainable profit. Consequently, over the long term, direct recycling offers significant advantages in terms of sustainability and economic viability.



**Tianran Liang** is a graduate student majoring in Electrical Engineering at the School of Electrical and Information Engineering, Zhengzhou University. She received the B.Sc. degree in electrical engineering and automation from the School of Electrical Engineering, Zhengzhou University, Zhengzhou, China, in 2023. Her research focuses on recycling cathode materials from spent lithium-ion batteries.



**Yi Chen** received his Ph.D. from University of Technology Sydney, Australia in 2020. He worked as a postdoctoral researcher at National Institute for Materials Science (NIMS), Japan from 2020 to 2023 and got the prestigious JSPS Postdoctoral Fellowship. He is currently an associate professor at School of New Energy and Electrical Engineering, Hubei University. His research interests focus on rechargeable batteries including lithium/sodium-sulfur batteries, solid-state batteries, lithium metal batteries, aqueous zinc-ion batteries, and sodium-ion batteries.



**Jing Xu** is a professor of Zhengzhou University. She is a young top-notch innovator of science and technology in central plains, and a high-level talent in Henan province. She also serves as a Youth Editorial Board Member for journals such as eScience, Nano-micro Letters, and Nano Research. She received her Ph.D (2018) with Prof. Guoxiu Wang from University of Technology Sydney. Her research interests focus on the next-generation batteries, including aqueous zinc-ion batteries, lithium-sulfur batteries. She has published more than 40 SCI-indexed journal papers, including *Science Advances*, *Advanced Materials*, *Advanced Energy Materials*, *Advanced Functional Materials*, *ACS Nano*, *Nano Energy*, and *Energy Storage Materials*. She has led projects funded by the National Natural Science Foundation of China and Henan Province.



**Yang Jin** received the B.Sc. degree in electrical engineering and automation from the School of Electrical Engineering, Zhengzhou University, Zhengzhou, China, in 2012 and the Ph.D. degree in electrical engineering from the School of Electrical Engineering, Xi'an Jiaotong University, Xi'an, China, in 2017. He is currently a Professor and a Deputy Dean with the School of Electrical and Information Engineering, Zhengzhou University, and the Director of the Research Center of Grid Energy Storage and Battery Application. He was a joint Ph.D. student with the Massachusetts Institute of Technology, Cambridge, MA, USA, and Stanford University, Stanford, CA, USA, in 2014 and 2015, respectively. His research interests include the application of artificial intelligence and large models in energy storage systems, fault diagnosis, and safety warnings for energy storage systems.

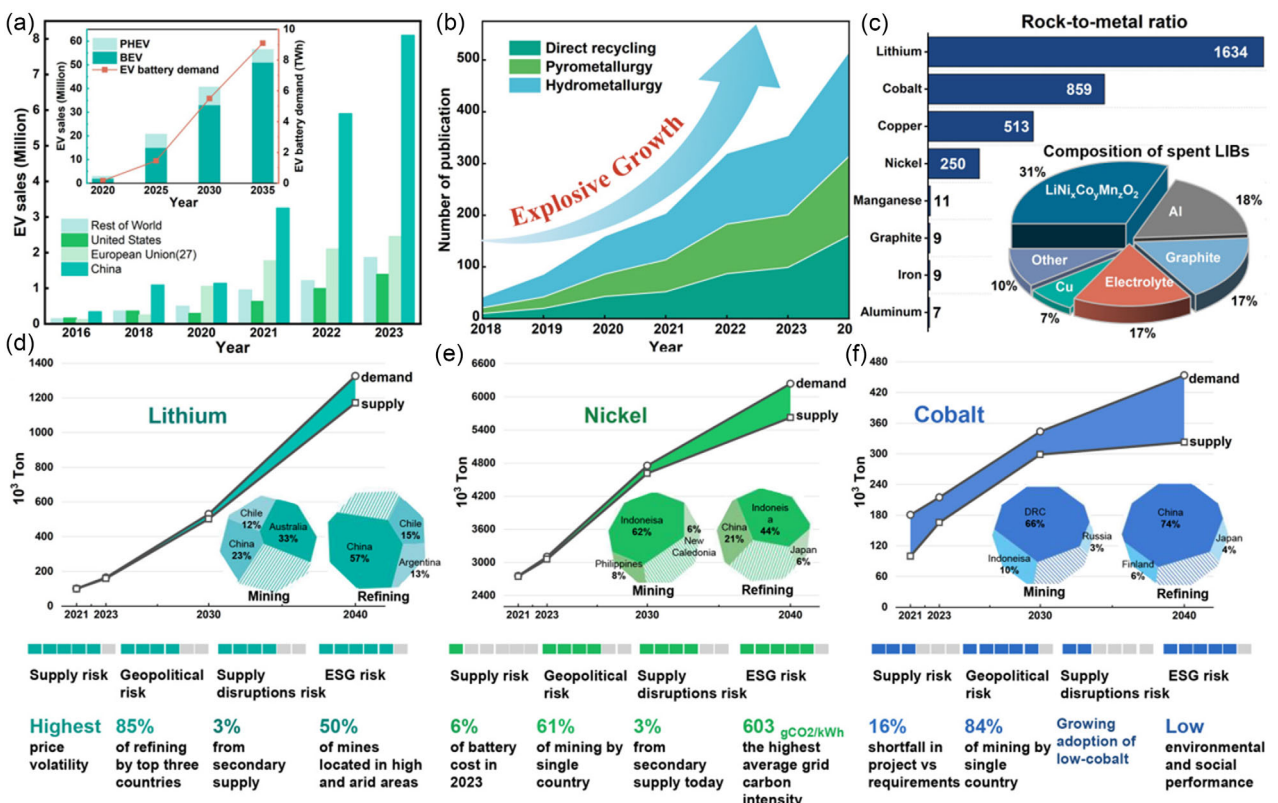


**Figure 1.** a) Sales of electric vehicles (including pure electric vehicles and hybrid electric vehicles) by main countries and regions between 2016 and 2023, as well as the projected growth of pure electric vehicles, hybrid electric vehicles, and electric vehicle power battery demand from 2020 to 2035.<sup>[273]</sup> b) Number of scientific publications on direct recycling, pyrometallurgy, and hydrometallurgy in 2018–2024 from Web of Science. c) Rock-to-metal ratio: The quantity of rock that has to be mined to produce one unit of metal. d–f) Demand projection based on the Announced Pledges Scenario (APS) for 2021–2040 and supply projection based on a detailed review of all announced projects, and the top three producers in 2030. Clean energy transitions risk assessments across supply risks, geopolitical risks, supply disruptions risk, and ESG (environmental, social, and governance) risks for (d) lithium,<sup>[276]</sup> (e) nickel,<sup>[277]</sup> and (f) cobalt.<sup>[278]</sup>

## 2. The Development of Spent Battery Recycling

### 2.1. Challenges of Direct Recycling for Spent LIBs

In China, the concept of direct recycling was proposed and led by Prof. Huiming Cheng (Academician of the Chinese Academy of Sciences). The researchers have innovated a shortcut for spent LIBs recycling—regenerating from molecule to molecule by repairing, and abandoning the traditional concept that recycling from molecules to atoms and finally back to molecules. Since the development of direct recycling, it has attracted widespread attention from researchers. To assess the current status and trends of spent LIBs recycling and better understand the significance of recycling, we conducted a thorough literature search in Web of Science by using keywords such as “spent lithium-ion batteries,” “direct recycling or direct regeneration,” “pyrometallurgy,” and “hydrometallurgy.” The search results indicate that the number of scientific publications on spent LIBs recycling has been significantly increasing over the past 5 years (Figure 1c). Since spent LIBs recycling involves multiple disciplines, knowledge from a single field is insufficient to address the complexity of

the recycling process; thus, the difficulties of recycling will accordingly increase.<sup>[38]</sup> As an emerging technology and research direction, direct recycling still faces obstacles in terms of recycling efficiency and applicability.<sup>[39]</sup> Currently, the LIBs recycling industry is in the early stages, and the difficulties in battery collection, dispersed sources, inconsistent recycling standards, and limitations of recycling technologies all restrict the sustainable development of the recycling industry. Though facing the above challenges, the industrialization of direct recycling technology has been gradually initiated worldwide. Johnson Matthey, a global leader in sustainable technology, has reached an agreement with OnTo Technology, the patent holder for direct battery recycling, to focus on the efficient recovery of electrode materials directly from lithium-ion battery production waste, upgrading OnTo’s laboratory-scale process to large-scale industrialized recycling.<sup>[40]</sup> BMW will set up a Cell Recycling Competence Centre (CRCC) in Bavaria to implement innovative direct recycling technologies for materials from production waste and whole spent batteries. The CRCC is scheduled to start up in the second half of 2025.<sup>[41]</sup> These major initiatives demonstrate that the direct recycling technology is transitioning from laboratory research to industrial application.

## 2.2. An Overview of Battery Recycling Policies for Different Countries and Regions

Based on this condition, various countries and regions focus on different stages of battery cycle life to regulate spent LIBs recycling, aiming to build a comprehensive recycling system that reduces environmental pollution. Due to the influence of local raw material shortages, Japan currently has the most advanced battery recycling system in the world. Since 1994, when Japan began to implement a battery recycling program, it has established a "reverse logistics" system. In this system, manufacturers collect spent batteries through the sales network.<sup>[42,43]</sup> The European Union (EU) was one of the first regions to address battery recycling. As early as 1991, the EU required that batteries must be separately collected, and the potential pollutants and recycling issues should be considered from production and design stages.<sup>[44]</sup> Recently, to improve power battery traceability and lifecycle management, the EU proposed that batteries should have labels and quick response (QR) codes, and power batteries should have a "battery passport."<sup>[45]</sup> The EU's Critical Raw Materials Act, adopted in 2024, primarily drives the development of the battery recycling industry by establishing mandatory recycling targets and content requirements of recycled materials, ensuring a secure supply of critical raw materials and building a circular economy system.<sup>[46]</sup> In the USA, the recycling system for spent LIBs is well-developed. In addition to establishing a deposit system for collecting used batteries, they also educate consumers about proper battery sorting through third-party organizations to reduce contamination in the recycling process.<sup>[47,48]</sup> According to the Inflation Reduction Act of 2022, Electric vehicle battery materials recycled in the USA are automatically recognized as "made in the United States" and eligible for subsidies regardless of their source. This policy could allow automakers that use recycled battery materials in the USA to qualify for electric vehicle production incentives.<sup>[49]</sup> In China, the corresponding policies were introduced in 2012 to encourage power battery manufacturers to promote spent LIB recycling. These policies also support the development of specialized battery recycling companies. At that time, the recycling industry was still in its early stages.<sup>[50,51]</sup> However, since 2018, with the introduction of pilot programs, the recycling industry has developed rapidly.<sup>[52]</sup> According to the Administrative Measures for Recycling and Utilization of Power Batteries for New Energy Vehicles of 2023, to strengthen the standardized management of the industry, the recycling and utilization of new energy vehicle power batteries have been promoted by laws and regulations in China.<sup>[53]</sup> China has gradually built a comprehensive legal and regulatory framework, which requires producers to take responsibility for battery recycling, thereby promoting complete life cycle management of resources for environmental responsibility.

## 2.3. Workflow of Different Recycling Methods for Spent LIBs

The design of modern LIBs presents challenges for direct recycling. As researchers did not consider recycling during the design

stage, this resulted in the need for a precise pretreatment of spent batteries in subsequent direct recycling.<sup>[39]</sup> Typically, pretreatment starts with mechanical or manual sorting based on the battery composition to prevent cross-contamination of cathode materials with different components and to avoid increasing unnecessary purification steps.<sup>[54]</sup> To ensure the safety of the recycling, passivation is necessary before recycling. Since spent LIBs contain various residual charges, ignoring the step may pose safety risks. Generally, residual charge is released by immersing the batteries in a salt solution for a specific period.<sup>[55]</sup> In pyrometallurgical recycling, after this step, batteries are directly crushed and treated at high-temperature. The high-temperature process removes separators, binders, conductive agents, electrolytes, and anodes, resulting in the corresponding metal alloys, which are separated to obtain material precursors for synthesizing cathode materials. The recycling process is simple, but it still causes carbon dioxide emissions.<sup>[56]</sup> In hydrometallurgical recovery, batteries are first crushed into small pieces and are separated into the shells, current collectors, and electrode materials. The separated cathode materials undergo acid or alkali leaching to obtain metal salts by precipitation, which can be used as raw materials in battery production. The recycling process is more complex and generates large amounts of wastewater.<sup>[57]</sup> Considering the degradation of cathode materials is primarily due to the loss of mobile lithium ions and damage to the crystal structure, direct recycling aims to restore the materials' original performance by replenishing lithium ions with lithium salts. Existing methods for direct recycling include solid-state recycling, hydrothermal repair, molten salt repair, and chemical relithiation (Figure 2). Compared with traditional recycling, direct recycling offers shorter processes with lower pollution, which has caused growing interest and attention.

To minimize cross-contamination and element mixing between different cathode materials, a series of pretreatment processes must be conducted before recycling. Through sorting, batteries are categorized, and material purification steps are simplified, which improves the recycling efficiency. Due to the lack of standardized manufacturing regulations in the LIB market, batteries with different shapes, sizes, and materials are widely used in various applications and regions, which poses challenges for the centralized collection, transportation, and recycling of spent batteries. Although the scaling up of the EV market has created favorable conditions for power battery recycling, the compositions of batteries from mobile devices vary significantly, and the sources are dispersed, making them difficult to trace. The outputs from the pretreatment step serve as the inputs for the subsequent recycling. Therefore, the classification of batteries according to the recycling requirements is essential. Battery sorting generally includes manual sorting, magnetic and nonmagnetic sorting, mechanical sorting based on shape and size, and automatic sorting based on weight and electrical parameters.<sup>[58]</sup> In addition to sorting batteries according to the above features, the atomic ratios of various elements in ternary cathode materials determine the different performance among the cathodes. Accurately classifying batteries based on the element ratios of the cathode material without disassembly presents a challenge.

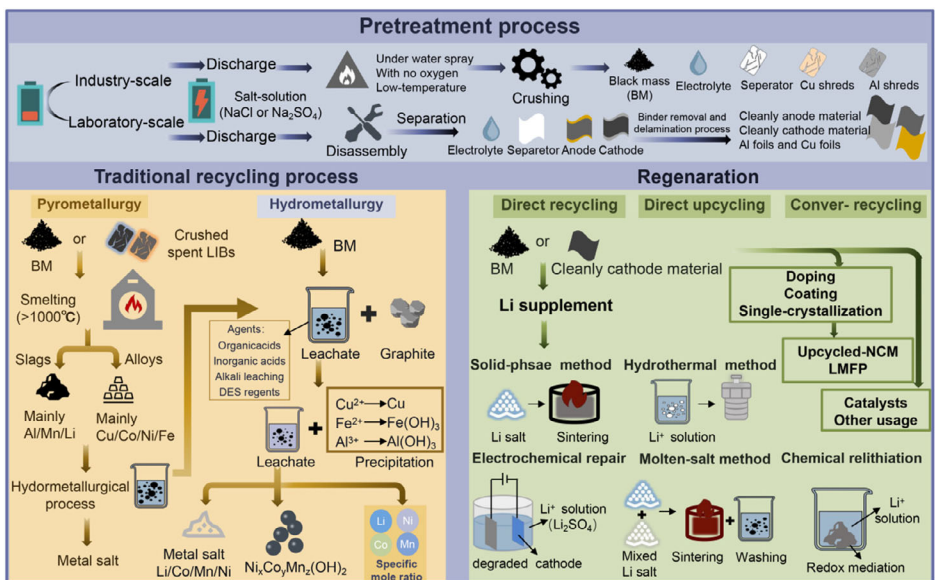


**Figure 2.** Pretreatment processes for spent LIBs: laboratory-scale and industrial-scale; and schematic diagrams of pyrometallurgy, hydrometallurgy, and direct recycling.

Current sorting methods cannot achieve the goal. This situation highlights the urgent need for nondestructive sorting technologies to classify materials with various atomic ratios, which can understand the inside information of batteries and may require the use of big data and AI. Furthermore, some batteries are labeled with information, such as the widely used NCR18650 battery. The label represents a cell with a diameter of 18 mm and height of 65 mm, and "NCR" indicates that the cathode material is nickel-cobalt-aluminum oxide (with the specific element ratio unknown). However, it has to be mentioned that the label information is often lost after long-term use, making classification more difficult. Thus, establishing a standardized naming system for LIBs may help facilitate AI automated classification.

When the remaining capacity of batteries falls to 80% or below, it is considered the end of battery life. Then, the tests are conducted to determine whether the battery can be reused for second-life application or be recycled. Even after retirement, spent batteries still retain a large amount of charge. Due to the presence of flammable organic electrolytes and lithium precipitation in the spent batteries, there exist some hazardous factors (such as short circuits and explosions) in storage and transport processes, and there is an explosion risk during the mechanical dismantling. Therefore, deep discharge treatment is required before battery disassembly to consume ≈90% of the battery capacity. The main discharge methods include physical techniques such as low-temperature freezing and perforation discharge, as well as chemical methods such as external resistance discharge, conductive solution discharge, and conductive powder discharge.<sup>[59,60]</sup> In the perforation process, short circuits may generate substantial residual heat, causing electrolyte decomposition to release harmful gases or even leading to explosions. For safety and large-scale processing considerations, the conductive solution discharge method is more commonly

employed. According to the "Battery Recycling and Reuse: Part 3—Discharge Specifications" proposed by the National Automotive Standardization Technical Committee in September 2020, discharging via an external circuit is only suitable for batteries with intact external structures and full function. The conductive solution method is applicable to all batteries, exhibiting broader applicability.<sup>[61]</sup> However, the conductive solution discharge method may lead to the corrosion of shells and the leakage of electrolyte. Compared with the conductive solution discharge method, the conductive powder discharge method does not produce pollutants, making it a cleaner technique. Wang et al.<sup>[62]</sup> assessed the discharge efficiency of different discharge media (NaCl, Na<sub>2</sub>SO<sub>4</sub>, MnSO<sub>4</sub> solutions, and flake graphite) by measuring the residual voltage after discharge. The assessment showed that the high concentration NaCl solutions exhibited higher discharge efficiency, and the flake graphite achieved zero emission during the discharge process.

Different components of spent batteries need to enter different recycling processes to achieve efficient recovery. Therefore, the flexible and precise separation of various components is crucial. With the development of LIB production technology and the extension of LIBs' application, the functions and compositions of batteries will become more complex, not only consisting of basic components such as cathodes, anodes, and current collectors, but also including fuses, overcharge protection, and electrical systems in battery packs. Based on the structure of battery packs, during disassembly, it is necessary to disconnect the batteries within the battery packs while maintaining the integrity of each battery. The subsequent disassembly process involves the precise separation of battery components. Given that the failed components typically are the electrolyte or electrodes, the ideal disassembly approach should focus on replacing failed parts without damaging other components. However, the current

technologies can not reach the goal because of the battery's structure. Therefore, disassembly strategies show significant research potential and are closely related to battery design.

Crushing is the primary method for large-scale disassembly.<sup>[63,64]</sup> Spent LIBs are firstly cut and then crushed, exposing the electrolyte and allowing gases to enter the exhaust treatment system. Then, the resulting pieces are further crushed into powder and sieved for coarse separation. However, the obtained powder contains not only cathode active materials, but also current collectors and anode materials. Although the disassembly method is simple, it introduces contamination into the subsequent recycling flow and affects recovery efficiency. Manual disassembly requires substantial labor and poses safety risks in an operating environment, but it can realize precise classification of battery components.<sup>[65,66]</sup> Moreover, the immaturity of automatic disassembly presents challenges in practical application. Automatic robot disassembly technologies that can replace manual operation require a high degree of intelligence and flexibility, making them a current research focus.<sup>[67]</sup>

To achieve efficient recycling of the obtained cathode and anode, it is essential to separate the active materials from other components successfully. Although the battery system continues to evolve, the composition of the cathode remains consistent, consisting of active materials, conductive agents, binders ( polyvinylidene fluoride, PVDF), and current collectors (Al foil).<sup>[68,69]</sup> Based on this, the complete separation of active cathode materials from cathodes is crucial for the subsequent recycling. Although the structure of anodes is similar to that of cathodes, the water-soluble binders in the anode can be dissolved easily in water.<sup>[70]</sup> Therefore, the separation of cathode materials requires deep research. The current separation methods based on Al foil typically use alkaline solutions to dissolve Al, exhibiting a significant separation effect.<sup>[71–73]</sup> Furthermore, the method can also be used to remove Al particles from Al-containing black mass (BM) generated by multistage crushing in industry. However, the method results in large amounts of alkaline wastewater, presenting challenges for wastewater recovery. Currently, researchers prefer to explore the separation methods by dissolving or decomposing the PVDF. For example, the PVDF can be dissolved by organic solvents.<sup>[74]</sup> However, due to particle agglomeration in materials, the reaction contact area will be reduced, resulting in low dissolution efficiency. To address the problem, researchers combined organic solvent immersion with ultrasonic treatment to accelerate the decomposition of PVDF and detachment of active materials. During this process, increasing the reaction temperature properly can further speed up the separation.<sup>[75]</sup> In addition to using high-polarity organic solvents for separation, such as N-methylpyrrolidone (NMP) and dimethyl carbonate (DMC), molten salts and deep eutectic solvents can also be used to dissolve PVDF.<sup>[76–82]</sup> Furthermore, heating the electrodes in an air or oxygen environment can also induce high-temperature pyrolysis of PVDF, simultaneously removing the conductive agent.<sup>[83,84]</sup> However, high-temperature treatment may damage the structure of the cathode materials, and the decomposition of PVDF generates F-containing acidic gases, which pollute the environment. Therefore, it is necessary to set the alkaline

solutions to adsorb the acidic gases at the furnace outlet.<sup>[85]</sup> The coating of the cathode material with a minor amount of calcium facilitated the conversion of the PVDF pyrolysis into metal deposits that were deposited on the surface of the particles, thereby eliminating the release of F-containing organic pollutants.<sup>[86]</sup> In conclusion, a well-designed pretreatment process can eliminate safety risks, precisely separate and enrich valuable components for subsequent recycling steps.

### 3. Direct Recycling of Spent Cathode Materials

The recycling of active cathode materials can be primarily divided into two aspects. Direct recycling involves the identification of appropriate methods to repair the material based on its failure mechanisms and defect levels, aiming to restore the chemical and cycling performance of materials to the original level. However, simply restoring failed materials to match the original materials may not meet the requirements of battery recycling in the future. As a result, direct upcycling has become an essential trend of battery recycling, as it regenerates materials with performance superior to that of original materials through techniques such as surface modification and element doping, thereby better aligning with the development needs of battery recycling. When cathode materials are severely degraded and regeneration is not feasible, or under other circumstances, utilizing the valuable elements of the materials and converting them into high-value-added products (such as catalysts) for other applications is also a critical development direction of battery recycling. Due to the different degradation mechanisms of various materials, understanding the defect formation mechanisms is key to selecting appropriate recycling methods. Moreover, as different recycling techniques are suitable for different cathode materials, it is critical to explore the degradation mechanisms of cathode materials to guide regeneration. Therefore, this study provides a detailed analysis of the degradation mechanisms of cathode materials, reviews the effective recycling methods, and discusses both historical and recent advancements.

#### 3.1. Direct Recycling Methods of Layer LiCoO<sub>2</sub> Cathode Materials

LCO was first proposed as a cathode material for LIBs in 1985. In 1991, Sony introduced the first commercial LIBs using LCO as the cathode for use in portable devices, such as Walkmans.<sup>[87,88]</sup> With the development of 3C electronic products, the market demand for LCO grew rapidly, and the energy density and cycle life of LCO were further improved. Despite the constant emergence of new cathode materials, LCO batteries are the primary power source for devices such as smartphones and tablets.<sup>[89]</sup> However, the elements of lithium and cobalt for LCO production face a critical supply crisis. It means that it is vital to explore the recycling methods of LCO.

The charge/discharge process of LIBs is highly related to the reversible shuttling of Li<sup>+</sup> between electrodes. Therefore, the

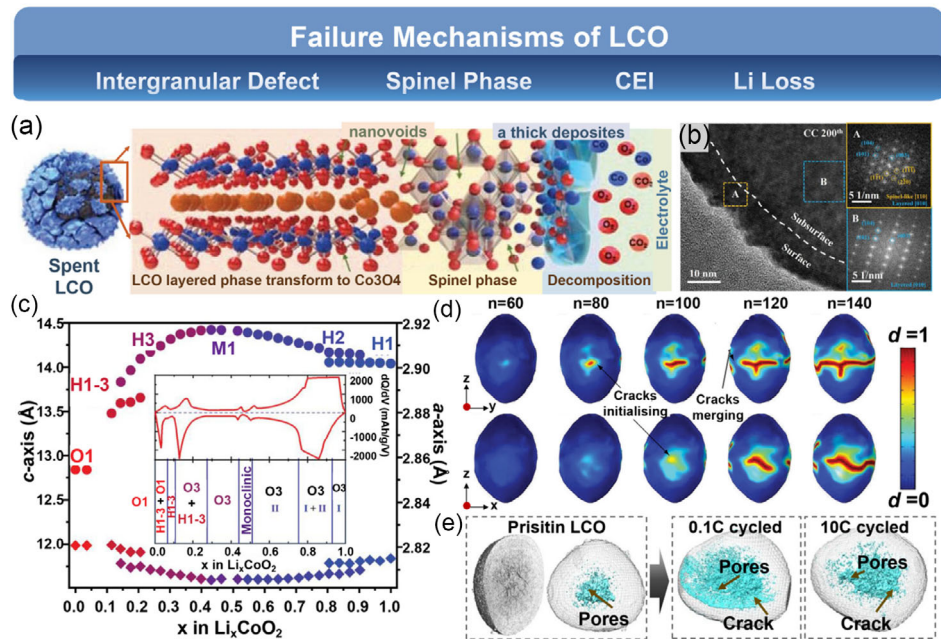


**Figure 3.** Multiscale structural degradation mechanisms of spent LCO. a) Schematic illustration of the degradation mechanisms of the cycled LCO (Reproduced with permission.<sup>[93]</sup> Copyright 2022, Wiley-VCH). b) TEM images of the LCO surface and subsurface structure features after the 200th cycle (Reproduced with permission.<sup>[279]</sup> Copyright 2023, Wiley-VCH). c) Phase transition and variation of lattice parameters (a,c) induced by lithium-ion intercalation/extraction in LCO (Reproduced with permission.<sup>[280]</sup> Copyright 2023, Wiley-VCH). d) 3D realistic electrode particle: evolution of the phase field contours for the following cycle numbers (n). d: describing the crack-solid interface (Reproduced with permission.<sup>[281]</sup> Copyright 2022, Elsevier). e) Visualization of internal pore structures and crack networks within cycled LCO particles (Reproduced with permission.<sup>[282]</sup> Copyright 2024, Springer Nature).

failure of LIBs is directly linked to the number of mobile active  $\text{Li}^+$  (Figure 3a).<sup>[90]</sup> Typically, LCO particles have a smooth and flat surface morphology. However, during cycling, repeated intercalation/extraction of  $\text{Li}^+$  causes lattice expansion and contraction, leading to uneven distribution of internal stress, which may result in lattice deformation and layer collapse.<sup>[91,92]</sup> As the cycle number increases, the above process eventually leads to the formation of intragranular cracks and intergranular cracks (Figure 3b). Due to lattice strain, the  $\text{Li}^+$  can no longer intercalate into the Li sites for the subsequent cycles, causing Li loss in materials, which is closely related to the degree of material failure. Therefore, the higher the degree of material failure is, the higher the concentration of lithium vacancies inside is (Figure 3c).<sup>[90]</sup> Moreover, when the loss of  $\text{Li}^+$  is significantly severe in the material ( $\text{Li}_x\text{CoO}_2, X \leq 0.5$ ), the Co  $t_{2g}$  energy level overlaps with the O 2p conduction band, leading to the loss of lattice oxygen from the material's surface.<sup>[93]</sup> As more lattice oxygen escapes from the surface, there will be many nanovoids and lithium-poor spinel  $\text{Co}_3\text{O}_4$  phases formed in the material (Figure 3a), limiting the reversible intercalation of  $\text{Li}^+$  during the discharge process, causing the  $\text{Li}^+$  to be trapped in the anode-CEI (cathode-electrolyte interface) structure and severe side reactions, which eventually lead to the dissolution of cobalt.<sup>[94,95]</sup> Due to the structural phase transition and rearrangement of LCO, the layered structure shifts to spinel or even rock-salt phase, forming the defective structures (Figure 3d,e). Therefore, during the regeneration of LCO, in addition to necessary  $\text{Li}^+$  replenishment, repairing the cracks and defects in its structure is crucial. The representative cases, the specific

regeneration conditions and results of LCO direct recycling and upcycling are summarized in Table 1.

### 3.1.1. Solid-State Recycling for LCO

As is well known, the solid-state reaction is the simplest method for synthesizing LCO, which involves thoroughly grinding and mixing lithium and cobalt sources, followed by high-temperature calcination to synthesize the LCO material.<sup>[96]</sup> Similarly, solid-state recycling can repair degraded LCO materials to a level comparable to that achieved in the synthesis process by mixing spent materials with Li source and calcining them at high temperatures to achieve  $\text{Li}^+$  supplementation and structural repair. Based on this condition, Nie et al. mixed spent LCO with  $\text{Li}_2\text{CO}_3$  and calcined it at 800 °C in air to obtain the regenerated-LCO (R-LCO).<sup>[97]</sup> Similarly, Shi et al. also used  $\text{Li}_2\text{CO}_3$  to repair spent LCO and compared it with other repair methods.<sup>[87]</sup> Moreover, Mu et al. found that during high-temperature sintering, Al impurities were introduced to the LCO surface, leading to poor cycling performance.<sup>[98]</sup> Through the alkaline washing method and adding LiOH, the Al impurities were removed, and the spent LCO was successfully repaired and regenerated. Given that the regeneration effect is significantly influenced by the temperature and the Li/Co ratio, Kong et al. explored the impact of regeneration temperature and element ratio on the regeneration of LCO, achieving optimal repair results at 850 °C with a Li/Co ratio of 1.0.<sup>[99]</sup>

With the steadily increasing consumption of LCO, there is a growing demand for higher energy density. To improve

**Tabel 1.** Summary of typical cases for the direct recycling and upcycling of LCO.

Cathode	Method	Key conditional	Initial capacity [mAh g <sup>-1</sup> ]	Capacity retention	References
LCO	Solid-phase recycling	Solid-state sintered with Li <sub>2</sub> CO <sub>3</sub> , 850–950 °C for 12 h	152.4 [0.2C, 3.0–4.3 V]	98% [100 cycle]	[97]
LCO	Solid-phase recycling	Solid-state sintered with Li <sub>2</sub> CO <sub>3</sub> , 850 °C for 12 h	152.1 [0.1C, 3.0–4.3 V]	89.0% [100 cycle]	[87]
LCO	Hydrothermal repair	Hydrothermal with LiOH 220 °C 4 h; annealing, 800 °C for 4 h (Ar)	153.1 [0.1C, 3.0–4.3 V]	91.2% [100 cycle]	[87]
LCO	Solid-phase recycling	Solid-state sintered with LiOH, 300 °C for 10 h, 850 °C for 8 h	145.0 [0.2C, 2.7–4.2 V]	94% [50 cycle]	[98]
LCO	Solid-phase recycling	Calcined at 600 °C for 2 h (air); sintered with Li <sub>2</sub> CO <sub>3</sub> , 850 °C for 12 h	138.9 [1C, 3.0–4.3 V]	89.9% [100 cycle]	[99]
LCO	Upcycling	Solid-state sintered with Li <sub>2</sub> CO <sub>3</sub> and Mg <sub>3</sub> (PO <sub>4</sub> ) <sub>2</sub> , 900 °C for 10 h	215.7 [0.1C, 3.0–4.6 V]	92.2% [100 cycle]	[100]
LCO	Upcycling	Sintered with Li <sub>2</sub> CO <sub>3</sub> , MgO, Al <sub>2</sub> O <sub>3</sub> , 900 °C for 10 h	220.4 [0.1C, 3.0–4.6 V]	79.7% [300 cycle]	[101]
LCO	Upcycling	Calcined at 500 °C for 2 h (air); high pressure crushing on 60 MPa, sintered 1000 °C for 10 h	175.2 [1.0C, 3.0–4.5 V]	88.8% [500 cycle]	[102]
LCO	Upcycling	Solid-state sintered with Li <sub>2</sub> CO <sub>3</sub> , NH <sub>4</sub> F, 450 °C for 5 h, 900 °C for 8 h	174.4 [1.0C, 3.0–4.5 V]	88.3% [500 cycle]	[103]
LCO	Upcycling	High pressure crushing on 60 MPa; sintered with manganese acetate, thiourea, Li <sub>2</sub> CO <sub>3</sub> , 850 °C for 10 h	188.2 [0.2C, 3.0–4.5 V]	92.5% [100 cycle]	[104]
LCO	Upcycling	Sintering with Ni-, Mn- solution and LiOH-H <sub>2</sub> O, 850 °C 16 h, 900 °C 10 h	159.0 [0.1C, 2.7–4.3 V]	82.1% [200 cycle]	[105]
LCO	Hydrothermal repair	Hydrothermal with LiOH, 220 °C for 45 min with microwave	151.5 [0.1C, 3.0–4.3 V]	94.5% [100 cycle]	[107]
LCO	Hydrothermal repair	Hydrothermal treatment with Li solution, H <sub>2</sub> O <sub>2</sub> , 90 °C for 6 h	132.1 [0.2C, 2.8–4.3 V]	96.74% [50 cycle]	[106]
LCO	DES repair	Reacted with CoO-DES, 120 °C 8 h annealing, 850 °C for 2 h	133.1 [0.1C, 2.0–4.2 V]	90% [100 cycle]	[108]
LCO	DES repair	Reacted with DES, 80 °C for 10 h	208.87 [NA, 3.0–4.6 V]	87.1% [200 cycle]	[110]
LCO	Molten salt	Sintered with LiOH-KOH-Li <sub>2</sub> CO <sub>3</sub> molten salt, 500 °C for 8 h	144.5 [0.1C, 3.0–4.3 V]	92.5% [200 cycle]	[111]
LCO	Molten salt	Sintered with LiOH-KOH molten salt, LiNO <sub>3</sub> , 300 °C 8 h, 500 °C 16 h	144.5 [0.1C, 3.0–4.2 V]	92.5% [200 cycle]	[112]
LCO	Molten salt	Sintered with KCl-LiNO <sub>3</sub> molten salt, CaO, 750 °C for 12 h	108.7 [4C, 3.0–4.5 V]	95.6% [50 cycle]	[113]
LCO	Redox mediation	Reacted with C <sub>2</sub> H <sub>5</sub> LiO (4 h/8 h/16 h), Annealing, 850 °C for 6 h	157.6 [1C, 2.8–4.3 V]	91.6% [200 cycle]	[114]
LCO	Redox mediation	Immersed in FL-Li/THF solution, 25 °C for 2 h; with Co <sub>3</sub> O <sub>4</sub> , 850 °C for 4 h	148.7 [0.2C, 3.0–4.3 V]	≈80% [1000 cycle]	[116]
LCO	Rapid Joule Heating	Rapidly Joule heating with Li <sub>2</sub> CO <sub>3</sub> , carbon paper, 1440 K for 8 s	133.0 [0.1C, 3.0–4.3 V]	75.2% [300 cycle]	[119]
LCO	Conve-cycling	Chemical delithiation;Electrochemical delithiation	NA	NA	[121]
NA: not available.					

the energy density of LCO, reducing the battery weight and enhancing the capacity of cathode materials are effective strategies. Since the thickness of current collectors, separators, and shells has approached their physical limits, increasing the capacity of LCO represents a feasible approach. The commercial upper limit for the cutoff charging voltage of LCO cathode materials is currently 4.45 V, but raising the cutoff voltage is necessary for the development of higher energy density batteries. Currently, the synthesis of high-voltage LCO is typically achieved through element doping or compound coating. In element doping, during Li-ion extraction from the bulk structure, these dopant atoms act as pillars to stabilize the layered structure.

Element doping relies on high-temperature diffusion, and the optimal timing for doping is before the Li sites are fully occupied. This is because, once Li ions fully occupy the Li sites, the diffusion and occupation of dopant atoms become challenging. For instance, Zhang et al. proposed a simple sintering process for recycling spent LCO by adding Mg<sub>3</sub>(PO<sub>4</sub>)<sub>2</sub> to achieve stable cycling of R-LCO at a high voltage of 4.6 V (Figure 4a).<sup>[100]</sup> During the recycling process, Mg<sup>2+</sup> was uniformly doped in the bulk lattice, and PO<sub>4</sub><sup>3-</sup> coating was formed as Li<sub>3</sub>PO<sub>4</sub> nanoparticles on the surface. Under the same cycle numbers, the doped R-LCO maintained relatively stable CEI interfacial resistance (R<sub>sf</sub>) throughout the cycles (Figure 4b). After recycling, the cracks and rough

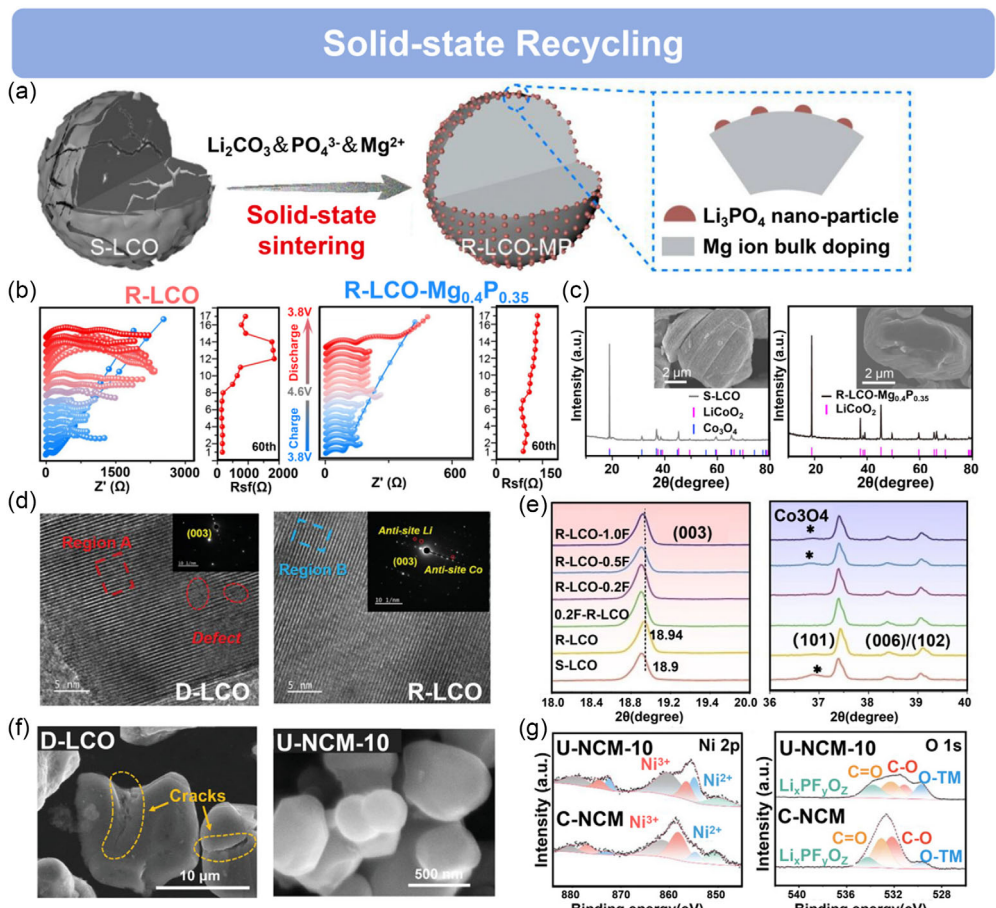


**Figure 4.** Solid-state recycling of spent LCO through elements doping to stabilize the crystal structure and enhance cycling performance. a) Schematic of dual-ion doping repairing particle structure in LCO solid-phase recycling and b) in situ EIS plots of regenerated LCO before and after dual-ion doping during 60 charge/discharge cycles (Reproduced with permission.<sup>[100]</sup> Copyright 2024, The Authors). c) XRD patterns and cross-sectional TEM images of pristine, failed, and doped-regenerated LCO (Reproduced with permission.<sup>[100]</sup> Copyright 2024, The Authors). d) SAED patterns of Co-upgraded regenerated LCO before/after 60 MPa crushing (Reproduced with permission.<sup>[102]</sup> Copyright 2024, Wiley-VCH). e) XRD patterns of F-doped regenerated LCO with different doping dosages and time (Reproduced with permission.<sup>[103]</sup> Copyright 2024, Wiley-VCH). f) SEM images of spent LCO particles before regeneration and Ni/Mn-doped regenerated NCM particles. g) High-resolution XPS spectra of regenerated NCM samples vs. commercial NCM (Reproduced with permission.<sup>[105]</sup> Copyright 2024, Wiley-VCH).

surface of the LCO were repaired, and R-LCO revealed diffraction peaks related to the  $\alpha\text{-NaFeO}_2$  layered structure in commercial LCO, as shown in X-ray diffraction (XRD) analysis (Figure 4c). Similarly, Wang et al. mixed spent LCO with  $\text{Al}_2\text{O}_3$ ,  $\text{MgO}$ , and  $\text{Li}_2\text{CO}_3$  and sintered for recycling.<sup>[101]</sup> The Li vacancies of LCO facilitated the diffusion and doping of Mg and Al. However, the doping dosage is critical for balancing battery capacity and cycling stability. In this recycling process, when cycling stability of the doped R-LCO was higher than that of the doped commercial LCO, the optimal dosage was 0.3 wt% for Mg and 0.6 wt% for Al. Instead, when excessive Mg and Al occupy Li sites, the capacity of doped R-LCO will decrease. Researchers confirmed the pillar effect of doping elements and emphasized their potential in the direct recycling of spent LCO. For example, Lei et al. directly regenerated spent LCO with evident cracks in particles through high-pressure crushing (60 MPa) and high-temperature sintering, introducing Li/Co antisite in R-LCO.<sup>[102]</sup> As shown in the selected area electron diffraction (SAED), the diffraction spots were

detected on Li sites, while some were absent on cobalt sites (Figure 4d). Generally, Li sites are not visible in SAED patterns unless occupied by other atoms. The result meant antisite Co acted as a “pillar” in Li sites, effectively promoting  $\text{Li}^+$  intercalation/extraction during cycling.

Considering the influence of battery structural design on the regeneration of spent LCO, F impurities often remain in the spent materials because of the use of binders and electrolytes. Therefore, exploring F-doped is practically significant for the efficient recovery of spent LCO. Unlike the elements occupying Li sites, F-doping utilizes oxygen vacancies in spent LCO as natural doping sites, which decreased the diffusion energy barrier of the F-element and contributed to successful regeneration. For example, Lei et al. precisely controlled F-doping levels to construct a gradient F-doped subsurface, significantly enhancing the electrochemical performance.<sup>[103]</sup> The result was attributed to the ordered migration of F in the crystal lattice, forming a robust  $\text{CoO}_2\text{F}$  structure. This process improved the redox activity

of Co-ions and physically strengthened surface oxygen, inhibiting irreversible oxygen release. As shown in XRD characteristic peaks, the R-LCO did not contain the  $\text{Co}_3\text{O}_4$  phase, indicating the spinel phase was effectively removed (Figure 4e). However, when excessive F reacted with Li sources to form LiF, it covered the LCO surface and hindered the restoration effect of  $\text{Li}_2\text{CO}_3$ . The doping-repair strategy addressed the multilevel challenges of Li deficiency, structural degradation, and irreversible oxygen release in spent LCO during recycling, achieving multi-dimensional and high-quality regeneration.

The cooperative effects of relithiation, elemental doping, and surface reconstruction more effectively restore and improve the electrochemical performance of degraded materials. For instance, Liu et al. mixed spent LCO with manganese acetate, thiourea, and  $\text{Li}_2\text{CO}_3$  to sinter, achieving triple restoration via relithiation, surface coating, and Mn/N/S doping.<sup>[104]</sup> As the crystal structure of LCO is similar to  $\text{LiNi}_{x}\text{Co}_y\text{Mn}_{1-x-y}\text{O}_2$  (NCM) materials and the production of LIBs with NCM cathodes is continuously increasing, upcycling spent LCO to NCM materials has substantial application potential. Given that LCO particles always possess a particle size of several tens of micrometers because of the high intrinsic electronic conductivity, whereas NCM particles with lower electronic conductivity should be smaller in size. Yang et al. simultaneously achieved relithiation, the reduction of particle size, and the formation of NCM particles.<sup>[105]</sup> As shown in scanning electron microscope (SEM) images, the crystal defects of LCO were recovered, and the LCO particles were transformed into smaller NCM particles ( $\approx 300\text{--}800\text{ nm}$ ) (Figure 4f). Meanwhile, X-ray photoelectron spectrometer (XPS) spectra of the regenerated materials confirmed the presence of Ni and Mn 2p peaks, indicating successful doping of Ni and Mn into the upgraded materials (Figure 4g). The innovative strategy is compatible with current industrial workflows, offering practicality and economic potential.

### 3.1.2. Hydrothermal Repair for LCO

To reduce energy consumption, researchers have explored a hydrothermal repair method for the direct recycling of LCO, which avoids the high-temperature calcination conditions and uses solutions as  $\text{Li}^+$  transport media, making it a more environmentally friendly and efficient regeneration method. However, the mild reaction conditions make it difficult to repair lattice cracks and defects. Therefore, introducing an annealing step in the final stage of the hydrothermal process can effectively compensate for this limitation. The combination of hydrothermal repair and short-time annealing treatment addresses the inherent shortcomings of hydrothermal reactions. For example, Shi et al. used LiOH solution to perform hydrothermal repair to spent LCO and explored the effects of different annealing temperatures and times for the recycling of LCO.<sup>[87]</sup> In addition, ultrasound-assisted hydrothermal repair is a promising direct recycling method. Zhao et al. successfully regenerated spent LCO cathode materials under the cooperative effect of ultrasonic cavitation and  $\text{H}_2\text{O}_2$  deep oxidation, effectively reconstructing blocked  $\text{Li}^+$  channels (Figure 5a).<sup>[106]</sup> Unlike ultrasound, which transfers energy through

mechanical vibrations, self-heating under microwave can form a highly efficient heat field in and around LCO particles (Figure 5b), influencing the particle crystallinity and microstructure. For instance, Liu et al. used microwave-assisted hydrothermal treatment to regenerate LCO materials.<sup>[107]</sup> Compared with traditional hydrothermal repairs, the approach can obtain higher purity powders with better crystallinity and more uniform microstructure in a shorter reaction time and at a lower reaction temperature. More uniform particles allow regenerated LCO batteries to achieve high capacity and high-rate performance, realizing stable regeneration.

### 3.1.3. Deep Eutectic Solvent Assisted Recycling for LCO

For LCO, the current hydrothermal relithiation process focuses primarily on  $\text{Li}^+$  supplementation under high pressure, ignoring cobalt loss. The ideal direct recycling method based on solution should meet the following requirements: a) the reaction should be operated in a solution without the need for high temperature and pressure; b) the solvent carrier should exhibit selectivity for ion transport, facilitating the supplementation of specific elements, such as lithium and cobalt; c) the reagents should be low-cost and readily available; and d) the method should have a broad applicability to different types of cathode materials.<sup>[108]</sup> To meet these requirements, a green deep eutectic solvent (DES) has attracted attention from researchers. Recently, DES has been used to dissolve spent cathodes to extract  $\text{Li}^+$  and  $\text{Co}^{2+}$ , which can be seen as an improvement of the hydrometallurgical process, as it uses less acid.<sup>[109]</sup> Therefore, the development of DES for the direct recycling of spent LCO is of significant importance. Based on this, Wang et al. utilized a DES composed of LiCl and  $\text{CH}_4\text{N}_2\text{O}$  to repair failed LCO directly (Figure 5c).<sup>[108]</sup> Unlike the hydrometallurgy method, which uses solvents to dissolve LCO materials, the solvent molecules in DES directly serve as selective transport carriers for Li and Co supplementation. During the process, Li supplementation restored the capacity of LCO to its initial capacity, while Co supplementation improved the capacity retention after long cycles. As shown in the transmission electron microscope (TEM), microcracks and fractures can be clearly seen on the surface of the LCO. At the same time, the regenerated LCO has a very different smooth surface (Figure 5d). Moreover, DES can be repeatedly recycled as a repair solvent and has excellent environmental and economic viability. Similarly, Fei et al. prepared a DES solvent by mixing a certain molar ratio of betaine, ethylene glycol lithium, and urea.<sup>[110]</sup> By controlling temperature variables, spent LCO was successfully regenerated at 80 °C and normal pressure conditions, reaching an initial discharge capacity of 209 mAh g<sup>-1</sup> at a high voltage of 4.6 V.

### 3.1.4. Molten Salt Recycling for LCO

Due to the large reactant contact area and fast ion diffusion rate, the molten salt assisted recycling method has attracted significant attention from researchers. Molten salts with low melting points and high Li content provide a stable and uniform liquid

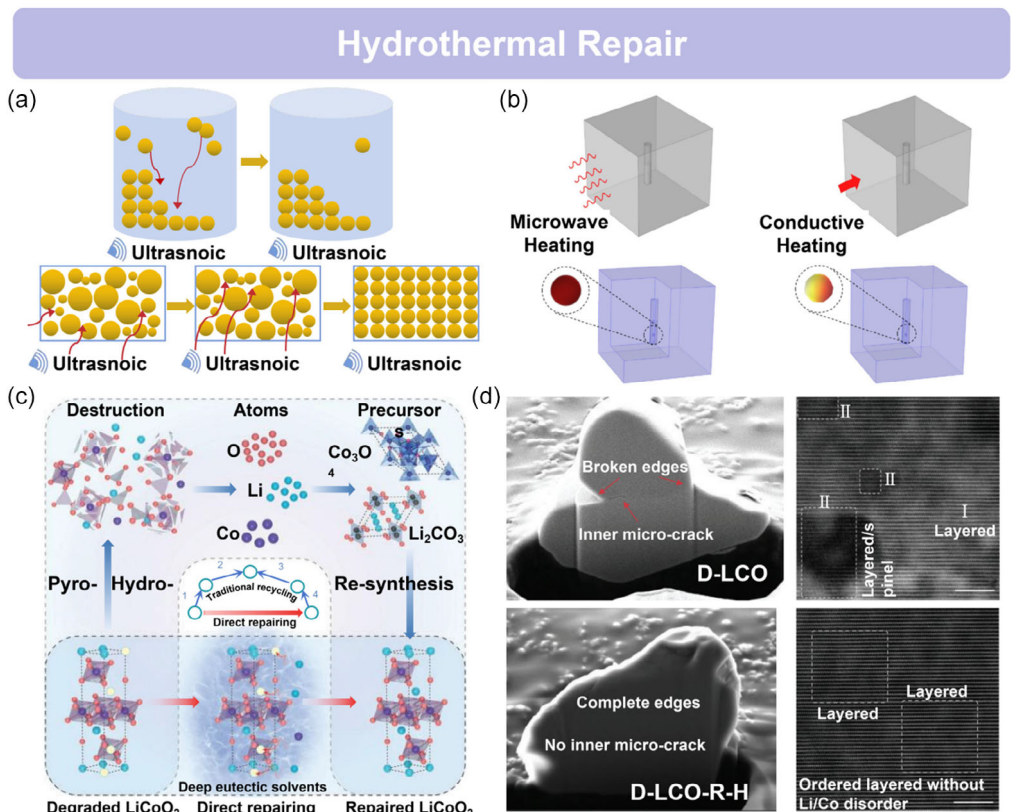


**Figure 5.** Ultrasonic/microwave-assisted hydrothermal repair and deep eutectic solvent (DES) recycling for spent LCO. a) Schematic of LCO crystal structure and particle size evolution under ultrasonic-assisted hydrothermal repair. b) Temperature distribution in LCO particles during microwave heating vs. conductive heating (Reproduced with permission.<sup>[107]</sup> Copyright 2022, Elsevier). c) Process flow comparison: conventional recycling vs. DES-based recycling for LCO and d) FIB-SEM and HRTEM characterization of LCO before and after DES regeneration (Reproduced with permission.<sup>[108]</sup> Copyright 2022, The Authors).

environment for material dissolution and crystal growth. Based on this, Yang et al. used a LiOH-KOH-Li<sub>2</sub>CO<sub>3</sub> molten salt to repair spent LCO materials in a molten environment (Figure 6a).<sup>[111,112]</sup> After recycling, the reversible capacity of LCO increased from 68.3 to 144.5 mAh g<sup>-1</sup>, reaching the theoretical capacity of LCO. Meanwhile, they also found that the alkaline environment with high solubility effectively removed impurities. In another research team, Yang et al. used three different eutectic molten salt systems (LiOH-KCl, LiOH-KOH, and Li<sub>2</sub>CO<sub>3</sub>-K<sub>2</sub>CO<sub>3</sub>) to regenerate spent LCO, discovering the significant impact of various molar ratios and different salt compositions on the direct recycling.<sup>[112]</sup> Additionally, by adding conductive agents, PVDF, and other impurities to the spent LCO, they observed that graphite and carbon black had a severe impact on the morphology of LCO, while PVDF had a smaller effect (Figure 6b). However, traditional molten salt methods always face the issue of uneven particle size and incomplete structural repairing. To address these problems, Gao et al. found that adding trace amounts of CaO to LiNO<sub>3</sub>-KCl molten salt could influence cathode regeneration by adjusting the growth kinetics of LCO.<sup>[113]</sup> The uniform occupation of Li sites by Ca<sup>2+</sup> also helped maintain the structural stability of LCO (Figure 6c). SEM images showed that the surface of LCO using only molten salts still formed substantial scratches and uneven aggregates; in contrast, LCO after doping with Ca<sup>2+</sup> presented a smooth surface and

homogeneous particle size (Figure 6d). Furthermore, the low cost of Ca<sup>2+</sup> also brought economic and performance advantages to this strategy.

### 3.1.5. Chemical Relithiation for LCO

Accurately measuring the Li content of materials to control the usage of Li salt for recycling in high throughput is extremely difficult and expensive. Due to the high price fluctuations of lithium salts, excessive use of lithium salts is negative for cost control. Chemical relithiation based on redox systems has a “self-terminating” lithium supplementation process, which eliminates the need for precise quantification of lithium content in recycling. For example, Zhao et al. used a redox system composed of C<sub>2</sub>H<sub>5</sub>LiO and O<sub>2</sub> to regenerate spent LCO by adding it to the C<sub>2</sub>H<sub>5</sub>LiO solution and stirring under oxygen.<sup>[114]</sup> The regeneration process was operated at room temperature and normal pressure without high-temperature sintering, which is consistent with the environmental, green, and sustainable recycling concept. In addition, Fei et al. successfully developed an autoxidative process to repair spent LCO.<sup>[115]</sup> By adding LiBr as a lithium source and dimethyl sulfoxide (DMSO) as a solvent and oxygen donor, an autoxidative relithiation process was achieved at low temperature and normal pressure. On this basis, Xu et al. explored further

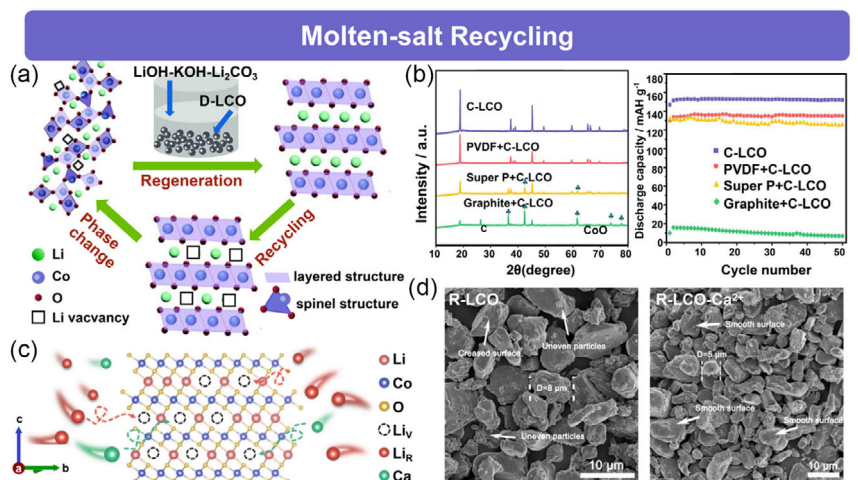


**Figure 6.** Simultaneous elements replenishment and doping in a molten environment for spent LCO recycling and upcycling. a) Schematic of structural evolution during LCO failure and molten salt recycling (Reproduced with permission.<sup>[111]</sup> Copyright 2020, Royal Society of Chemistry). b) XRD patterns and cycling performance at 0.2 C rate for impurity-containing LCO samples in LiOH-KOH molten salt (Reproduced with permission.<sup>[112]</sup> Copyright 2021, Elsevier). c) Intercalation mechanism of  $\text{Ca}^{2+}$  into lithium vacancies in LCO crystal lattice and d) SEM images of LCO repaired with  $\text{LiNO}_3\text{-KCl}$  molten salt and  $\text{Ca}^{2+}$  doped co-modification (Reproduced with permission.<sup>[113]</sup> Copyright 2024, Elsevier).

developments, achieving the regeneration of spent LCO cathodes via 9-fluorenone-mediated Li supplementation and subsequent structural repair (Figure 7a).<sup>[116]</sup> Due to the “redox-potential matching principle,” the relithiation reaction will spontaneously stop once all Li vacancies in spent LCO are filled, thus avoiding precise quantification of Li content in the solution. After Li supplementation (R-FL-LCO), annealing was conducted to obtain R-FL-LCO-ht. As shown in XRD, spinel phases were not completely eliminated in R-FL-LCO due to slight Co loss in the lattice (Figure 7b). Therefore, Co source ( $\text{Co}_3\text{O}_4$ ) was added during the annealing step, resulting in a well-ordered and uniform lattice structure of LCO.

### 3.1.6. Other Methods for LCO

Similarly, electrochemical relithiation for LCO materials also did not require quantification of lithium deficiency before the recovery process. For example, Yang et al. achieved electrochemical relithiation for LCO in lithium-containing solutions by using spent LCO electrode or powder as the working electrode, Ag/AgCl as the reference electrode, and a Pt mesh or pristine LCO as the counter electrode.<sup>[117]</sup> Zhang et al. used a constant current to insert  $\text{Li}^+$  into the spent LCO successfully.<sup>[118]</sup> During the process, they also found that the time to reach complete relithiation could be shortened with increasing Li concentration in the solution or higher current density. Therefore, the regeneration system with spontaneous stopping of the lithiation reaction eliminates the need for precise lithium content in the reagent, avoiding the risk of over-lithiation. The advantages are important for the large-scale recycling of spent batteries at different levels of degradation.

Proven effective direct recycling methods generally require high-temperature sintering or annealing steps to repair the crystal structure of cathode materials. Therefore, to achieve

high energy and time efficiency in regeneration, Yin et al. proposed a nondestructive ultra-fast method to regenerate spent LCO in just eight seconds (Figure 7c).<sup>[119]</sup> Compared with traditional solid-phase recycling, the ultra-fast repair used rapid Joule heating with a fast heating rate and adjustable temperature, minimizing Li loss at high temperatures, which offered significant advantages in terms of energy and time efficiency. The method provided effective evidence for exploring ultra-fast high-temperature regeneration of spent LIBs, opening up a new feasible path.

While the LIB industry is actively working to reduce the usage of Co, it must be acknowledged that Co plays a crucial role in various applications, particularly in catalysis. The production of LCO and other Co-containing battery materials currently accounts for over 70% of global cobalt resource consumption. Therefore, recycling Co resources for other applications can reduce the demand for additional Co mining and refining. Researchers are focusing on developing various potential applications for cathode materials from spent LIBs. For instance, Liu et al. explored integrated cobalt single-site catalysts (Co-ssc) with strong photothermal conversion, high catalytic activity, and stability, efficiently catalyzing the glycolysis of polyesters (PET).<sup>[120]</sup> The method proves the feasibility of Co-ssc for large-scale plastic recycling (Figure 7d). Lou et al. converted spent LCO cathodes into photothermal catalysts for PET upcycling, turning them into high-value monomers.<sup>[121]</sup> To simulate spent LCO cathode materials, the original LCO was charged under different cutoff voltages to achieve various degrees of delithiation. As shown in Figure 7e, the catalytic activity was found to be closely related to the degree of cathode material lithiation. By combining spent LIBs recovery with environmental waste management, these methods confirmed the great potential of multifaceted and efficient recovery of spent LCO.

When the layered structure of LCO degrades to a spinel structure, it represents material failure. However, it is the opposite in

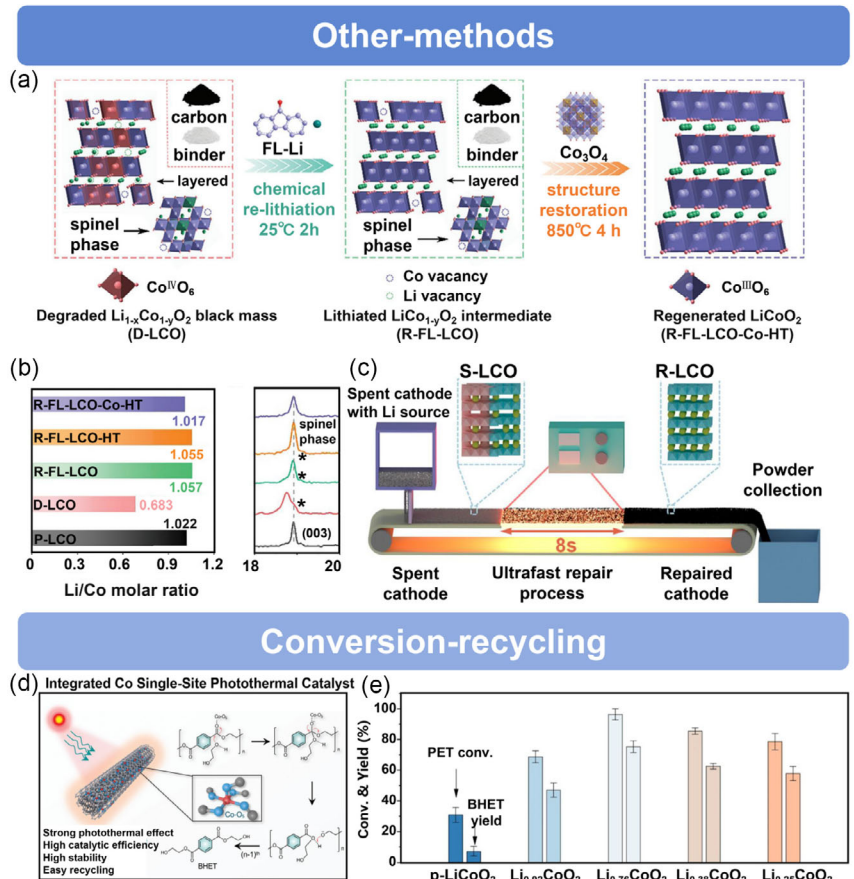


**Figure 7.** Efficient chemical lithiation, electrode-level ultrafast repair, and value-added transformation strategies of spent LCO for plastic recycling.  
 a) Schematic of LCO regeneration combining fluorenone-mediated chemical lithiation with cobalt-phase structural restoration and b) Li/Co molar ratios (ICP-AES) and spinel-phase XRD patterns of LCO under different regeneration conditions (Reproduced with permission.<sup>[116]</sup> Copyright 2024, Wiley-VCH).  
 c) Schematic of roll-to-roll regeneration for LCO via ultrafast repair (Reproduced with permission.<sup>[119]</sup> Copyright 2023, American Chemical Society).  
 d) Integrated functionality of Co-SSCs and photothermal catalytic mechanism in PET glycolysis (Reproduced with permission.<sup>[283]</sup> Copyright 2022, Wiley-VCH). e) PET glycolysis conversion rate and BHET yield with LCO at varying lithiation degrees (Reproduced with permission.<sup>[121]</sup> Copyright 2024, The Authors).

catalysis, and the spinel structure shows higher catalytic activity in the oxygen evolution reaction (OER) compared with other structures. Based on this, Chen et al. found that as the number of cycles increased, the surface structure of LCO was destroyed, which leads to an increase in the area of the catalyst and in catalytic activity.<sup>[122]</sup> Similarly, Huang et al. exfoliated the spent LCO into ultra-thin CoOOH nanosheets, which provided more electrochemical catalytic sites.<sup>[123]</sup> In addition, spent LCO has shown potential for application in battery-related catalysts. For example, Liu et al. applied spent LCO on the separator of lithium-sulfur batteries to improve cycling performance and multiplicity performance.<sup>[120]</sup> Yang et al. converted spent LCO into nano-sized Co<sub>3</sub>O<sub>4</sub> as a cathode for zinc-air batteries, which opened up the possibility of spent LCO materials in advanced metal-air batteries.<sup>[124]</sup> As spent LIBs are diverse, the conversion regeneration method also provides new ideas and possibilities for exploring regeneration methods for LiFePO<sub>4</sub> (LFP) and NCM.

The direct recycling of spent LCO aims to restore its electrochemical performance through relithiation and structural reconstruction. Various repair methods exhibit significant

differences in mechanisms, applicability, and efficiency. The solid-state method, based on high-temperature sintering, enabled effective bulk structural recovery and elemental doping.<sup>[104]</sup> However, it was energy-intensive and sensitive to the amount of lithium source, which required precise control. The hydrothermal repair achieved mild recovery based on liquid-phase ion transport, but often required an additional annealing step to compensate for insufficient repair of microscopic defects.<sup>[87]</sup> The molten salt method exhibited high ionic conductivity and uniform mass transfer, achieving relithiation and the removal of electrode impurities.<sup>[113]</sup> However, the design of molten salt composition must consider the introduction of impurities. Electrochemical and chemical lithiation methods relied on redox potential regulation to achieve self-limiting and selective lithium compensation, avoiding high-temperature side reactions.<sup>[114]</sup> Therefore, future development of LCO direct recycling should focus on low-energy and efficient processes, while remaining compatible with industrial applications, facilitating the transition of direct recycling from laboratory research to large-scale implementation.

### 3.2. Direct Recycling Methods of Layer Ternary $\text{LiNi}_x\text{Co}_y\text{Mn}_{1-x-y}\text{O}_2$ Cathode Materials

NCM is currently the most widely used cathode material in power batteries.<sup>[34]</sup> During the development of cathode materials of LIBs, because of the same layered structure as LCO,  $\text{LiNiO}_2$  and  $\text{LiCoO}_2$  are considered potential substitutes for LCO. However, poor stability limits their widespread application. To address the problem, researchers found that replacing part of the Ni with other metal elements (such as Co, Mn, Al) can improve stability.<sup>[125]</sup> Based on this, various NCM and NCA cathode materials with different ratios have been developed, with NCM being more common. Japanese battery manufacturers began exploring the commercialization of ternary materials in 1999, and these materials were widely used in consumer electronics starting in the 21st century.<sup>[125]</sup> With the growth of the EV market and the advantages of energy density, ternary materials have gradually gained favor from both manufacturers and consumers. To date, ternary materials have captured more than 60% of the market share in EV power batteries.<sup>[126]</sup>

NCM and LCO have similar O3-type structures, so they have identical physical and chemical properties. During the process of charge/discharge, NCM undergoes complex phase transitions like LCO, which leads to structural damage (Figure 8a).<sup>[127,128]</sup> Thereby, the spatial changes caused by phase transitions lead to intracrystalline defects (Figure 8b). During the intercalation and extraction process in cycling, the  $\text{Li}^+$  concentration gradient induces local stress accumulation in the layered structure, forming local dislocations.<sup>[129]</sup> As the number of cycles increases, this

eventually results in severe staircase slippage and rupture of the material (Figure 8c).<sup>[130]</sup> Furthermore, since the ionic radius of  $\text{Ni}^{2+}$  is close to that of  $\text{Li}^+$ , a certain degree of Li/Ni intermixing typically exists in ternary material, especially in materials with a higher Ni content.<sup>[131,132]</sup> This is due to the migration of  $\text{Ni}^{2+}$  to the Li vacancy after  $\text{Li}^+$  is removed from the cathode, making the  $\text{Li}^+$  intercalation and extraction process partially irreversible.<sup>[133]</sup> While the impact of moderate Li/Ni intermixing on the performance of ternary materials is debatable, excessive element antisites are the primary reason for the formation of spinel and rock-salt phases (Figure 8d).<sup>[134]</sup> Moreover, oxygen loss from the surface can also lead to a decrease in the valence state of Ni, further exacerbating the Li/Ni antisites and triggering irreversible degradation of electrochemical performance.<sup>[133]</sup> Similar to other materials, side reactions caused by the organic electrolyte form a CEI film at the cathode-electrolyte interface. The process not only consumes available  $\text{Li}^+$  but also leads to the dissolution of transition metals (Mn, Co) after prolonged cycling.<sup>[135–137]</sup> Therefore, in addition to necessary lithium supplementation, the loss of transition metal elements and structural defects must also be considered for ternary materials with higher levels of degradation. The representative cases, the specific regeneration conditions and results of NCM direct recycling and upcycling are summarized in Table 2.

#### 3.2.1. Solid-State Recycling for NCM

For degraded layered materials, the rock-salt phase near the particle surface hinders the reversible insertion of Li, thereby

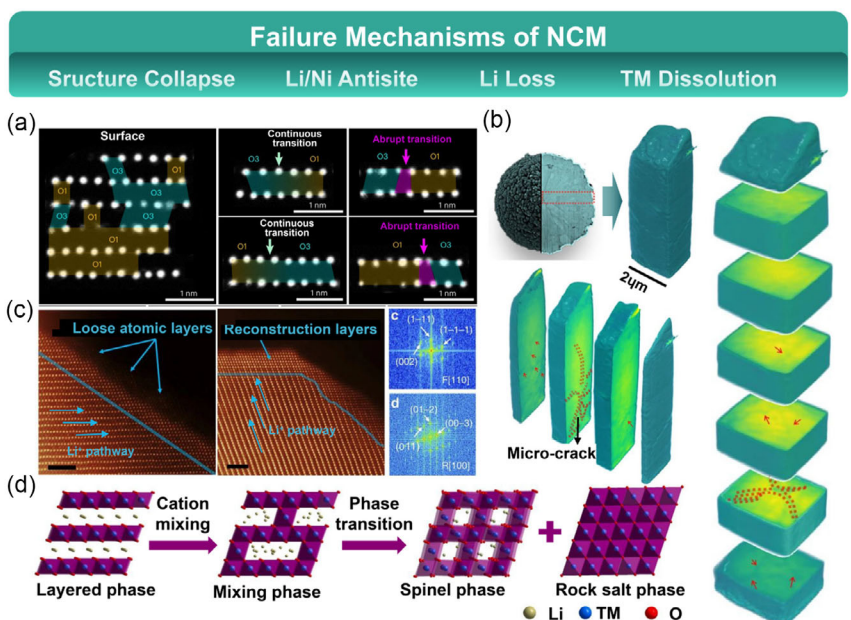


**Figure 8.** Multiscale failure mechanisms of NCM cathodes involving surface phase transition, microcrack propagation, and cation disorder-induced structural degradation. a) Coexisting O1 and O3 phases on NCM particle surfaces with abrupt O1-O3 interfacial transition zones (Reproduced with permission.<sup>[284]</sup> Copyright 2023, Springer Nature). b) 3D X-ray tomography of cycled secondary particles (left-right and top-bottom cross-sections) revealing microcrack propagation pathways (Reproduced with permission.<sup>[285]</sup> Copyright 2021, The Authors). c) FFT patterns of NCM bulk layered structure (R-3m) and surface reconstruction layer (Fm-3m) (Reproduced with permission.<sup>[286]</sup> Copyright 2014, Springer Nature). d) Failure mechanism schematic of NCM523 showing phase transition induced by cation mixing (Reproduced with permission.<sup>[287]</sup> Copyright 2021, Elsevier).

**Tabel 2.** Summary of typical cases for the direct recycling and upcycling of NCM.

Cathode	Repair method	Key conditional	Initial capacity [mAh g <sup>-1</sup> ]	Capacity retention	References
NCM	Solid-phase recycling	Intensive ball milling; sintered with LiOH-H <sub>2</sub> O 500 °C 2 h, 800 °C 16 h	174.3 [0.1C, 3.0–4.3 V]	90% [200 cycle]	[140]
NCM111	Solid-phase recycling	Solid-state sintered 450 °C; 500 °C for 2 h, (800–900 °C) for 12 h	169.7 [0.1C, 2.8–4.3 V]	86.9% [200 cycle]	[142]
NCM	Solid-phase recycling	Ultrasonic washing with HNO <sub>3</sub> ; solid-state sintered with Li <sub>2</sub> CO <sub>3</sub> 850 °C for 10 h	171.4 [0.1C, 2.8–4.4 V]	82.1% [200 cycle]	[289]
NCM111	Solid-phase recycling	Annealing with LiOH	Close to the original material	Close to the original material	[144]
NCM523	Solid-phase recycling	Intensive ball milling with TM(OH) <sub>2</sub> , LiOH for 20 min; solid-state sintered 500 °C for 5 h, 900 °C for 2 h	>145 [0.5C, 2.5–4.3 V]	95.7% [100 cycle]	[145]
NCM523	Hydrothermal repair	Hydrothermal treatment with LiOH 220°C for 4 h; annealing with Li <sub>2</sub> CO <sub>3</sub> 850 °C for 4 h	≈160 [1C, 3.0–4.3 V]	80.2% [100 cycle]	[146]
NCM111	Hydrothermal repair	Hydrothermal treatment with LiOH 220 °C for 4 h; annealing with Li <sub>2</sub> CO <sub>3</sub> 850 °C for 4 h	158.4 [1C, 3.0–4.3 V]	80.0% [100 cycle]	[146]
NCM111	Hydrothermal repair	Hydrothermal treatment with LiOH 220 °C for 4 h; annealing with Li <sub>2</sub> CO <sub>3</sub> 850 °C for 4 h	155.0 [0.1C, 3.0–4.3 V]	98% [100 cycle]	[147]
NCM622	Hydrothermal repair	Hydrothermal treatment with LiOH 220 °C for 4 h; annealing with Li <sub>2</sub> CO <sub>3</sub> 850 °C for 4 h	176.0 [0.1C, 3.0–4.3 V]	94% [200 cycle]	[147]
NCM523	Hydrothermal repair	Hydrothermal treatment with LiOH 220 °C for (1–3 h); annealing with LiOH 600 °C for 4 h, 810 °C for 6 h	166.1 [0.1C, 2.8–4.35 V]	90.8% [500 cycle]	[149]
NCM523	Hydrothermal repair	–	150.5 [1C, 3.0–4.2 V]	94.25% [500 cycle]	[149]
NCM111	Hydrothermal repair	–	NA	>90% [500 cycle]	[149]
NCM111	Hydrothermal repair	Hydrothermal treatment with LiOH 220 °C for 4 h; annealing with Li <sub>2</sub> CO <sub>3</sub> 850 °C for 4 h	155.0 [C/10, 3–4.3 V]	98% [100 cycle]	[148]
NCM622	Hydrothermal repair	Hydrothermal treatment with LiOH 220°C for 4 h; annealing with Li <sub>2</sub> CO <sub>3</sub> 850 °C for 4 h	176.0 [0.1C, 3.0–4.3 V]	94% [200 cycle]	[148]
NCM111	Hydrothermal repair	Hydrothermal treatment with LiOH + KOH 160–220 °C for 1–6 h; annealing with Li <sub>2</sub> CO <sub>3</sub> or LiOH	156.4 [0.1C, 3.0–4.3 V]	93.1% [50 cycle]	[150]
NCM622	Hydrothermal repair	Hydrothermal treatment with LiOH; annealing with H <sub>3</sub> BO <sub>3</sub> , 300 °C for 5 h 850 °C	177.0 [0.1C, 3.0–4.2 V]	92.3% [100 cycle]	[152]
NCM111	Hydrothermal repair	Hydrothermal treatment with LiOH; annealing with H <sub>3</sub> BO <sub>3</sub> , 300 °C for 5 h 850 °C	147.7 [0.1C, 3.0–4.2 V]	82.7% [100 cycle]	[152]
NCM523	Hydrothermal repair	Water washing; hydrothermal treatment 220 °C 4 h; annealing with Li <sub>2</sub> CO <sub>3</sub> 850 °C 4 h	163.09 [0.1C, 3–4.3 V]	92.69% [50 cycle]	[153]
NCM523	Hydrothermal repair	Hydrothermal treatment with NH <sub>4</sub> OH 180 °C for 6 h; annealing with LiOH, 500 °C for 2 h, 850 °C for 10 h	152.0 [0.5C, 2.5–4.3 V]	90% [100 cycle]	[154]
NCM523		–	155.0 [0.5C, 2.5–4.3 V]	92.5% [100 cycle]	[154]
NCM622		–	167.0 [0.5C, 2.5–4.3 V]	90% [100 cycle]	[154]
NCM622	Upcycling	Hydrothermal treatment with LiOH, TBT, EG, 140 °C for 8 h; annealing with LiOH, 800 °C for 4 h	183.0 [0.1C, 2.7–4.3 V]	79.3% [200 cycle]	[155]
NCM523	Molten salt	Sintered with LiOH-Li <sub>2</sub> CO <sub>3</sub> molten salt 440 °C for 5 h, 850 °C for 12 h	146.3 [1C, 2.8–4.3 V]	89.6% [200 cycle]	[156]
NCM523	Molten salt	Sintered with Li <sub>1</sub> -LiOH molten salt, Co <sub>2</sub> O <sub>3</sub> , MnO <sub>2</sub> , 200 °C for 4 h, 850 °C for 5 h	≈170 [0.1C, 2.5–4.3 V]	>80% [200 cycle]	[157]
NCM523	Molten salt	Sintered with LiOH-H <sub>2</sub> O-LiNO <sub>3</sub> -CCL-2H <sub>2</sub> O 400 °C for 4 h; annealing with Li <sub>2</sub> CO <sub>3</sub> , 850 °C 6 h	160.0 [0.5C, 3.0–4.3 V]	93.7% [100 cycle]	[158]
NCM	Molten salt	Sintered with LiOH-H <sub>2</sub> O-Na <sub>2</sub> SO <sub>4</sub> 900 °C for 15 h; annealing 850 °C for 10 h	153.2 [1C, 3.0–4.3 V]	89.5% [300 cycle]	[160]
NCM523	Upcycling	Sintered with LiOH-H <sub>2</sub> O-NaCl 850–900 °C for 15–20 h; annealing 800 °C for 10 h with LiOH	180.1 [1C, 3.0–4.3 V]	86.5% [200 cycle]	[161]

**Table 2.** Continued.

Cathode	Repair method	Key conditional	Initial capacity [mAh g <sup>-1</sup> ]	Capacity retention	References
NCM523	Upcycling	Sintered with LiNO <sub>3</sub> -LiOH, Al particle 300 °C for 4 h; annealing 800 °C for 8 h with LiOH	158.6 [0.1C, 2.8–4.3 V]	89.6% [200 cycle]	[162]
NCM83 NCM523 NCM622	Upcycling	Sintered with NaCl-KCl-LiOH, Al particle, Cu(OH) <sub>2</sub> , 500 °C for 3 h + 850 °C for 8 h; annealing 720 °C for 5 h	215.0 [0.1C, 2.6–4.6 V] ≈ 160 [0.1C, 2.6–4.5 V] ≈ 170 [0.1C, 2.6–4.5 V]	93.3% [100 cycle] 94.8% [100 cycle] 94.8% [100 cycle]	[163]
NCM523	Upcycling	Sintered with LiOH-LiNO <sub>3</sub> , LiC <sub>7</sub> H <sub>5</sub> O <sub>2</sub> , 300 °C for 4 h	150.0 [0.5C, 2.5–4.3 V]	70% [700 cycle]	[164]
NCM111	Redox mediation	Reacts with DTBQ, Li 10–60min; annealing 850 °C for 4 h	170.6 [1.0C, 3.0–4.3 C]	NA	[165]
Battery	Other method	Injection of Li-Naph for constant voltage (CV) treatment with disassembly	Close to initial capacity	80% [100 cycle]	[169]

NA: not available.

obstructing the complete compensation of Li and the effective repair of spent NCM. Based on the solid-phase synthesis process of NCM materials, solid-phase recycling of spent NCM mixed with a lithium source and sintered, which may achieve a certain degree of repairing of the spent NCM. During the solid-state recycling, a moderate excess of lithium salts is typically required to ensure full lithium compensation. For example, Li et al. supplemented lithium according to different stoichiometries to explore the effect of different Li contents on the performance of regenerated NCM.<sup>[138]</sup> Fan et al. used LiOH to successfully repair the spent NCM cathode.<sup>[139]</sup> To improve the efficient use of lithium salts, Jin et al. divided the solid-state recycling process into two steps: mechanical prelithiation and high-temperature calcination (**Figure 9a**).<sup>[140]</sup> As shown in Figure 9b,c, the simultaneous presence of adjacent lithium-oxygen vacancies favored the adsorption of LiOH. So the ball milling process is employed to induce oxygen vacancies on the NCM surface, facilitating the adsorption of Li and improving the pre-lithiation efficiency. Similarly, Han et al. performed a ball-milling activation treatment in solid-phase sintering to facilitate subsequent regeneration.<sup>[141]</sup> In fact, the surface of degraded or stored NCM materials is typically covered with side reaction products composed of lithium. And most of these impurities have also been proven to be Li<sub>2</sub>CO<sub>3</sub>, which can be used as a lithium source during repairing. For instance, Chi et al. successfully regenerated spent NCM cathodes without an external lithium source, enabling efficient reuse of the lithium-containing products on the materials' surface (**Figure 9d**).<sup>[142]</sup>

Before recycling, spent batteries are usually separated and crushed to obtain their final form—black mass (BM). Compared with the whole battery, BM is easier and safer to transport, avoiding thermal runaway. Thus, BM is the most common form of material in battery recycling. However, BM may contain impurities, such as current collector fragments and residual interface reaction products. Guo et al. found that the residual impurities mainly come from the electrolyte rather than the binder.<sup>[143]</sup> By minute-scale washing to selectively remove these impurities

through using HNO<sub>3</sub>, the spent NCM was regenerated by simple solid-state recycling. The strategy highlights impurity levels often overlooked in laboratory-scale recycling and offers a feasible solution. Similarly, Ross and others considered the impact of F on cathode materials when removing PVDF, thereby using an excess of LiOH-H<sub>2</sub>O to react with fluoride and prevent lithium removal, and fluoride doping of the cathode in the process.<sup>[144]</sup> Due to lithium-oxygen loss on the surface and side reactions at the CEI, layered structures are continuously degrading into spinel and rock salt phases, hindering lithium diffusion. To convert the surface rock-salt phase into a layered structure with fast migration pathways for lithium ions, creating an oxidative environment is crucial. However, common cheap oxidants like O<sub>2</sub> lead to slow and incomplete oxidation. Therefore, Zheng et al. introduced polycrystalline Ni<sub>0.5</sub>Co<sub>0.2</sub>Mn<sub>0.3</sub>(OH)<sub>2</sub> [TM(OH)<sub>2</sub>, TM: transition metal] as a surface catalyst and simple solid-state sintering to eliminate the rock-salt phase on the SNCM surface and perform overall structural repair.<sup>[145]</sup> During recycling, the catalyst TM(OH)<sub>2</sub> (primarily Ni(OH)<sub>2</sub>) forms an active reaction zone on the material surface, where oxygen vacancies generated by dehydration at high temperatures help activate the redox process, triggering the formation of reactive oxygen species. The O 1s XPS patterns show that under thermodynamic driving forces, the formation of reactive oxygen facilitates the transition from rock-salt NiO to layered NiOOH and Ni(OH)<sub>2</sub> eventually (**Figure 9e**). In the rate-determining step, the energy barrier decreases from 3.99 to 3.38 eV (**Figure 9f**). Surface catalytic repair promotes the reformation of layered structures by introducing highly reactive reaction sites and reactive oxygen species, thereby rapidly establishing lithium ion diffusion pathways (**Figure 9g**).

### 3.2.2. Hydrothermal Repair for NCM

Hydrothermal repair has been proven to effectively recycle various types of spent cathode materials. Compared with solid-state recycling, hydrothermal repair offers broader applicability. In

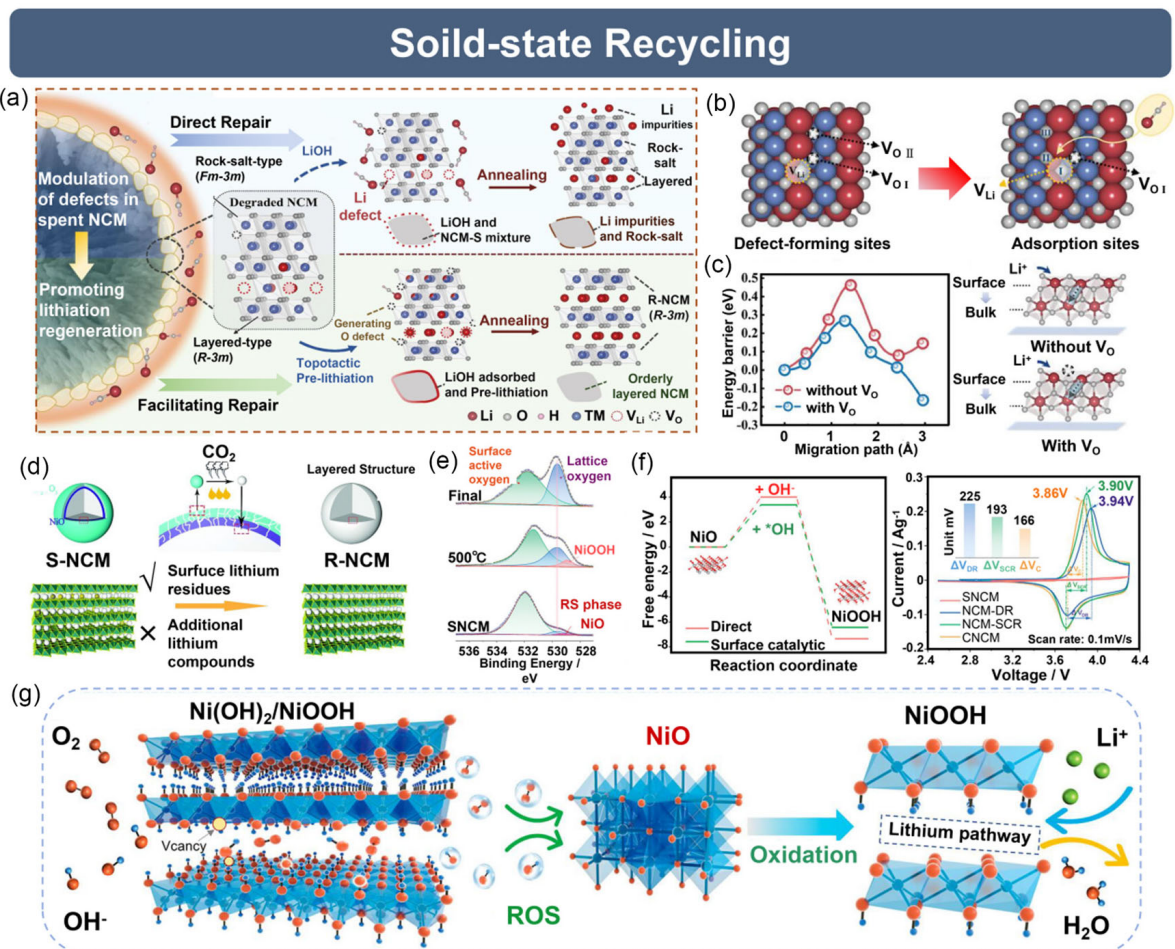


**Figure 9.** Advanced solid state recycling strategies for NCM via surface defect engineering and catalytic processes. a) Schematic of promoting relithiation regeneration through regulation of surface defects in NCM and direct high-temperature regeneration and b) top view of non-adjacent lithium-oxygen vacancies and adjacent lithium-oxygen vacancies in NCM structure and c) diffusion energy barriers and schematic of lithium-ion diffusion from surface to bulk structure with/without oxygen vacancies (Reproduced with permission.<sup>[140]</sup> Copyright 2024, Wiley-VCH). d) Schematic of NCM regeneration process without external lithium source (Reproduced with permission.<sup>[142]</sup> Copyright 2021, Royal Society of Chemistry). e) O 1s XPS spectra of samples at different stages during TM(OH)<sub>2</sub> surface catalyst-assisted regeneration and f) free energy of rate-determining steps and initial cyclic voltammetry (CV) curves at 0.1 mV s<sup>-1</sup> scan rate during regeneration processes with/without TM(OH)<sub>2</sub> surface catalyst assistance and g) schematic of Ni(OH)<sub>2</sub> surface catalyst enabling oxidative regeneration through adsorption of O<sub>2</sub> and OH<sup>-</sup> on NCM impurity phases and reactive oxygen species release (Reproduced with permission.<sup>[145]</sup> Copyright 2024, American Chemical Society).

addition to milder reaction conditions and lower energy consumption, researchers have found that direct solid-state sintering in air gets good regeneration results only for NCM111 with lower nickel content, and does not fully restore NCM523 and NCM622. That's because the latter has higher nickel content and requires an increase in oxygen partial pressure during regeneration to restore high-nickel NCM effectively. Therefore, Shi et al. added degraded NCM into LiOH solution for hydrothermal repair, followed by short annealing steps to address the inherent limitations of the hydrothermal process.<sup>[146]</sup> This strategy achieved the complete restoration of the degraded NCM materials for the first time. After LiOH successfully repaired the NCM via water-based treatment (validated by teams such as Kwak et al. and Guo et al.),<sup>[147-149]</sup> Gupta et al. extended the use of LiOH solution for repair to the BM level, demonstrating the industrial applicability of this strategy (Figure 10a).<sup>[148]</sup> Based on this, Xu et al. optimized the experimental procedure by replacing

the commonly used 4 M LiOH solution with a cost-effective mixture of 0.1 M LiOH and 3.9 M KOH, minimizing energy and raw materials costs.<sup>[150]</sup> In the hydrothermal process, the high temperature and pressure conditions are major problems for its scaling. Therefore, Yu et al. reduced the regeneration temperature from 220 to 100 °C and the pressure from 26 bar to 1 bar, by using low-cost ethanol, H<sub>2</sub>O<sub>2</sub>, and ethylene glycol as redox mediators (Figure 10b).<sup>[151]</sup> The approach offered high economic efficiency and safety (Figure 10c).

Generally, the impurity residue level and air interface stability risks of NCM after hydrothermal treatment are high. This is because the spent cathode must be fully immersed in the lithium solution during relithiation. Therefore, removing surface alkaline contaminants is critical for fully restoring electrochemical performance. Typically, the operation is achieved through complex washing steps, not only generating significant wastewater, but also exacerbating the instability of the material through excessive

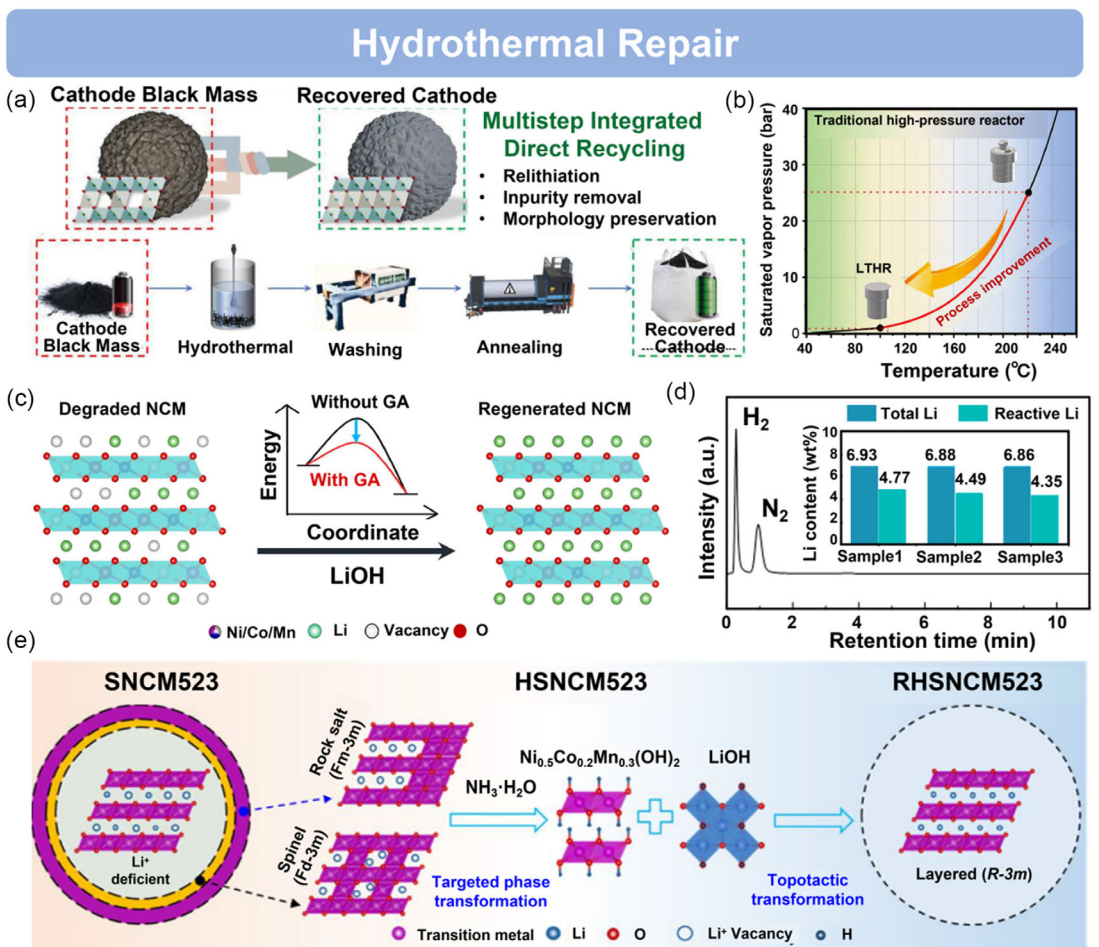


**Figure 10.** Advanced hydrothermal repair techniques: scalable method, anode lithium extraction for cathode, and topological phase conversion for NCM recycling. a) Schematic of a scalable hydrothermal repair method integrating multistep for BM (Reproduced with permission.<sup>[148]</sup> Copyright 2022, Wiley-VCH). b) Schematic of reduced-pressure reaction at 100 °C (conventional 220 °C high-pressure conditions) enabled by redox mediator addition under hydrothermal process, and c) schematic of degraded NCM materials regeneration with/without redox mediators (Reproduced with permission.<sup>[151]</sup> Copyright 2022, Elsevier). d) Quantitative characterization of total lithium content and active lithium content in spent graphite through GC chromatographic analysis of gases generated by water immersion (Reproduced with permission.<sup>[153]</sup> Copyright 2024, Elsevier). e) Schematic of direct recycling method converting impurity phases to layered phases via topological structural transformation in NCM523 (Reproduced with permission.<sup>[154]</sup> Copyright 2023, American Chemical Society).

or insufficient washing. Based on this, Yu et al. proposed to couple a multifunctional scavenging material into hydrothermal relithiation (SAHR).<sup>[152]</sup> The strategy can remove lithium salts remaining on the surface, simultaneously forming a fast Li<sup>+</sup> conductive LiBO<sub>2</sub> (LBO) and successfully improving the stability of the regenerated cathode in air. The use of additional lithium sources leads to higher overall recovery costs. To address the problem, releasing active lithium ions trapped in the anode can be used as a lithium source for recycling cathodes. For example, Liu et al. used a lithium-rich solution for hydrothermal repair of spent cathodes, whereas the lithium source was derived from spent anode graphite.<sup>[153]</sup> TGC (thermogravimetric-gas chromatography) quantification revealed that ≈65% of the residual lithium could react with water for subsequent cathode regeneration (Figure 10d). Li<sup>+</sup> lost from the cathode is reintroduced into the cathode, eliminating the need for an additional lithium source and avoiding the introduction of impurity. Therefore, the method

effectively reduces recycling costs and the environmental impact associated with raw materials.

In contrast to the above repair processes, Jia et al. provided a unique perspective.<sup>[154]</sup> The rock-salt phase/spinell phase was converted to the layered phase Ni<sub>0.5</sub>Co<sub>0.2</sub>Mn<sub>0.3</sub>(OH)<sub>2</sub> by pretreating the spent NCM with NH<sub>4</sub>OH. The regenerated NCM (RNCM) was obtained by replenishing lithium by mixing it with lithium salt. The method was demonstrated to be successfully extendable to NCM622, LCO, and BM-NCM523 (Figure 10e). Recent studies on high-nickel materials have shown that coating is a simple and effective method to enhance electrochemical performance. A typical Li<sub>4</sub>Ti<sub>5</sub>O<sub>12</sub> (LTO) coating has been extensively reported as an effective functional coating for layered oxide materials. The LTO coating improves the Li diffusion kinetics and forms a barrier between the layered material and the electrolyte to prevent direct contact. Based on this, Chen et al. introduced Li<sup>+</sup> and Ti<sup>4+</sup> ions during a hydrothermal process to achieve both lithium

replenishment and LTO coating.<sup>[155]</sup> A thin and uniform LTO coating significantly enhanced the electrochemical performance of NCM. Similarly, Guo et al. also formed an in situ coated LiF film on the surface of spent NCM, which successfully enhanced the cycling stability of the cathode material.<sup>[149]</sup>

### 3.2.3. Molten Salt Recycling for NCM

Molten salt mixtures exhibit suitable solubility, a uniform thermal environment, abundant  $\text{Li}^+$ , and high ionic diffusion rates. These advantages help to enable impurity decomposition and  $\text{Li}^+$  supplementation via a “dissolution-recrystallization” mechanism, repairing damaged structures. For example, Jiang et al. found that the  $\text{Li}_2\text{CO}_3\text{-LiOH}$  binary molten salt with a new eutectic melting point (Figure 11a), which can effectively repair spent NCM in the molten state (Figure 11b).<sup>[156]</sup> Compared with a single lithium salt, a binary molten salt lowered the reaction temperature while ensuring performance recovery. In the continued exploration of reducing temperature, Ma et al. made further discoveries by choosing the eutectic lithium salt  $\text{LiLiOH}$  with the lowest

eutectic melting point to provide a lithium-rich environment (Figure 11c).<sup>[157]</sup> Additionally, considering that highly degraded NCM materials may also retain some degree of dissolution of transition metal, they added  $\text{Co}_2\text{O}_3$  and  $\text{MnO}_2$  during regeneration. In addition to binary molten salts, multicomponent molten salts also exhibit excellent lithium supplementation capabilities. For instance, Qin et al. found that eutectic salts with different components have respective eutectic points and regeneration temperatures.<sup>[158]</sup> They also found that the addition of acetate salts to molten salts can lower the melting point to some extent. The team then added lithium acetate to  $\text{LiNO}_3\text{-LiOH}$  and regenerated the spent NCM materials at a moderate temperature (400 °C). In a word, inorganic lithium salts have been proven to have good regeneration effects on spent NCM with a certain integrity of structure. However, for low state of health (SOH) materials, these salts show insufficient repairing ability. Therefore, Liu et al. added organic lithium salicylate (LSA) to the known  $\text{LiOH-LiNO}_3$  molten salt system to regenerate spent NCM.<sup>[159]</sup> XPS spectra showed that after adding LSA, the lattice oxygen ratio in the regenerated material significantly increased

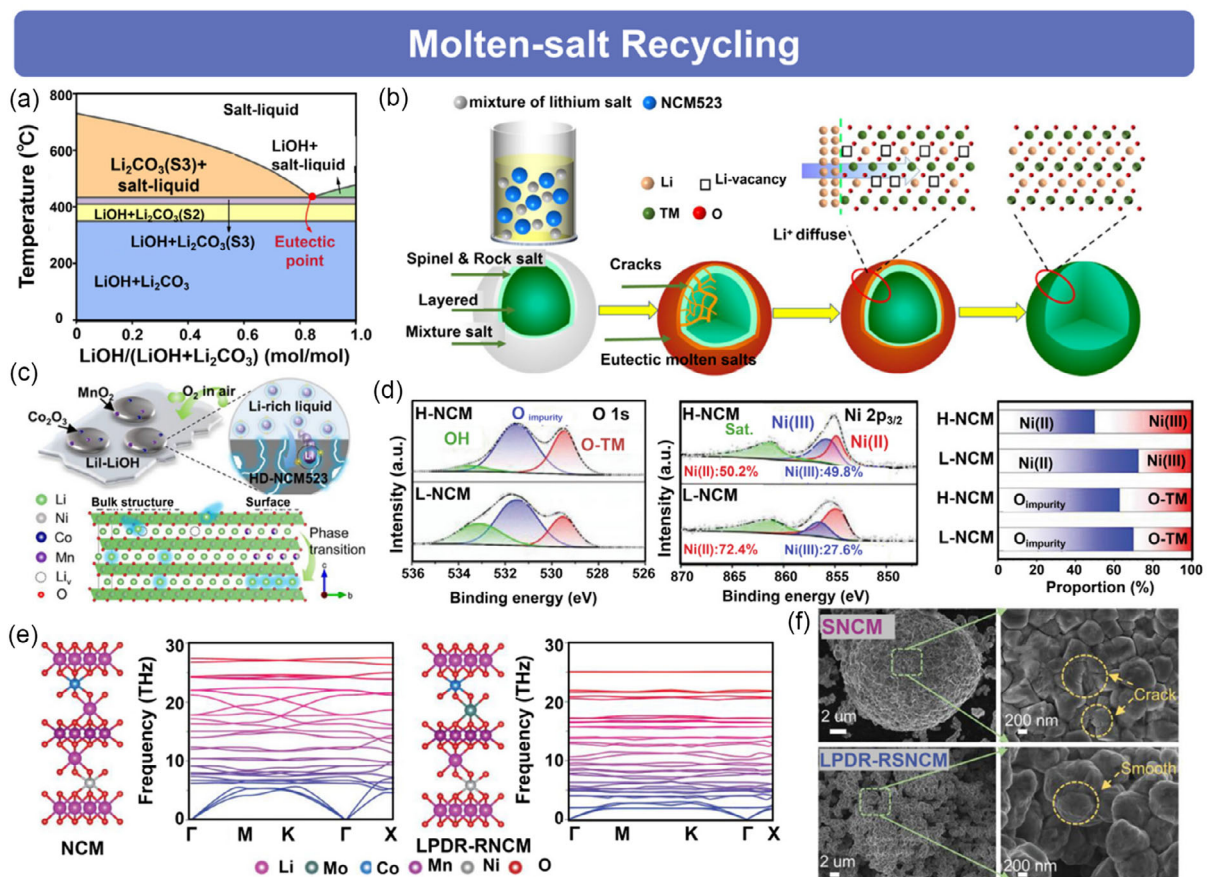


**Figure 11. Molten-salt recycling and elemental doping for efficient repair of degraded NCM.** a) Eutectic point diagram of  $\text{LiOH}$  and  $\text{Li}_2\text{CO}_3$  at different molar ratios, and b) schematic of NCM structure repair and lithium replenishment via eutectic salt method (Reproduced with permission.<sup>[156]</sup> Copyright 2020, American Chemical Society). c) Schematic of repairing severely degraded NCM by adding  $\text{Co}_2\text{O}_3$  and  $\text{MnO}_2$  in the  $\text{LiLiOH}$  eutectic salt system (Reproduced with permission.<sup>[157]</sup> Copyright 2022, American Chemical Society). d) XPS spectra of O 1s and Ni 2p<sub>3/2</sub> before/after molten salt recycling, with Ni and O content ratio variations (Reproduced with permission.<sup>[159]</sup> Copyright 2023, Wiley-VCH). e) Phonon dispersion characteristics of Mo-doped and pristine NCM materials at 300 K, and f) SEM images of NCM particle surfaces before and after Mo-doped regeneration (Reproduced with permission.<sup>[164]</sup> Copyright 2024, Wiley-VCH).

(Figure 11d). The result proved that the oxidative atmosphere provided by LSA at high temperatures reduced Li/Ni disorder, facilitating subsequent regeneration.

Direct upcycling is the future trend of direct recycling. During molten-salt recycling, the improvement of performance can be achieved by reducing particle size, realizing element doping, and other measures. For example, Qin et al. explored the regeneration of failed NCA using a LiOH-Li<sub>2</sub>SO<sub>4</sub> eutectic salt, upcycling the failed material to high-value-added single-crystalline lithium-rich materials.<sup>[160]</sup> This method can also be successfully extended to other cathode materials such as NCM and ternary mixed materials. Currently, solid-state sintering and hydrothermal repair are difficult to apply directly to high-nickel ternary cathodes, which are the most promising development direction for next-generation cathode materials. As the nickel content increases, the capacity decreases, and the structural instability of ternary materials becomes more severe during cycling. These are caused by not only lithium loss, but also oxygen release, Li/TM mixing, and transition metal mixing. These problems interact and promote each other, making direct recycling of high-nickel cathodes difficult. Based on this, Qin et al. combined low-temperature lithium supplementation and high-temperature molten salt transformation to achieve the reconstruction of particle morphology and crystal structure.<sup>[161]</sup> The method regenerated high-nickel NCM to single-crystalline materials with higher structural stability and stronger ability to inhibit oxygen release and crack generation.

In industrial recycling processes, the widely applied solvent-free disassembly methods inevitably introduce Al impurities into the spent NCM. Inspiringly, trace controllable Al doping can stabilize the layered structure of NCM cathode materials. For instance, Xing et al. used Al impurity to repair spent NCM cathodes in a LiNO<sub>3</sub>-LiOH molten salt system.<sup>[162]</sup> Similarly, Ji et al. utilized dual-site doping with Al and Cu to transform spent high-nickel materials into high-voltage 4.6 V cathode materials using a molten salt system.<sup>[163]</sup> The obtained material effectively overcame the challenges of strain accumulation and oxygen release under high voltage. Jia et al. used an organic-inorganic composite molten salt system (LiOH-LiNO<sub>3</sub>-LiC<sub>7</sub>H<sub>5</sub>O<sub>2</sub>) to regenerate spent NCM BM.<sup>[164]</sup> By doping with Mo, they introduced localized lattice stress into the regenerated cathode to construct a new phonon dispersion relation for TM-O covalent bonds, lowering the bending and stretching vibration frequencies of TM-O covalent bonds during cycles (Figure 11e). Before Mo doping, the lattice dispersion relation exhibited dispersive characteristics, with high-frequency lattice vibrations between different wave vectors and a large slope in the phonon spectrum. After Mo doping, the dispersion curve became relatively flatter. The SEM image (Figure 11f) shows that the establishment of the new low-frequency dispersion relation effectively alleviated the collapse of the cathode lattice structure and the formation of surface cracks on the particles.

### 3.2.4. Other Methods for NCM

In addition to the above common repair methods, Park et al. employed a redox medium to repair the spent NCM at room

temperature by adding Li metal into an electrolyte containing 3,5-di-tert-butyl-o-benzoquinone (DTBQ) to prepare the lithiation reagent.<sup>[165]</sup> Due to the inability to efficiently identify the lithium content in spent materials, it is challenging to sort materials for direct recycling during the recovery process. Therefore, Li et al. used TGC for the rapid determination of lithium content and developed an electrochemical lithiation method for direct recycling based on this.<sup>[166]</sup> Adding additional raw materials is the prospect of direct recycling and upcycling. However, Ma et al. took an alternative route and changed the addition strategy for upcycling.<sup>[167]</sup> Instead, they chose to remove some cobalt and nickel from the NCM to obtain a new high-voltage cathode material of Co-doped LNMO. Since Co has an important role in the structural stability of anode materials, it is necessary and reasonable to retain a moderate amount of Co.

Researchers have attempted to utilize natural solar energy to repair spent cathode materials. For example, Wang et al. used concentrated solar radiation to directly repair the electrode by ultra-strong radiation and ultra-high temperature in a short time, which not only provided energy for the regeneration but also inhibited side reactions.<sup>[168]</sup> Concentrated solar radiation combined with photocatalysis and photothermal effects to directly repair the electrode without separating the cathode active material and collector. Ogihara et al. even omitted the step of disassembling the battery to obtain the electrode.<sup>[169]</sup> Through directly injecting lithiation reagents into the battery to restore the capacity, "cell to cell" recycling of spent batteries was achieved. This method is expected to provide the shortest path for battery regeneration. However, the direct injection of lithiation reagents for recycling is only applicable to batteries, which failed due to carrier loss.

The direct recycling of spent NCM materials aims to restore their initial performance through external lithium supplementation and structural reconstruction, with particular emphasis on addressing issues of high-nickel cathodes, such as surface degradation, complex phase transitions, and cation mixing. The solid-phase method relied on high-temperature thermal treatment to achieve bulk-phase lithiation and structural reconstruction by introducing external lithium sources or utilizing inherent lithium-containing impurities (e.g., Li<sub>2</sub>CO<sub>3</sub>). It can also introduce dopants (e.g., Al, Cu) for upcycling to enhance the stability of the layered structure.<sup>[162]</sup> The hydrothermal method facilitated ion transport and relithiation in a liquid-phase environment under mild conditions. It effectively removed residual lithium salts and improves stability in air, avoiding side reactions at high temperatures. Moreover, the introduction of redox mediators in hydrothermal systems was expected to realize recovery under low-temperature and ambient-pressure conditions, significantly reducing energy consumption and equipment requirements.<sup>[151]</sup> The molten salt method achieved uniform and efficient lithium replenishment and impurity removal via a "dissolution-recrystallization" mechanism. And the melting points can be lowered by adjusting molten salt compositions, while introducing doping elements (e.g., Mo, Al-Cu, etc.) to enhance structural and improve performance.<sup>[163]</sup> Upcycling has emerged as a significant trend in NCM direct recycling, aiming to improve materials performance through particle size reduction, elemental doping, and surface modification. The molten salt method exhibited

considerable potential in this field. Furthermore, direct recycling strategies were expanding from the material level to the electrode and even cell levels.<sup>[169]</sup> As a result, NCM direct recycling has evolved from simple lithium compensation to multi-level upcycling. The development of low-destruction regeneration strategies on material, electrode, and cell levels will contribute to the establishment of a closed-loop, low-carbon battery recycling technology system.

### 3.3. Direct Recycling Methods of Olivine LiFePO<sub>4</sub> Cathode Materials

Based on economic needs, the new material LFP was discovered in 1997.<sup>[170]</sup> Because the new material does not contain cobalt, and the elements Fe and P are very inexpensive, the market price of LFP is only a quarter of that of ternary materials.<sup>[171]</sup> Before 2015, LFP served as the primary material for power batteries, which was attributed to the advantages of LFP in safety, cost, and cycle life.<sup>[172–174]</sup> However, after 2015, with the development of high-energy-density materials (such as ternary materials) and the changing demands of the EV market, the market share of LFP was affected.<sup>[174,175]</sup> But in

recent years, due to the frequent safety incidents related to ternary materials, researchers have refocused on LFP again.<sup>[176,177]</sup>

LFP has a regular olivine structure with high rigidity and is not prone to collapse.<sup>[178]</sup> The structural framework does not undergo drastic volume changes during Li<sup>+</sup> intercalation/extraction, which is very different from layered oxides (Figure 12a).<sup>[42,179,180]</sup> During charging, LFP forms the FePO<sub>4</sub> phase as Li<sup>+</sup> is removed, and during discharging, the process is reversibly restored as Li<sup>+</sup> re-intercalates. However, the anisotropy of LFP causes uneven lithiation and delithiation spatially, leading to irreversible phase changes after long-term cycling (Figure 12b-d).<sup>[181,182]</sup> Furthermore, once the 1D Li<sup>+</sup> transport channels are occupied by Fe<sup>2+</sup>, it becomes difficult for Li<sup>+</sup> to re-intercalate.<sup>[183]</sup> During the use of LFP, the addition of conductive agents plays a critical role in material performance. Therefore, the failure of conductive agents causes LFP to decompose or even peel off, thus accelerating the degradation process (Figure 12e).<sup>[181]</sup> Based on these, unlike ternary materials, LFP requires a reduction environment and avoids the effects of oxidants. In addition to external lithium supplementation, the repair of the conductive agent carbon coating helps to ensure the overall conductivity of the material. The representative cases,

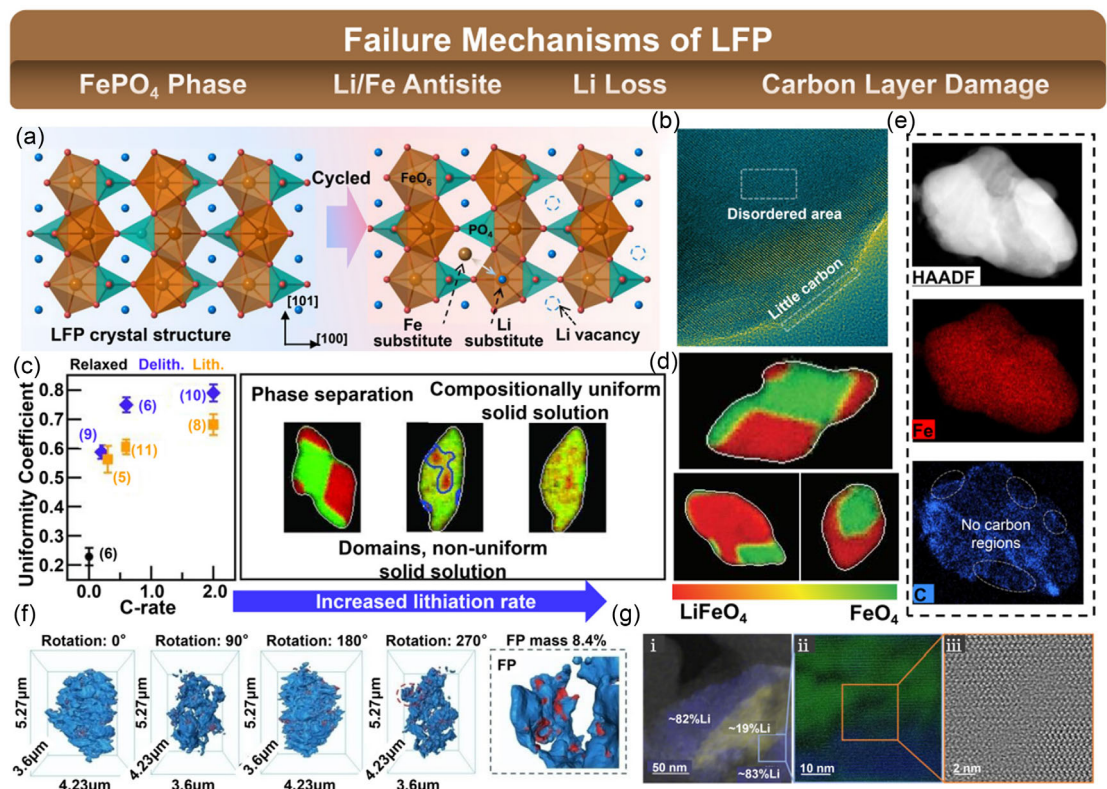


**Figure 12.** Multiscale degradation mechanisms in LFP cathodes: atomic defects, LFP/ FePO<sub>4</sub> phase separation and carbon layer damage. a) Schematic of lithium vacancies and Li-Fe antisite defects formed in olivine-phase LFP and b) HRTEM image of cycled LFP with structural degradation (Reproduced with permission.<sup>[181]</sup> Copyright 2023, The Authors). c) EDS elemental mapping of Fe and C distribution in degraded LFP and d) enhanced lithium-ion uniformity coefficient during lithiation compared to delithiation with increasing C-rates (Reproduced with permission.<sup>[182]</sup> Copyright 2016, Science). e) Phase-separated particles after structural relaxation (Reproduced with permission.<sup>[181]</sup> Copyright 2023, The Authors). f) Synchrotron radiation X-ray 3D nano-CT images of FP in LFP substrates at different rotation angles (Reproduced with permission.<sup>[192]</sup> Copyright 2024, Wiley-VCH). g) Phase map of a partially lithiated LFP crystal. (i) depicting areas of varying lithiation in LFP. Lithiated areas are shown in blue, delithiated areas in green. Magnified view (ii) of the phase boundary highlighted in (i). (iii) HR-iDPC image of the phase boundary showing a continuous transition between the lithiated and delithiated phase (Reproduced with permission.<sup>[288]</sup> Copyright 2024, The Authors).

**Tabel 3.** Summary of typical cases for the direct recycling and upcycling of LFP.

Cathode	Repair method	Key conditional	Initial capacity [mAh g <sup>-1</sup> ]	Capacity retention	References
LFP	Solid-phase recycling	Solid-state sintered 650 °C 1 h (Ar/H <sub>2</sub> )	147.0 [0.2C, 2.5–4.2 V]	95.2% [95 cycle]	[184]
LFP	Solid-phase recycling	Solid-state sintered with Li <sub>2</sub> DHBN, 800 °C for 6 h (Ar/H <sub>2</sub> )	157.0 [0.1C, 2.5–4.3 V]	88% [400 cycle]	[181]
LFP	Solid-phase recycling	Solid-state sintered 650–800 °C for 1–4 h (Ar)	130.7 [0.1C, 2.5–4.2 V]	96.9% [300 cycle]	[185]
LFP	Solid-phase recycling	Calcination in air for preoxidation; solid-state sintered with C <sub>6</sub> H <sub>12</sub> O <sub>6</sub> 700 °C for 10 h	167.8 [0.2C, 2.5–4.2 V]	92% [300 cycle]	[186]
LFP	Solid-phase recycling	Calcination in air 550 °C for 2 h; solid-state sintered with Li <sub>2</sub> CO <sub>3</sub> , C <sub>6</sub> H <sub>12</sub> O <sub>6</sub> , TiO <sub>2</sub> 700 °C for 8–12 h (N <sub>2</sub> )	155.7 [0.5C, 2.5–3.8 V]	95.8% [100 cycle]	[187]
LFP	Solid-phase recycling	Calcination in air 550 °C for 2 h; solid-state sintered with Li <sub>2</sub> CO <sub>3</sub> , C <sub>6</sub> H <sub>12</sub> O <sub>6</sub> , TiO <sub>2</sub> 700 °C for 8–12 h (N <sub>2</sub> )	147.3 [0.1C, 2.5–3.8 V]	>94% [100 cycle]	[188]
LFP	Solid-phase recycling	Calcination in air 500 °C; solid-state sintered with CuO, C <sub>6</sub> H <sub>12</sub> O <sub>6</sub> , Li <sub>2</sub> CO <sub>3</sub> , 350 °C 4 h + 700 °C 10 h (Ar/H <sub>2</sub> )	141.5 [0.5C, 2.5–4.2 V]	≈100% [300 cycle]	[189]
LFP	Hydrothermal repair	Hydrothermal treatment with CCL, L-threonine, 180 °C for 6 h	155.1 [0.1C, 2.5–4.3 V]	86% [500 cycle]	[190]
LFP	Hydrothermal repair	Hydrothermal treatment with TA, TU, 140 °C for 7 h; annealing with C <sub>6</sub> H <sub>12</sub> O <sub>6</sub>	151.3 [0.1C, 2.5–4.3 V]	72% [1000 cycle]	[191]
LFP	Hydrothermal repair	Hydrothermal treatment with LiOH, glycerol, 180 °C for 10 h	138.0 [1.0C, 2.5–4.3 V]	93.1% [500 cycle]	[192]
LFP	Hydrothermal repair	Hydrothermal treatment with ethanol, lithium acetate, PVP 180 °C for 5 h; annealing, 700 °C for 5 h (Ar)	170.0 [0.1C, 2.5–4.3 V]	80% [1000 cycle]	[193]
LFP	Solution relithiation	Mixed with LiOH, H <sub>2</sub> O <sub>2</sub> ; annealing with Li <sub>2</sub> CO <sub>3</sub> , 700 °C 10 h	158.0 [0.1C, 2.5–4.3 V]	92.0% [300 cycle]	[194]
LFP	Solution relithiation	Mixed with LiOH, CA 80 °C for 5 h; annealing with Li <sub>2</sub> CO <sub>3</sub> , 600 °C 2 h (N <sub>2</sub> )	159.0 [0.5C, 2.5–3.8 V]	>99% [100 cycle]	[195]
LFP	Solution relithiation	Mixed with LiOH, C <sub>6</sub> H <sub>12</sub> O <sub>6</sub> , NaCl freeze drying; annealing, 550 °C for 3 h (Ar)	169.7 [0.1C, 2.5–4.2 V]	>95.7% [200 cycle]	[196]
LFP	Solution relithiation	Annealing with LiOH, C <sub>6</sub> H <sub>12</sub> O <sub>6</sub> 550 °C for 3 h (Ar); use of ZnDEA as a structural modifier	167.0 [0.1C, 2.0–4.2 V]	96.3% [1500 cycle]	[197]
LFP	Solution relithiation	Immersed in LiTBH for 6 min at room temperature	164.4 [0.1C, 2.5–3.6 V]	84.6% [100 cycle]	[198]
LFP	Electrochemical repair	Graphite prelithiations	145.8 [0.1C, 2.5–4.0 V]	65.5% [200 cycle]	[199]
LFP	Electrochemical repair	Separator prelithiation	152.0 [0.05C, 2.5–4 V]	90.7% [292 cycle]	[200]
LFP	Electrochemical repair	Electrodes prelithiationannealing, 500 °C for 2 h (Ar)	135.2 [1C, 2.5–4.3 V]	95.3% [500 cycle]	[201]
LFP	Electrochemical repair	Electrodes prelithiation	153.0 [C/12, 2.0–3.8 V]	110% [225 cycle]	[202]
LFP	Electrochemical repair	Electrodes prelithiation	–	96% [274 cycle]	[203]
LFP	DES	Immersed in DES; calcination with LiOH, NH <sub>4</sub> H <sub>2</sub> PO <sub>4</sub> 350 °C 6 h, 650 °C 10 h (Ar)	152.0 [0.1C, 2.5–4.5 V]	99.5% [200 cycle]	[204]
LFP	Upcycling	Calcination with FePO <sub>4</sub> , Li <sub>2</sub> CO <sub>3</sub> , C <sub>6</sub> H <sub>12</sub> O <sub>6</sub> , MnCO <sub>3</sub> , 450 °C for 4 h, 700 °C for 16 h	161.3 [0.1C, 2.5–4.5 V]	95.6% [800 cycle]	[290]
NA: not available.					

the specific regeneration conditions, and results of LFP direct recycling and upcycling are summarized in Table 3.

### 3.3.1. Solid-State Recycling for LFP

Traditional pyrometallurgical and hydrometallurgical recycling have been proven effective for layered structure materials. But

they are not economically viable for spent LFP, as the only valuable recoverable element in spent LFP is lithium, without precious metal salts. Direct recycling methods for degraded layered structure materials require an oxidative environment for regeneration. However, the degradation mechanism of LFP determines that the regeneration process must be achieved in a reduction environment without oxygen. Therefore, innovative methods are needed

to address these specific challenges. For example, Chen et al. found that after heat treatment at an appropriate temperature, spent LFP powder could be reused in LIBs.<sup>[184]</sup> To replenish the Li<sup>+</sup> lost during cycling, Ji et al. developed a multifunctional organic lithium salt ((3,4-dihydroxybenzonitrile dilithium, Li<sub>2</sub>DHBN) to regenerate spent LFP by solid-state sintering directly.<sup>[181]</sup> During heating, the composite lithium salt undertook the task of lithium replenishment, simultaneously creating a reducing atmosphere through its strongly reducing cyano groups to inhibit the formation of Fe<sup>3+</sup>. In addition to the inherent defects of Li loss and the Fe<sup>3+</sup> phase considered in other methods, this method considers the lack of an efficient conductive layer, which directly affects the rate performance. The advantage of organic lithium salt is to generate an amorphous carbon layer on the surface of LFP particles during pyrolysis as a carbon source (Figure 13a). As shown in Figure 13b, this direct recycling route is more economically competitive than other battery technologies. In spent LFP batteries, the Al foil is coated not only with active LFP material but also with lithium- and carbon-containing substances, such as the electrolyte LiPF6 and conductive carbon. Based on this, Wang et al. utilized these lithium- and carbon-containing impurities attached to the cathode as lithium and carbon sources, achieving in situ regeneration of the failed LFP through high-temperature calcination.<sup>[185]</sup>

Researchers found the pre-oxidation process could remove impurities such as binders, conductive agents, and organic materials. Then, simple solid-phase methods could successfully regenerate spent LFP. For instance, Zeng et al. promoted subsequent lattice reconstruction and ion diffusion behavior

by pre-oxidation.<sup>[186]</sup> Similarly, Li et al. achieved the decomposition of residual impurities through a pre-oxidation process, forming LFP particles co-coated with carbon and Li<sub>3</sub>PO<sub>4</sub> during regeneration (Figure 13c).<sup>[187]</sup> In addition, Li and his team also found that doping with Ti improves the ionic conductivity of regenerated LFP (Figure 13d).<sup>[188]</sup> Metal ion doping has been shown to improve the electrochemical performance of LFP. In laboratory-scale regeneration, artificial disassembly was applied to completely separate the active materials from the cathodes. However, in traditional industrial mechanical separation, Cu foil is inevitably introduced into the recycled cathode. By using Cu impurity as a doping resource, Zeng et al. successfully suppressed the formation of Li/Fe antisites and enhanced the Li<sup>+</sup> storage capacity.<sup>[189]</sup>

### 3.3.2. Hydrothermal Repair for LFP

The high solubility of Li<sup>+</sup> in aqueous solutions leads to a large effective contact area between the Li<sup>+</sup> and the spent LFP particle; simultaneously, it also reduces the likelihood of impurity phase formation. Therefore, these advantages of hydrothermal repair have attracted the attention of researchers. The key to hydrothermal repair is the choice of reducing agent. However, adding a single carbon source and reducing agent can complicate the recovery process, potentially increasing the regeneration cost and decreasing its economic feasibility and scalability. Therefore, more researchers are exploring multifunctional additives to enable a one-step regeneration of spent LFP. For instance, Tang et al. proposed a hydrothermal method

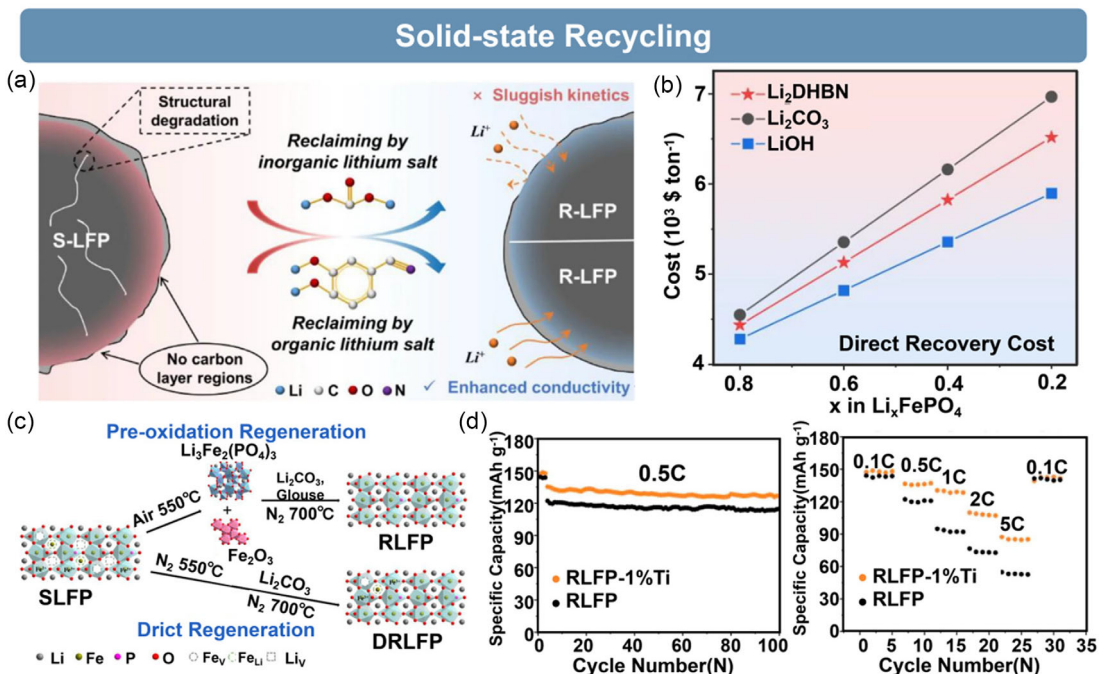


**Figure 13.** Solid-phase recycling of spent LFP based on organic lithium salt, pre-oxidation strategy. a) Schematic comparison of solid-phase recycling for LFP using organic vs. inorganic lithium salts and b) economic analysis of LFP regeneration via Li<sub>2</sub>CO<sub>3</sub>, LiOH, and organic lithium salt routes (Reproduced with permission.<sup>[181]</sup> Copyright 2023, The Authors). c) Process flow diagrams of pre-oxidized solid-phase recycling vs. direct recycling for spent LFP, and d) cycling performance and rate capability of regenerated LFP with/without 1% Ti doping (Reproduced with permission.<sup>[188]</sup> Copyright 2023, American Chemical Society).

using a natural, low-cost L-threonine as a multifunctional reductant (Figure 14a).<sup>[190]</sup> During recycling, the reducing environment created by this amino acid is crucial for reduction, which not only transforms the impurity  $\text{FePO}_4$  phase into the LFP phase, but also helps reconstruct  $\text{Li}^+$  diffusion channels. At the same time, the amino acid acts as a nitrogen source to modify the carbon layer on the surface of LFP particles, exhibiting multiple roles and opening up possibilities for future exploration of other multifunctional reducing agents for direct recycling of spent LFP.

In terms of selecting reducing agents, Cao et al. chose thiourea (TU) as the reducing agent for recovery, and tannic acid (TA) was chosen to attach to the particle surface.<sup>[191]</sup> While TA formed a dense carbon coating on LFP, it provided a mildly acidic environment to enhance the reducibility of TU. XPS spectra confirm the effective coating of N/S (Figure 14b). After doping, the Fe—O and P—O bonds on the surface of the regenerated LFP were enhanced. XRD patterns (Figure 14c) show that the  $\text{FePO}_4$  phase disappears after regeneration, indicating the completion of the reduction process. In addition, Feng et al. found that glycerol has rich functional groups to provide electron donors and create

a reducing environment.<sup>[192]</sup> Therefore, glycerol was chosen as both a solvent and a reducing agent to repair the LFP with LiOH as the lithium source (Figure 14d). As a solvent, glycerol's high viscosity effectively inhibits the Ostwald ripening process, causing the broken small particles to aggregate and reconstruct. Moreover, considering the subsequent treatment of reducing agents and their environmental impact is vital for the sustainable development of recycling methods; ethanol has great potential in the regeneration of spent LFP. In LFP, the migration of iron ions is closely related to the stability of the Fe—O bond, which is very sensitive to the energy bands of iron. According to the d-band center theory, the movement of the d-band close to the Fermi level will result in weaker bonding with surrounding atoms (Fe—O). Thus, raising the d-band position is an effective method for increasing the bond strength between transition metal atoms and surrounding atoms. Based on the theory, Jia et al. used ethanol as a reducing agent in regeneration.<sup>[193]</sup> By constructing a stable interface between nitrogen-doped carbon and LFP particles, they elevated the d-band center of the iron atoms to improve cycling stability (Figure 14e).

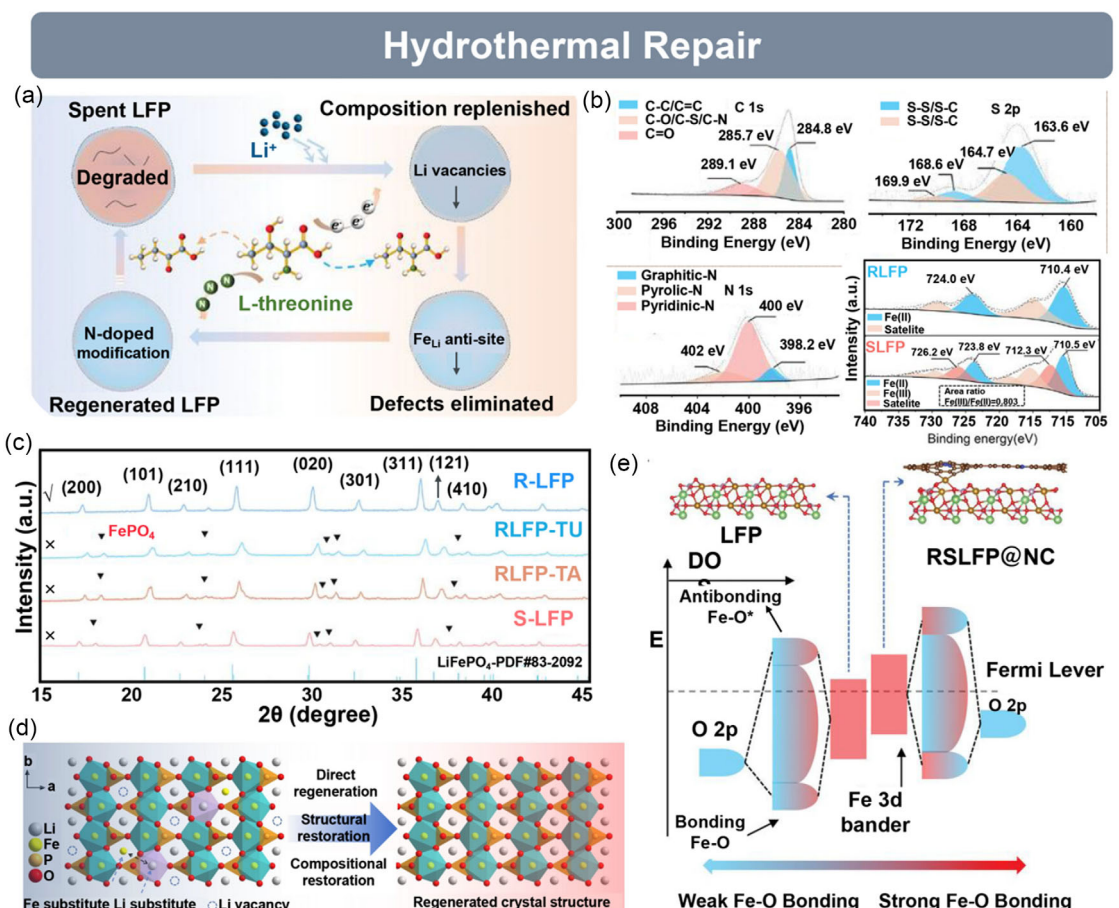


**Figure 14.** Multifunctional role of different additives (L-threonine, TA/TU) in LFP hydrothermal repair and carbon layer doping modification. a) Multifunctional roles of L-threonine in direct recycling process (Reproduced with permission.<sup>[190]</sup> Copyright 2023, Wiley-VCH). b) XPS spectra of C 1s, S 2p, N 1s in N/S co-doped R-LFP and Fe 2p spectra comparison before and after regeneration and c) XRD pattern comparison: TA-TU synergistically treated R-LFP vs. individually treated RLFP-TA/RLFP-TU vs. untreated SLFP (Reproduced with permission.<sup>[191]</sup> Copyright 2024, Wiley-VCH). d) Structural reconstruction mechanism of LFP failure and regeneration process (Reproduced with permission.<sup>[192]</sup> Copyright 2024, Wiley-VCH). e) Schematic of d-band center upshift in nitrogen-doped carbon modified R-LFP (Reproduced with permission.<sup>[193]</sup> Copyright 2022, Wiley-VCH).

### 3.3.3. Chemical Relithiation for LFP

The high-temperature and high-pressure regeneration conditions present safety risks, which hinder commercialization and large-scale application to some extent. To address these challenges, Xu et al. proposed a mild chemical reduction method by utilizing  $H_2O_2$  in LiOH solution to reduce and repair structural defects in spent LFP without heating or pressurization.<sup>[194]</sup> In this recycling method,  $H_2O_2$  is a relatively green reducing agent and does not produce any impurities in the decomposition process, which significantly reduces the complexity of post-treatment and environmental pollution. Similarly, citric acid (CA) is a low-cost and readily available option as a reducing agent for spent LFP. Therefore, Xu et al., in another team, successfully repaired LFP using LiOH solution with CA, which only produced  $CO_2$ ,  $H_2O$ , and  $C_5H_6O_5$  during relithiation.<sup>[195]</sup> Notably,  $C_5H_6O_5$  is an important intermediate for drug synthesis, which means that the LFP recycling process can couple with the synthesis of other valuable organic molecules.

Adding a carbon source to build a carbon coating during recycling has been proven to be an effective recycling method for

LFP. However, controlling the structural form of the carbon coating remains challenging. Overly dense or uneven coatings can negatively affect the transport of lithium ions. Based on this, Sun et al. introduced a salt template agent NaCl to the pre-reduction step with spent LFP, glucose, and LiOH (Figure 15a).<sup>[196]</sup> During recycling, freeze-drying helped embed NaCl into the glucose coating on particles, and the annealing process enabled the glucose to form a unique 3D porous carbon network on LFP particles. The template agent NaCl can be recovered and reused through washing. During the charge/discharge cycles, the LFP/FePO<sub>4</sub> phase transition affects the interfacial kinetics and increases the  $Li^+$  migration barrier. Therefore, using repair agents to alleviate the adverse effects of FePO<sub>4</sub> is an effective method. Zhao et al. used a ligand-chain Zn-complex (ZnDEA) as a structural regulator to promote the direct recycling of highly degraded LFP.<sup>[197]</sup> Spent LFP was generated by treating it in a lithium aqueous solution and adding glucose. The obtained LFP, together with conductive agents and ZnDEA, was used to prepare electrodes. During charge and discharge, ZnDEA expanded the crystal structure without disrupting its integrity, thereby mitigating the

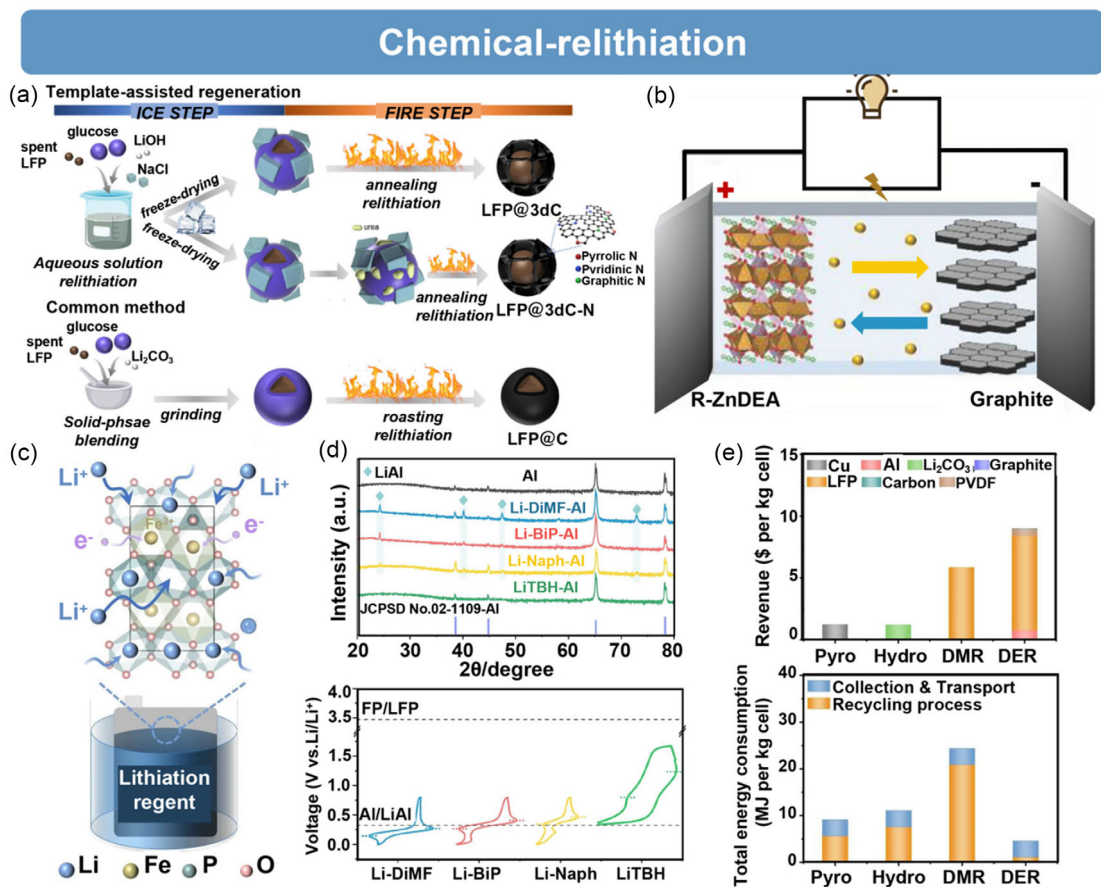


**Figure 15.** Chemical relithiation based on templating agents and novel lithiation reagents, and the economic advantages of direct recycling. a) Schematic of NaCl template-assisted “ice and fire” direct recycling and conventional solid-phase recycling (Reproduced with permission.<sup>[196]</sup> Copyright 2023, Elsevier). b) Full-cell configuration with ZnDEA-modified LFP cathode and graphite anode (Reproduced with permission.<sup>[197]</sup> Copyright 2024, Wiley-VCH). c) Immersion regeneration process of intact electrode sheet in lithiation reagent, and d) XRD patterns and redox potential profiles of Al foil exposed to Li-dimethylformamide (Li-DiMF), Li-biphenyl (Li-Bip), Li-naphthalene (Li-Naph), and Li-tert-butoxide (LiTBH) solutions, and e) Revenue and energy consumption for recycling 1 kg spent batteries via pyrometallurgy, hydrometallurgy, direct material recycling, and direct electrode recycling (Reproduced with permission.<sup>[198]</sup> Copyright 2024, Wiley-VCH).

negative effects of LFP and  $\text{FePO}_4$  phase transitions (Figure 15b). To avoid complicating the recycling process, it is necessary to restore the electrode without damaging its structure, so that the repaired electrode can be used directly. For instance, Yang et al. used lithium triethylborohydride/tetrahydrofuran (LiTBH) solution as the relithiation agent to replenish Li loss and regenerate spent LFP at room temperature.<sup>[198]</sup> This solution can reduce  $\text{Fe}^{3+}$  to  $\text{Fe}^{2+}$  without separating LFP and Al collector, regenerating spent LFP by simply immersing it in the solution within approximately six minutes (Figure 15c). By observing the LiAl peak in the XRD of different lithium reagents, they compared the usability of each reagent (Figure 15d). Compared with direct material recycling methods, this direct electrode recycling method reduces total energy consumption by 80% while increasing revenue by 53% (Figure 15d). The exploration of lithium reagents that can be used in air and further simple recycling steps will further promote the development of spent LFP recycling.

### 3.3.4. Other Methods for LFP

In addition to the common methods, electrochemical recycling and DES have also been explored for the direct recycling of LFP. For example, Wang et al. achieved graphite prelithiation by assembling graphite and lithium foils into batteries.<sup>[199]</sup> The degree of prelithiation was controlled by adjusting the cutoff voltage, and the lithiated graphite was then assembled with spent LFP to regenerate. The method achieved simple, low-cost, green recycling of cathodes. Unlike prelithiation of the anode, Fan et al. chose to perform separator prelithiation by coating a lithium-containing film on a commercial separator, which acted as a lithium source.<sup>[200]</sup> Similarly, lithium-containing electrolytes can also successfully supplement lithium in spent LFP. For instance, Peng et al. immersed the spent LFP in a lithium-containing solution and caused automatic embedding of lithium due to concentration gradients.<sup>[201]</sup> At the same time, a continuous output current drives successful regeneration of LFP. Larouche et al. also achieved the regeneration of degraded LFP by using lithium-containing solutions.<sup>[202]</sup> In degraded cathodes, Li loss is primarily stored in the anode in the form of SEI (solid electrolyte interface) or dead lithium. Zhao et al. utilized the lithium source in the anode for deep discharge to replenish lithium loss in spent LFP.<sup>[203]</sup> Currently, the recovery and direct recycling of many key metals focus on single cathode components. Therefore, the direct recycling of mixed materials remains a significant challenge. To address this, Ji et al. used DES to upcycle a mixture of spent LFP and LMO into a high-voltage polyanionic cathode material, ensuring complete recovery of all elements.<sup>[204]</sup> Furthermore, DES can be reused, and the new generation of phosphate cathode materials demonstrated improved structural stability and conductivity.

In typical recycling methods, valuable lithium elements are selectively leached for recycling, and the residual  $\text{FePO}_4$  is considered waste. However, in actual recycling, degraded LFP materials may vary due to different batches and unknown historical usage paths and origins, which lead to additional challenges

to direct recycling. Therefore, it is preferable for recycling to begin from waste  $\text{FePO}_4$ . For instance, Zhou et al. added the element manganese to  $\text{FePO}_4$  to form a gradient-doped structure of particles.<sup>[205]</sup> The electrochemical performance of the new material even exceeded the original material.  $\text{FePO}_4$  particles vary in size and often have micro/nanocracks on the surface, which facilitates subsequent element replenishment and serves as diffusion channels for Li and Mn doping. This regeneration method is expected to be effectively applied to new regenerated materials with various Mn/Fe ratios and doped with different elements. It provides an effective value-adding treatment method for leached  $\text{FePO}_4$ .

The direct recycling of spent LFP materials focuses on restoring their electrochemical performance through relithiation and reduction of  $\text{Fe}^{3+}$ , while simultaneously addressing issues such as degraded conductivity and structural defects. Establishing a reducing atmosphere is essential to prevent  $\text{Fe}^{2+}$  from being oxidized to  $\text{Fe}^{3+}$ , which would occupy additional lithium sites. Different methods focused on creating a reducing environment and repairing the conductive layer. The solid-phase method typically mixed spent LFP with lithium sources followed by high-temperature thermal treatment, enabling both lithium replenishment and reduction of  $\text{Fe}^{3+}$  along with carbon coating.<sup>[181]</sup> The hydrothermal method utilized multifunctional reducing agents under mild conditions to achieve relithiation,  $\text{Fe}^{3+}$  reduction, and antisite defect repair simultaneously.<sup>[190]</sup> Chemical methods relied on green reducing agents for reductive repair under relatively low temperature and pressure, ensuring high safety and low cost.<sup>[194]</sup> Notably, direct recycling for LFP was expanding from the material level to the electrode and even cell level, significantly reducing energy consumption and costs.<sup>[199]</sup> Therefore, the future development of LFP direct recycling should concentrate on the design of multifunctional repair that can combine lithiation, reduction, and conductivity enhancement in a single process.

## 4. Direct Recycling of Spent Graphite Anode Materials

As the key components of LIBs, anode active materials play a vital role in determining the safety and electrochemical performance of batteries.<sup>[206]</sup> Although cathode materials are constantly being updated and iterated, graphite-based carbon materials have consistently dominated the field of anodes, accounting for  $\approx 91\%$  of the commercial LIB anode market, because of their high conductivity, long cycle life, high capacity, and low working potential.<sup>[207,208]</sup> With the continuous expansion of the new energy industry, the demand for graphite is rapidly increasing. Graphite anodes account for about 15–20 wt% of LIBs and nearly 10% of the total battery cost.<sup>[208,209]</sup> Therefore, with the growing number of spent LIBs, a large amount of spent graphite will be produced. However, currently, the recycling of spent LIBs focuses on cathode materials, and spent graphite is typically separated and removed as an impurity, making it difficult to recycle effectively.<sup>[210]</sup> Therefore, developing efficient and environmentally

friendly strategies to recover carbon materials from spent anode is greatly significant. Particularly, spent graphite obtained from unregulated dismantling (no-discharge dismantling) contains a large amount of residual lithium, which further increases the value of spent graphite.<sup>[211]</sup> Moreover, spent graphite often contains metal impurities, binders, and flammable electrolytes, which may cause environmental pollution if not properly treated. As a result, recycling spent anode materials not only alleviates environmental and supply pressures but also promotes the sustainable utilization of resources.

Since spent graphite does not contain transition metals, it has traditionally been treated by landfilling or incineration.<sup>[212]</sup> Unlike the degradation mechanism of the cathode, spent graphite maintains a relatively intact crystal structure even after long-term cycling. Graphite has a typical hexagonal layer structure, with weak van der Waals forces between the layers.<sup>[213]</sup> This structure facilitates the intercalation/extraction of Li<sup>+</sup>, forming graphite intercalation compounds. During charging, Li<sup>+</sup> inserted into the graphite layers, generating a series of lithium–carbon compounds (LiC<sub>X</sub>, X = 6, 12, 18) and forming a unique gradient structure.<sup>[214]</sup> However, this phase transition process inevitably leads to strain accumulation, and the residual strain is not fully released after the lithiation/delithiation. With the increasing number of cycles, the irreversible phase transitions gradually accumulate, causing structural defects or even layer peeling off, leading to the degradation of graphite. In addition to Li<sup>+</sup> entering the graphite layer, some solvent molecules may also intercalate into the graphite layers during charging, which may cause irregular deposits and dimensional expansion after long-term cycling.<sup>[215]</sup> For example, Wang et al. observed that the interlayer spacing of graphite increased from 0.335 to 0.37 nm after cycling.<sup>[216]</sup> Moreover, the SEI formed at the anode–electrolyte interface is another major factor causing the degradation of graphite. During the lithiation/delithiation process, the SEI layer undergoes continuous tensile and compressive strain, leading to the formation of cracks. Electrolyte diffuses through these cracks and generates new SEI growth sites to form a thick and uneven SEI layer finally, which reduces the electrical conductivity of the material.<sup>[217,218]</sup> In addition, the attachment of metal impurities and organic binders also leads to the gap between spent graphite and commercial graphite. Based on the failure mechanism, the recycling strategy for anode should focus on the release of Li<sup>+</sup>, as well as the removal of SEI and metal impurities, to restore the original layer structure.

The maintenance of high temperatures during pyrometallurgical recycling facilitates the decomposition and detachment of impurities, as well as the graphitization of the spent anode. Yu et al. treated spent graphite at 3000 °C for 6 h under N<sub>2</sub> atmosphere, which achieved higher capacity and excellent cycle stability of the regenerated graphite.<sup>[219]</sup> However, the use of ultra-high temperatures results in high energy consumption, which limits its feasibility for large-scale applications. Therefore, Yi et al. reduced the graphitization temperature to 1400 °C and successfully obtained regenerated graphite by heating the anode under N<sub>2</sub> atmosphere for 4 h.<sup>[220]</sup> During the heat treatment, the copper current collector melted into spherical particles, which

could be removed through sieving. Similarly, Gao and his team obtained regenerated graphite with an ordered structure through calcination at 1500 °C.<sup>[221]</sup> Considering the formation of HF during recycling, Liu et al. used a NaOH roasting approach to recover LiF and avoid HF release.<sup>[222]</sup>

However, it is difficult to remove impurities completely by high temperatures alone. Therefore, adding extra purification steps is necessary. The hydrometallurgical recycling can efficiently remove metal impurities from spent graphite through acid treatment. For example, Li et al. removed binders and conductive agents via calcination, followed by immersing in sulfuric acid to dissolve metal impurities.<sup>[223]</sup> Subsequent KOH etching and high-temperature calcination restored the structural defects and pore structure of graphite, increasing the even size of the pores and enhancing Li<sup>+</sup> mobility. Similarly, based on surfactant-assisted purification, Liu et al. achieved successful regeneration of spent graphite using methanesulfonic acid (MSA).<sup>[224]</sup> Given the secondary pollution caused by acid use in the above methods, Shi et al. introduced a bioleaching strategy.<sup>[225]</sup> Strains on the surface of spent graphite not only facilitated impurity removal but also formed biofilms coating to fill surface cracks. Subsequently, these surface biofilms were heat-treated to decompose into amorphous carbon and create carbon core–shell structure of graphite, allowing them to repair and regenerate.

While pyrometallurgical recycling can reconstruct the graphite structure at high temperatures, the high energy input should be avoided for recycling. Hydrometallurgical recycling consumes large volumes of acid, and the problems with secondary wastewater treatment also create obstacles. DES, as green, biodegradable, and low-cost solvents, has already demonstrated excellent performance in cathode recycling. Due to the coordination ability with metals, DES can selectively extract metal impurities. Therefore, DES may replace acid as a leaching agent for spent graphite for efficient recycling. For instance, Lai et al. reported that DES was more effective in removing impurities than conventional acid for spent graphite.<sup>[226]</sup> Moreover, organic binders and electrolytes could dissolve due to hydrogen bonding with DES, which allowed efficient removal of PVDF and enabled graphite regeneration under mild conditions.

In the recovery of graphite materials, simple water treatment can be used to remove surface impurities. For example, Bhar et al. proposed a method for recovering spent graphite using deionized water as a leaching medium, followed by DMC washing and calcination at 750 °C to remove residual impurities further.<sup>[227]</sup> Similarly, Wang et al. found that residual lithium in graphite can react with water to generate H<sub>2</sub>, which facilitates the removal of thick and uneven SEI layers.<sup>[228]</sup> At the same time, this process also eliminated most of the impurities and reopened the Li<sup>+</sup> diffusion channels. Yang et al. also regenerated graphite successfully using water leaching.<sup>[229]</sup> Researchers have found that lithium trapped on the surface and within the bulk structure of graphite can be extracted into water through leaching and efficient utilization of this lithium solution can improve the economic value of the recycling process. For example, using lithium extracted from the anode as a lithium source to repair the cathode. Wang et al. extracted Li<sup>+</sup> from spent graphite into an aqueous

solution to regenerate NCM or LCO materials.<sup>[90]</sup> Additionally, delithiated graphite can be regenerated by calcination in an Ar atmosphere with NaOH as a flux. In the method, the regeneration of the cathode and the anode was connected through the cycle of lithium. Similarly, Liu et al. used water as a medium to remove lithium impurities from graphite and regenerated graphite.<sup>[153]</sup> The resulting lithium solution was used for the regeneration of cathode through hydrothermal repair.

The regenerated graphite is still limited by anisotropy and poor rate capability during cycling. Therefore, Yuan et al. used NH<sub>4</sub>F as the removal and modified agents to introduce effective pores on graphite, successfully regenerating spent graphite at 1400 °C.<sup>[230]</sup> The abundant surface pores help to enhance ion diffusion and slow down the voltage dropping, thus accelerating electrochemical kinetics. However, continuous thermal treatment and decontamination during regeneration are time-consuming and costly; therefore, researchers have explored more efficient and environmentally friendly approaches. Chen et al. developed an ultrafast flash regeneration method for spent graphite anodes.<sup>[231]</sup> The temperature of ≈2850 K broke down resistive impurities (SEI, binder, etc.) in a few seconds of heating time. It formed a tightly contacted carbon layer while maintaining the graphite particle morphology. Similarly, Shan et al. employed a microwave field to remove impurities and restore the graphitic structure within 30 s.<sup>[232]</sup> Fan et al. compared microwave-assisted calcination with conventional methods, demonstrating that microwave treatment enabled efficient regeneration of spent anode graphite at lower energy input.<sup>[233]</sup> In the exploration of recovery time, Zhang et al. achieved 98.7% recovery ratio of graphite and 100% recovery ratio of copper foil within just 1 s of transient heating, enabling a roll-to-roll recycling for spent anode.<sup>[234]</sup> This approach minimizes energy input and waste generation compared to other methods, and helps facilitate continuous and automatic recycling, making it promising to be extended to other battery anode materials.

Recently, researchers have proposed the use of expanded graphite (EG) as a new anode material. Due to its unique porous structure, EG provides abundant active sites for lithium storage and shows great potential for improving battery rate performance, which suggests that upcycling spent graphite into EG may be a promising direction. Moreover, graphene has unlimited possibilities for application in batteries because of its ultra-high electronic and thermal conductivity, as well as its large surface area. During the preparation of graphene, it can be exfoliated from layered graphite by the shear stripping method. Obviously, the small particle size and narrow interlayer spacing of spent anode graphite make direct exfoliation difficult. However, after upcycling the graphite to EG, the graphite layer spacing is enlarged, thus increasing the feasibility of preparing graphene. For this reason, Yang et al. proposed an innovative strategy to synthesize high-performance EG and graphene oxide from spent graphite.<sup>[235]</sup> During the process, FeCl<sub>3</sub> was used as an intercalant to enlarge the interlayer spacing, allowing H<sub>2</sub>O<sub>2</sub> molecules to penetrate. Then, the in-situ reaction between FeCl<sub>3</sub> and H<sub>2</sub>O<sub>2</sub> generated O<sub>2</sub> gas within the graphite layers, promoting further expansion of gas. The obtained EG and graphene products show good cycling

stability in both lithium-ion and sodium-ion batteries. The strategy is no longer limited to decontamination and purification, but rather moves toward higher performance regenerated graphite derivatives. Similarly, Gong et al. separated impurities and regenerated to expand the volume of the graphite. KMnO<sub>4</sub> simultaneously oxidized and expanded the graphite structure, and the generated gas molecules significantly increased the interlayer spacing. The method exhibits excellent removal and expansion effects.<sup>[236]</sup>

## 5. Artificial Intelligence Assisted Battery Direct Recycling and Development

The rapid advancement of artificial intelligence (AI) provides new opportunities for advancing direct recycling. Spent LIBs typically originate from various sources and differ in materials, sizes, and degradation levels. The lack of classification hinders the direct recycling of spent batteries. Moreover, the obscurity of key information such as manufacturing data, usage history, and recycling pathways across multiple platforms further complicates the recycling process. Machine learning (ML) is one of the most useful and widely used methods in AI.<sup>[237–239]</sup> In recent years, it has become a viable tool for solving complex problems in the battery field, including battery classification, remaining useful life prediction, efficient disassembly, and recycling process optimization.<sup>[240]</sup>

### 5.1. Lifetime Estimation of Spent LIBs for Clustering

To ensure the safe operation of batteries and accurate classification of spent batteries, predicting the remaining useful life and evaluating the state of health (SOH) of batteries are particularly critical. Currently, the clustering methods for spent LIBs can be broadly summarized as follows.<sup>[241]</sup> Traditional methods rely on full charge-discharge testing to determine the remaining capacity of spent batteries.<sup>[242]</sup> Electrochemical impedance spectroscopy (EIS) measures the response of current to voltage perturbations to obtain impedance across a wide frequency range, and statistical machine learning is employed to correlate these measurements with battery health.<sup>[243]</sup> The pulse testing applies a series of current pulses to mimic real operational conditions.<sup>[244]</sup> If the same amount of electricity is charged or discharged to/from LIBs with different aging under the same initial voltage and ambient temperature, LIBs of dissimilar SOH reflect varied voltage rise or drop. Pulse test is efficient and reflects battery SOH. Combined with ML, the pulse test can sort LIBs and estimate SOH. In recent years, artificial intelligence has been widely applied to assess the SOH of LIBs.<sup>[245,246]</sup>

Lu et al. pointed out that AI plays a significant role in LIB modeling.<sup>[247]</sup> By training on large-scale, time-scale datasets, ML is expected to estimate the lifetime of batteries. Multiple ML methods can be applied to estimate battery condition. For example, Li et al. and Jiang et al. employed Bayesian models for lifetime prediction by using existing datasets.<sup>[248,249]</sup> Chen et al. developed an ML-based framework that uses electrochemical signatures recorded cycle-by-cycle to distinguish

degradation modes.<sup>[250]</sup> Their study demonstrated that failure mode classification and prediction can be achieved even without knowledge of the anode type and a complete training set. Similarly, Zhang et al. combined EIS with Gaussian process machine learning.<sup>[251]</sup> By building a large dataset, they accurately predicted battery lifetime accurately without complete information of historical conditions. Ran et al. proposed a two-step method involving model training and short-pulse testing to assess the health status of LIBs.<sup>[241]</sup> After full discharge, batteries are charged to 5% state of charge (SOC) for short-pulse testing. Extracted features are clustered using unsupervised K-means and Gaussian mixture models, achieving a correlation coefficient over 98% and reducing sorting time by more than 80%.

## 5.2. Cathode Classification for Recycling Process

Direct recycling highly relies on the cathode. Although pyrometallurgical and hydrometallurgical methods can extract metals from mixed materials, interactions between different cathode types during recycling will seriously affect the quality of the recovered products. Therefore, identifying the type of cathode material plays a crucial role in determining recycling strategies and ensuring the performance of regenerated materials. Recent studies have proposed the establishment of battery cycle life tracking systems and the concept of a “battery passport” to enable precise material identification.<sup>[252,253]</sup> However, a large number of LIBs have already been used, retired, and currently entered recycling process. The need for classification remains critical, regardless of whether batteries are reused for second-life or directly recycled.

Although ML has shown great potential in various aspects of LIB research, studies focused on cathode material classification are still limited, mainly due to the lack of accessible historical data. DiKMEN et al. developed an electrochemical approach to identify unknown cathode types.<sup>[254]</sup> By connecting batteries to two different loads and recording voltage-current responses, they applied artificial neural networks and decision tree algorithms to achieve 100% classification. Similarly, Zhong et al. collected electrochemical data of cathodes from the past 5 years.<sup>[255]</sup> Then, they trained an ML model named DRX to extract key features and enable rapid cathode identification. However, the availability of battery cycling data remains limited due to barriers to data sharing among manufacturers, users, and academic institutions. Ensuring database interoperability is essential for accurate cathode classification and preserving data privacy. Tao et al. demonstrated the applicability of federated ML in intelligent battery recycling.<sup>[240]</sup> It enables decentralized model training across multiple data owners without exposing sensitive information. Each participant trains the model locally and then only transmits model parameters to a central coordinator for aggregation. Compared with centralized data sharing, this method is much faster, more secure, and cost-effective.

## 5.3. Automated Disassembly for Direct Recycling

Disassembly is a necessary step in the recycling of spent LIBs. Currently, manual disassembly is still the dominant method. It

is labor-intensive, inefficient, and economically unsustainable. In recent years, the application of industrial robotics has promoted the development of automated mechanical disassembly, significantly improving operational efficiency and reducing labor and time costs.<sup>[256,257]</sup> However, achieving accurate and flexible robotic disassembly still faces several technical challenges. The advantage of industrial robots is efficient and repetitive work. They cannot process the complex uncertainties during disassembly.<sup>[258]</sup> Spent battery modules vary in specifications, dimensions, and configurations. And after prolonged use, some components may change shape. These factors make it impossible for robots to perform a single operation in complex working conditions.

Human–robot collaboration balances efficiency and cost. Wegener et al. developed a cooperative disassembly system.<sup>[259]</sup> They used a visual recognition system to locate fasteners (e.g., bolts), facilitating subsequent disassembly tasks. Computer vision has been increasingly utilized to model end-of-life batteries, providing critical support for automated disassembly processes. Poschmann et al. employed computer vision for target identification, enabling precise and distributed disassembly.<sup>[260]</sup> In human–robot collaborative disassembly, the planning and scheduling of disassembly tasks can be further enhanced through the use of advanced intelligent strategies. Zaatar et al. improved Task-Parameterized Learning from Demonstration (TP-LfD) to enhance robotic applicability.<sup>[261]</sup> Using TP-LfD, robots learn from human demonstration paths and optimize new disassembly operations. Zhou et al. employed the Stackelberg model to optimize disassembly operations.<sup>[262]</sup> Additionally, they designed a particle swarm optimization Pareto algorithm (PSO-Pareto) to improve further the efficiency and safety of human–robot collaboration in disassembly tasks.

## 5.4. Process Optimization for Direct Recycling

The development and utilization of battery materials and devices involve complex multivariate problems. Traditional trial-and-error approaches often rely on extensive experimental work by researchers. AI, with its powerful data processing capabilities, especially ML, has demonstrated outstanding potential in evaluating multidimensional data and identifying feature patterns.<sup>[263]</sup> This offers opportunities for advancing the discovery of battery designs, materials synthesis, and device fabrication. The preparation of electrodes represents emerging application areas for ML. Each step in these processes involves multiple parameters, such as slurry composition ratios, powder pre-mixing time and speed. In many cases, manufacturers lack the fundamental physical understanding of these parameters. ML can autonomously collect production line data, optimizing manufacturing through data-driven modeling and analysis.<sup>[264]</sup> Similarly, direct recycling in battery recycling shares similarities with battery material synthesis and involves complex multivariable production steps. It is reasonable to infer that ML can also be employed to collect operational data from recycling lines and apply data training models to achieve recycling process optimization.

### 5.5. Typical Applications and Cases

Traditional recycling methods require manual disassembly, which is costly and inefficient. Consequently, given the huge decommissioning market, many batteries were ultimately shredded, which limited the value of recovered components. To address this issue, researchers at the Fraunhofer Institute in Magdeburg, Germany, have developed iDEAR (intelligent Disassembly, Remanufacturing and Recycling of electronic devices).<sup>[265]</sup> The iDEAR achieves data acquisition with 3D camera and optical sensor system. Based on these data, AI core algorithms (machine learning) enable real-time identification and classification of materials, plastics, and components. These systems not only enable identification but also assess component condition, detect, and evaluate the status of connecting elements. The robots will be guided to complete the disassembly task with the results of the algorithms. Furthermore, European startup Circu Li-Ion has developed an AI-assisted disassembly platform with 3D camera and robotics to accurately identify, separate, and recover battery components.<sup>[266]</sup> This approach not only minimizes material cross-contamination but also identifies batteries suitable for second-life applications. Similarly, Hunan Brunn Recycling Technology has successfully industrialized a fully automated disassembly system for power batteries at the minute level.<sup>[267]</sup> The advancement of automated disassembly is becoming a cornerstone in AI-assisted LIB recycling.

## 6. Summary and Prospect

Each cathode material corresponds to different failure mechanisms, which in turn require distinct repair mechanisms and goals. With a thorough understanding of the failure mechanisms, the importance of repair needs to be redefined. The choice of direct recycling method directly determines the extent of the repair. For LCO materials, the overall recycling benefit is generally lower than that of NCM. This is because the performance of the restored material often fails to return to its initial level, and its economic value is also lower than recycled high-nickel NCM materials. Therefore, for LCO, upcycling to higher-performance materials is more promising than direct recycling. Furthermore, due to its high cobalt content, LCO can be converted into high-value cobalt-containing catalysts. For LFP materials with strong structural rigidity, mild solution-based lithiation repair methods may be the future direction for direct recycling. At the same time, the relatively intact structure also limits the entry of heteroatom dopants to some extent, so the upcycling methods are more focused on coating and conductive agent doping. On the other hand, for NCM materials, whose bulk structure is severely damaged after long cycles, the primary repair goal is to restore the original structure. Simple elemental supplementation may not meet the commercial material repair standards, and a high-temperature environment is still needed to promote structural reconstruction. Unlike LFP, the fractured structure and elemental vacancies in NCM materials facilitate the entry of dopant atoms. Therefore, upcycling of ternary materials is more

economically viable and sustainable than direct recycling, making it a better choice for future recycling. The recycling of graphite anode materials requires first removing SEI layers, binders, and other impurities. Acid leaching and high-temperature calcination can effectively address these issues. Currently, ultra-fast high-temperature and instant heating technologies, which have shown effectiveness in cathode recycling, have also achieved successful results in anode material recycling. This approach is expected to enable the consistent recycling of both anode and cathode materials after failure.

To comprehensively evaluate the advantages and disadvantages of recycling spent batteries, particularly sustainability, we analyzed life cycle assessment (LCA) and life cycle cost (LCC) studies of spent batteries.<sup>[38]</sup> LCA focuses on assessing the environmental burden of a product or process throughout its entire life cycle, including stages from raw material acquisition to final recycling.<sup>[268]</sup> Generally, the environmental impact associated with recycling spent LIBs largely depends on the chosen recycling technology. Wu et al. reported that regenerating 1 kg of LCO cathode material from recycled cobalt resulted in 67–286 kg carbon dioxide equivalent ( $\text{CO}_{2\text{eq}}$ ) and 1164–4349 MJ.<sup>[269]</sup> In contrast, the direct recycling process resulted 21–154 kg  $\text{CO}_{2\text{eq}}$  and consumed 267–2251 MJ to regenerate 1 kg of LCO cathode material. In addition to assessing environmental trade-offs, the economic impact of recycling spent LIBs was evaluated through LCC analysis.<sup>[38]</sup> Some researchers have demonstrated positive net income from recycling spent LIBs.<sup>[48,270]</sup> For example, the profit obtained from recycling 1 ton of spent LCO powder is approximately \$28016.2, whether through pyrometallurgical or hydrometallurgical methods.<sup>[42]</sup> Alipanah et al. estimated that the potential average profit ranged between 17% and 26%.<sup>[271]</sup> Furthermore, direct recycling has been demonstrated to be the highest revenue-generating method compared to other methods. That's because direct recycling tends to exhibit lower energy and reagent costs, as well as reduced fixed equipment costs. Currently, the global LIB recycling rate is estimated to be only 5%.<sup>[272]</sup> By addressing economic barriers, improving the recycling rate becomes feasible, thereby promoting the sustainable development of the LIB industry. LCA and LCC analyses indicated that direct recycling had economic benefits and reduced greenhouse gas emissions. 1. The collection of different types and failure levels of batteries in a mixed batch adds extra burden to the recycling process. The choice of recycling method is closely related to the type of electrode material and the extent of failure. Further exploration of failure modes and accurately assessing the battery's condition before cell disassembling can have a significant impact on the selection and implementation of recycling. The combination of battery sorting and AI, including machine learning and computer vision, may enable efficient sorting of spent batteries, with initial sorting based on size, source, material type, and remaining capacity, therefore supporting the direct recycling process. 2. Trace amounts of impurity elements can significantly affect the level and effectiveness of recycling. It is necessary to investigate the impact of trace impurities on the performance of regenerated cathodes. Recycling purity cathode materials requires innovative research on the

separation of mixed anode and cathode materials, the separation of active materials from conductive agents and binders, and the separation of active materials from the electrode. Research is also needed to develop water-soluble and alcohol-soluble binders that are easy to separate for recycling. Currently, the concept of decomposition and recycling in conventional recycling is a key factor leading to impurities. Direct recycling, which avoids separating the active material from the current collector, is a promising direction for future recycling, aiming for roll-to-roll recovery of electrodes. In addition, self-supporting electrodes that do not require current collectors fundamentally reduce the potential for impurities and represent one of the future directions for electrode material design. 3. Research on direct recycling methods is now primarily focused on specific active materials. The optimal direct recycling method for a specific material remains uncertain. It is necessary to find a universal method that can recycle all types of electrode materials. For example, we hope electrode materials with different remaining capacities can be directly recycled using the same method. Similarly, materials with different elemental compositions are supposed to be fully recycled. For instance, in a low oxygen pressure environment, the repair effect for high nickel-content ternary materials is poor. When the nickel content exceeds 0.5, the material becomes more sensitive to moisture in the air. This requires careful consideration when choosing the recycling method. Moreover, different types of materials require different gas atmospheres during the repair process, which poses a challenge in selecting a universal recycling method. For example, based on failure mechanisms, ternary materials require control of oxygen partial pressure for recycling, whereas LFP requires avoiding oxidation to prevent further degradation. 4. Currently, the rapid evolution of cathode materials, along with advancements in battery technology and scaling, also demands the revision and upgrading of direct recycling. Direct recycling that focuses on the initial formula and structure will gradually become obsolete as cathode materials develop at high speed. For example, NCM111, due to its high cost and low energy density, is being replaced by NCM523 or NCM622, which better align with the market trends. Moreover, the trend of increasing nickel content, higher voltage, and single-crystal development in ternary materials indicates the future development direction of upcycling. Upcycling, which produces materials with better performance, will gradually replace direct recycling as the new trend. Additionally, due to the valuable elements such as Co and Ni, transforming spent batteries into new functional materials for other fields broadens the scope of recycling technologies and overcomes the limitations in this field. 5. Future development trends indicate a shift toward low cobalt or cobalt-free high energy-density cathode materials. The direct recycling of LFP and other cobalt-free cathode materials (e.g., LMFP, LNMO) faces severe challenges. Compared with high-value NCM cathodes, the economic drivers for LFP recycling are weaker due to the lower cost. Therefore, it is necessary to develop lower-cost direct recycling processes compared to other materials. In addition to the repair goals of lithium-ion replenishment and structural reconstruction, regenerating conductive carbon networks of LFP typically requires additional carbon sources and high-temperature

treatment, which remains a significant challenge for recycling benefits. Moreover, the extension of LFP direct recycling system to other cobalt-free systems will introduce new technical challenges, such as the dissolution of elements such as iron and manganese and structural instability under high pressure. 6. The development of recycling technologies should not only focus on efficiency and environmental friendliness but also on the compatibility of these technologies with existing production lines. These factors are critical in determining their potential for industrial-scale implementation. There is often a gap between the effectiveness of recycling at the laboratory scale and its feasibility in industrial applications. Even the most efficient recycling technologies will lose much of their practical value if they cannot be integrated into current production and recycling systems. Future research into recycling methods should not only validate the effectiveness of these technologies at the laboratory scale but also assess their potential for integration with industrial production lines. Therefore, future recycling research needs to focus on the compatibility of technologies with existing processes. 7. Direct recycling is intended to improve toward lower energy consumption and reduced greenhouse gas (GHG) emissions. However, it is essential to establish a unified, transparent, and widely accepted evaluation system that incorporates a range of research methods and goals. This evaluation system should be more comprehensive and scientific, encompassing the entire process from the collection, classification, and pretreatment of spent LIBs to the recycling process. A standardized set of indicators should be developed to assess energy consumption, GHG emissions, water resource usage, material recovery rates, and economic feasibility for different recycling technologies, enabling quantification and evaluation. Furthermore, to ensure the system's broad applicability, the development of this evaluation framework should consider the technological levels and energy structures of different countries and regions, and be dynamically adjusted to maintain its scientific rigor and forward-looking nature.

## Acknowledgements

J.X. acknowledges financial supports from the National Natural Science Foundations of China Grant (52002358) and the Henan Provincial Natural Science Foundation General Program.

## Conflict of Interest

The authors declare no conflict of interest.

**Keywords:** artificial intelligence-assisted recycling • direct recycling • electrode materials • spent lithium-ion batteries

- [1] N. Kittner, F. Lill, D. M. Kammen, *Nat. Energy* 2017, 2,17125, <https://doi.org/10.1038/nenergy.2017.125>.
- [2] J. Liao, R. S. Longchamps, B. D. McCarthy, F. Shi, C. Wang, *ACS Energy Lett.* 2024, 9, 771, <https://doi.org/10.1021/acsenergylett.3c02823>.

- [3] Z. Zhu, T. Jiang, M. Ali, Y. Meng, Y. Jin, Y. Cui, W. Chen, *Chem. Rev.* **2022**, 122, 16610, <https://doi.org/10.1021/acs.chemrev.2c00289>.
- [4] T. Raj, K. Chandrasekhar, A. N. Kumar, P. Sharma, A. Pandey, M. Jang, B.-H. Jeon, S. Varjani, S.-H. Kim, *J. Hazard. Mater.* **2022**, 429, 128312, <https://doi.org/10.1016/j.jhazmat.2022.128312>.
- [5] IEA, *Global EV Outlook 2024*, <https://www.iea.org/reports/global-ev-outlook-2024> (accessed: April, 2025).
- [6] P. Li, S. Luo, Y. Lin, J. Xiao, X. Xia, X. Liu, L. Wang, X. He, *Chem. Soc. Rev.* **2024**, 53, 11967, <https://doi.org/10.1039/d4cs00362d>.
- [7] T. Or, S. W. D. Gourley, K. Kaliyappan, A. Yu, Z. Chen, *Carbon Energy* **2020**, 2, 6, <https://doi.org/10.1002/cey2.29>.
- [8] Y. Chen, Y. Kang, Y. Zhao, L. Wang, J. Liu, Y. Li, Z. Liang, X. He, X. Li, N. Tavajohi, B. Li, *J. Energy Chem.* **2021**, 59, 83, <https://doi.org/10.1016/j.jechem.2020.10.017>.
- [9] S. Chu, S. Guo, H. Zhou, *Chem. Soc. Rev.* **2021**, 50, 13189, <https://doi.org/10.1039/d1cs00442e>.
- [10] S. Yang, Y. Wang, H. Pan, P. He, H. Zhou, *Nature* **2024**, 636, 309, <https://doi.org/10.1038/s41586-024-08117-1>.
- [11] A. Zeng, W. Chen, K. D. Rasmussen, X. Zhu, M. Lundhaug, D. B. Müller, J. Tan, J. K. Keiding, L. Liu, T. Dai, A. Wang, G. Liu, *Nat. Commun.* **2022**, 13, 1341, <https://doi.org/10.1038/s41467-022-29022-z>.
- [12] H.-H. Ryu, H. H. Sun, S.-T. Myung, C. S. Yoon, Y.-K. Sun, *Energy Environ. Sci.* **2021**, 14, 844, <https://doi.org/10.1039/d0ee03581e>.
- [13] C. B. Tabelin, J. Dallas, S. Casanova, T. Pelech, G. Bournival, S. Saydam, I. Canbulat, *Miner. Eng.* **2021**, 163, 106743, <https://doi.org/10.1016/j.mineng.2020.106743>.
- [14] T. Yang, D. Luo, A. Yu, Z. Chen, *Adv. Mater.* **2023**, 35, 2203218, <https://doi.org/10.1002/adma.202203218>.
- [15] J. T. Frith, M. J. Lacey, U. Ulissi, *Nat. Commun.* **2023**, 14, 420, <https://doi.org/10.1038/s41467-023-35933-2>.
- [16] J. Roy, S. Rarotra, V. Krikstolaityte, K. W. Zhuoran, Y. D.-la Cindy, X. Y. Tan, M. Carboni, D. Meyer, Q. Yan, M. Srinivasan, *Adv. Mater.* **2022**, 34, <https://doi.org/10.1002/adma.202103346>.
- [17] K. K. Jena, A. AlFantazi, A. T. Mayyas, *Energy Fuels* **2021**, 35, 18257, <https://doi.org/10.1021/acs.energyfuels.1c02489>.
- [18] J. Liu, H. Shi, X. Hu, Y. Geng, L. Yang, P. Shao, X. Luo, *Sci. Total Environ.* **2022**, 816, 151621, <https://doi.org/10.1016/j.scitotenv.2021.151621>.
- [19] G. Xu, L. Huang, C. Lu, X. Zhou, G. Cui, *Energy Storage Mater.* **2020**, 31, 72, <https://doi.org/10.1016/j.jesm.2020.06.004>.
- [20] X. Zheng, Z. Zhu, X. Lin, Y. Zhang, Y. He, H. Cao, Z. Sun, *Engineering* **2018**, 4, 361, <https://doi.org/10.1016/j.eng.2018.05.018>.
- [21] K. Jia, G. Yang, Y. He, Z. Cao, J. Gao, H. Zhao, Z. Piao, J. Wang, A. M. Abdelkader, Z. Liang, R. V. Kumar, G. Zhou, S. Ding, K. Xi, *Advanced Materials* **2024**, 36, 2313273, <https://doi.org/10.1002/adma.202313273>.
- [22] Y. Li, W. Lv, H. Huang, W. Yan, X. Li, P. Ning, H. Cao, Z. Sun, *Green Chem.* **2021**, 23, 6139, <https://doi.org/10.1039/d1gc01639c>.
- [23] P. Meshram, B. D. Pandey, T. R. Mankhand, *Chem. Eng. J.* **2015**, 281, 418, <https://doi.org/10.1016/j.cej.2015.06.071>.
- [24] J. Heelan, E. Gratz, Z. Zheng, Q. Wang, M. Chen, D. Apelian, Y. Wang, *JOM J. Miner. Met. Mater. Soc.* **2016**, 68, 2632, <https://doi.org/10.1007/s11837-016-1994-y>.
- [25] X. Zhang, L. Li, E. Fan, Q. Xue, Y. Bian, F. Wu, R. Chen, *Chem. Soc. Rev.* **2018**, 47, 7239, <https://doi.org/10.1039/c8cs00297e>.
- [26] A. Holzer, L. Wiszniewski, S. Windisch-Kern, H. Raupenstrauch, *Metals* **2022**, 12, 1642, <https://doi.org/10.3390/met12101642>.
- [27] A. Holzer, S. Windisch-Kern, C. Ponak, H. Raupenstrauch, *Metals* **2021**, 11, 149, <https://doi.org/10.3390/met11010149>.
- [28] Z. Liu, J. G. Sederholm, K.-W. Lan, E. J. Cho, M. J. Dipto, Y. Gurumukhi, K. F. Rabbi, M. C. Hatzell, N. H. Perry, N. Miljkovic, P. V. Braun, P. Wang, Y. Li, *J. Power Sources* **2023**, 580, 233345, <https://doi.org/10.1016/j.jpowsour.2023.233345>.
- [29] M. A. Rajaeifar, M. Raugei, B. Steubing, A. Hartwell, P. A. Anderson, O. Heidrich, Life Cycle Assessment of Lithium-Ion Battery Recycling Using Pyrometallurgical Technologies. *J. Ind. Ecol.* **2021**, 25, 1560, <https://doi.org/10.1111/jiec.13157>.
- [30] X.-H. Zhu, Y.-J. Li, M.-Q. Gong, R. Mo, S.-Y. Luo, X. Yan, S. Yang, *Angew. Chem., Int. Ed.* **2023**, 62, 202300074, <https://doi.org/10.1002/anie.202300074>.
- [31] W. Lv, Z. Wang, H. Cao, Y. Sun, Y. Zhang, Z. Sun, *ACS Sustainable Chem. Eng.* **2018**, 6, 1504, <https://doi.org/10.1021/acssuschemeng.7b03811>.
- [32] S. Wang, C. Wang, F. Lai, F. Yan, Z. Zhang, *Waste Manage.* **2020**, 102, 122, <https://doi.org/10.1016/j.wasman.2019.10.017>.
- [33] P. Xu, D. H. S. Tan, B. Jiao, H. Gao, X. Yu, Z. Chen, *Adv. Funct. Mater.* **2023**, 33, 2213168, <https://doi.org/10.1002/adfm.202213168>.
- [34] C. Xu, Q. Dai, L. Gaines, M. Hu, A. Tukker, B. Steubing, *Commun. Mater.* **2020**, 1, 99, <https://doi.org/10.1038/s43246-020-00095-x>.
- [35] J. Wang, J. Ma, Z. Zhuang, Z. Liang, K. Jia, G. Ji, G. Zhou, H.-M. Cheng, *Chem. Rev.* **2024**, 124, 2839, <https://doi.org/10.1021/acs.chemrev.3c00884>.
- [36] W. Wang, Y. Wu, *Resourc. Conserv. Recycl.* **2017**, 127, 233, <https://doi.org/10.1016/j.resconrec.2017.08.019>.
- [37] B. E. Murdock, K. E. Toghill, N. Tapia-Ruiz, *Adv. Energy Mater.* **2021**, 11, 210208, <https://doi.org/10.1002/aenm.202102028>.
- [38] B. K. Biswal, B. Zhang, P. Thi Minh Tran, J. Zhang, R. Balasubramanian, *Chem. Soc. Rev.* **2024**, 53, 5552, <https://doi.org/10.1039/d3cs00898c>.
- [39] Y. Dong, H. Ji, X. Wu, N. Zheng, J. Wang, G. Ji, Y. Chen, G. Zhou, Z. Liang, *MetalMat* **2024**, 1, 5, <https://doi.org/10.1002/metm.5>.
- [40] J. Matthey, *Johnson Matthey to Improve the Sustainability of Li-Ion Battery Manufacturing with Partners OnTo Technology and the UK Battery Industrialisation Centre*, <https://matthey.com/documents/161599/166306/BMR-OnTo-press-release-FINAL.pdf> (accessed: August, 2025).
- [41] C. Marxstand B. Group, *Innovative Direct Recycling at the BMW Group: New Competence Centre in Lower Bavaria Returns Battery Cell Raw Materials to the Loop*, <https://www.press.bmwgroup.com/global/article/detail/T0446534EN/> (accessed: August, 2025).
- [42] E. Fan, L. Li, Z. Wang, J. Lin, Y. Huang, Y. Yao, R. Chen, F. Wu, *Chem. Rev.* **2020**, 120, 7020, <https://doi.org/10.1021/acs.chemrev.9b00535>.
- [43] Act on the Promotion of Effective Utilization of Resources, <https://www.japaneselawtranslation.go.jp/en/laws/view/3819/en> (accessed: April, 2025).
- [44] Council Directive 91/157/EEC of 18 March 1991 on Batteries and Accumulators Containing Certain Dangerous Substances, <https://eur-lex.europa.eu/eli/dir/1991/157/oj> (accessed: March, 2025).
- [45] Regulation (EU) 2023/1542 of the European Parliament and of the Council of 12 July 2023, <https://eur-lex.europa.eu/eli/reg/2023/1542> (accessed: May, 2025).
- [46] Critical Raw Materials, [https://single-market-economy.ec.europa.eu/sectors/raw-materials/areas-specific-interest/critical-raw-materials\\_en](https://single-market-economy.ec.europa.eu/sectors/raw-materials/areas-specific-interest/critical-raw-materials_en) (accessed: August, 2025).
- [47] Electronic Waste Recycling Act of 2003: Covered Battery-Embedded Products, [https://leginfo.legislature.ca.gov/faces/billTextClient.xhtml?bill\\_id=202120220SB1215](https://leginfo.legislature.ca.gov/faces/billTextClient.xhtml?bill_id=202120220SB1215) (accessed: September, 2024).
- [48] X. Wang, G. Gaustad, C. W. Babbitt, K. Richa, *Resourc. Conserv. Recycl.* **2014**, 83, 53, <https://doi.org/10.1016/j.resconrec.2013.11.009>.
- [49] CNBC, *Dead EV batteries turn to gold with US incentives*, <https://www.cnbc.com/2023/07/21/dead-ev-batteries-turn-to-gold-with-us-incentives.html> (accessed: August, 2025).
- [50] M. O. L. A. I. Technology, *Joint Notice on Promoting the Coordinated and Stable Development of the Lithium-Ion Battery Industrial Chain and Supply Chain Issued by the Two Departments* [https://www.gov.cn/zhengce/zhengceku/2022-11/20/content\\_5727976.htm](https://www.gov.cn/zhengce/zhengceku/2022-11/20/content_5727976.htm) (accessed: February, 2025).
- [51] M. O. E. Protection, *Announcement on Issuing the Technical Policy for Pollution Prevention and Control in Lead-Acid Battery Remanufacturing and Production and the Technical Policy for Spent Battery Pollution Prevention and Control* [https://www.mee.gov.cn/gkml/hbb/bgg/201612/t20161228\\_378325.htm](https://www.mee.gov.cn/gkml/hbb/bgg/201612/t20161228_378325.htm) (accessed: February, 2025).
- [52] M. O. I. A. I. Technology, *Joint Notice on Organizing and Conducting the Pilot Program for Recycling of New Energy Vehicle Power Batteries*, [https://www.gov.cn/xinwen/2018-03/05/content\\_5270958.htm](https://www.gov.cn/xinwen/2018-03/05/content_5270958.htm) (accessed: February, 2025).
- [53] MIIT, *Administrative Measures for Recycling and Utilization of Power Batteries for New Energy Vehicles*, [https://www.miit.gov.cn/jgsj/jns/gzdt/art/2023/art\\_43c4326b13974aa2b78045c85d7bc583.html](https://www.miit.gov.cn/jgsj/jns/gzdt/art/2023/art_43c4326b13974aa2b78045c85d7bc583.html) (accessed: August, 2025).
- [54] F. Larouche, F. Tedjar, K. Amouzegar, G. Houlachi, P. Bouchard, G. P. Demopoulos, K. Zaghib, *Materials* **2020**, 13, 801, <https://doi.org/10.3390/ma13030801>.
- [55] Y. Yang, Z. Liu, J. Zhang, Y. Chen, C. Wang, *J. Alloys Compd.* **2023**, 947, 169660, <https://doi.org/10.1016/j.jallcom.2023.169660>.
- [56] G. Harper, R. Sommerville, E. Kendrick, L. Driscoll, P. Slater, R. Stolkin, A. Walton, P. Christensen, O. Heidrich, S. Lambert, A. Abbott, K. Ryder, L. Gaines, P. Anderson, *Nature* **2019**, 575, 75, <https://doi.org/10.1038/s41586-019-1682-5>.

- [57] Z. H. I. Sun, Y. Xiao, J. Sietsma, H. Agterhuis, G. Visser, Y. Yang, *Hydrometallurgy* **2015**, *152*, 91, <https://doi.org/10.1016/j.hydromet.2014.12.013>.
- [58] J. J. Roy, D. M. Phuong, V. Verma, R. Chaudhary, M. Carboni, D. Meyer, B. Cao, M. Srinivasan, *Carbon Energy* **2024**, *6*, 492, <https://doi.org/10.1002/cey2.492>.
- [59] Y. Hua, S. Zhou, Y. Huang, X. Liu, H. Ling, X. Zhou, C. Zhang, S. Yang, *J. Power Sources* **2020**, *478*, 228753, <https://doi.org/10.1016/j.jpowsour.2020.228753>.
- [60] S. Ojanen, M. Lundström, A. Santasalo-Aarnio, R. Serna-Guerrero, *Waste Manage.* **2018**, *76*, 242, <https://doi.org/10.1016/j.wasman.2018.03.045>.
- [61] M. O. I. A. I. Technology, *Recovery of Traction Battery Used in Electric Vehicle—Recycling—Part 3 : Specification for Discharging*, <https://openstd.samr.gov.cn/bzgk/gb/newGblinfo?hcno=5CEDE34989D8702192CB593537DA1E9F> (accessed: February, 2025).
- [62] H. Wang, G. Qu, J. Yang, S. Zhou, B. Li, Y. Wei, *J. Energy Storage* **2022**, *54*, 105383, <https://doi.org/10.1016/j.est.2022.105383>.
- [63] D. Thompson, C. Hyde, J. M. Hartley, A. P. Abbott, P. A. Anderson, G. D. J. Harper, *Resour. Conserv. Recycl.* **2021**, *175*, 105741, <https://doi.org/10.1016/j.resconrec.2021.105741>.
- [64] Y. Yao, M. Zhu, Z. Zhao, B. Tong, Y. Fan, Z. Hua, *ACS Sustainable Chem. Eng.* **2018**, *6*, 13611, <https://doi.org/10.1021/acssuschemeng.8b03545>.
- [65] X. Zeng, J. Li, H. Xie, L. Liu, *Chemosphere* **2013**, *93*, 1288, <https://doi.org/10.1016/j.chemosphere.2013.06.063>.
- [66] L. Li, R. Chen, F. Sun, F. Wu, J. Liu, *Hydrometallurgy* **2011**, *108*, 220, <https://doi.org/10.1016/j.hydromet.2011.04.013>.
- [67] M. Choux, E. Martí Bigorra, I. Tyapin, *Metals* **2021**, *11*, 387, <https://doi.org/10.3390/met11030387>.
- [68] D. L. Thompson, J. M. Hartley, S. M. Lambert, M. Shiref, G. D. J. Harper, E. Kendrick, P. Anderson, K. S. Ryder, L. Gaines, A. P. Abbott, *Green Chem.* **2020**, *22*, 7585, <https://doi.org/10.1039/d0gc02745f>.
- [69] L. Wang, T. Liu, X. Peng, W. Zeng, Z. Jin, W. Tian, B. Gao, Y. Zhou, P. K. Chu, K. Huo, *Adv. Funct. Mater.* **2018**, *28*, 1704858, <https://doi.org/10.1002/adfm.201704858>.
- [70] Y. Zhao, Y. Kang, M. Fan, T. Li, J. Wozny, Y. Zhou, X. Wang, Y.-L. Chueh, Z. Liang, G. Zhou, J. Wang, N. Tavajohi, F. Kang, B. Li, *Energy Storage Mater.* **2022**, *45*, 1092, <https://doi.org/10.1016/j.ensm.2021.11.005>.
- [71] L. Kong, F. Liu, X. Hu, Z. Shi, A. Liu, X. Wang, *Energy Sourc., Part A: Recov., Utiliz. Environ. Eff.* **2023**, *45*, 877, <https://doi.org/10.1080/15567036.2023.2172105>.
- [72] E. Gratz, Q. Sa, D. Apelian, Y. Wang, *J. Power Sources* **2014**, *262*, 255, <https://doi.org/10.1016/j.jpowsour.2014.03.126>.
- [73] G. P. Nayaka, Y. Zhang, P. Dong, M. Wang, Z. Zhou, J. Duan, X. Li, Y. Lin, Q. Meng, K. V. Pai, J. Manjanna, G. Santhosh, *J. Environ. Chem. Eng.* **2019**, *7*, 102854, <https://doi.org/10.1016/j.jece.2018.102854>.
- [74] W. Yang, Z. Tong, X. Bu, L. Dong, *J. Ind. Eng. Chem.* **2025**, *148*, 27, <https://doi.org/10.1016/j.jiec.2024.12.074>.
- [75] Z. Qin, J. Li, T. Zhang, Z. Wen, Z. Zheng, Y. Zhang, N. Zhang, C. Jia, X. Liu, G. Chen, *J. Mater. Chem. A* **2022**, *10*, 23905, <https://doi.org/10.1039/d2ta06959h>.
- [76] G. Zeng, J. Yao, C. Liu, X. Luo, H. Ji, X. Mi, C. Deng, *ACS Sustainable Chem. Eng.* **2021**, *9*, 16133, <https://doi.org/10.1021/acssuschemeng.1c04806>.
- [77] Y. Xu, D. Song, L. Li, C. An, Y. Wang, L. F. Jiao, H. Yuan, *J. Power Sources* **2014**, *252*, 286, <https://doi.org/10.1016/j.jpowsour.2013.11.052>.
- [78] K. Liu, F.-S. Zhang, *J. Hazard. Mater.* **2016**, *316*, 19, <https://doi.org/10.1016/j.jhazmat.2016.04.080>.
- [79] M. Wang, Q. Tan, L. Liu, J. Li, *ACS Sustainable Chem. Eng.* **2019**, *7*, 8287, <https://doi.org/10.1021/acssuschemeng.8b06694>.
- [80] L. Li, J. B. Dunn, X. X. Zhang, L. Gaines, R. J. Chen, F. Wu, K. Amine, *J. Power Sources* **2013**, *233*, 180, <https://doi.org/10.1016/j.jpowsour.2012.12.089>.
- [81] D. Wang, H. Wen, H. Chen, Y. Yang, H. Liang, *Chem. Res. Chin. Univ.* **2016**, *32*, 674, <https://doi.org/10.1007/s40242-016-5490-2>.
- [82] M. Wang, Q. Tan, L. Liu, J. Li, *J. Hazard. Mater.* **2019**, *380*, 120846, <https://doi.org/10.1016/j.jhazmat.2019.120846>.
- [83] E. Fan, L. Li, X. Zhang, Y. Bian, Q. Xue, J. Wu, F. Wu, R. Chen, *ACS Sustainable Chem. Eng.* **2018**, *6*, 11029, <https://doi.org/10.1021/acssuschemeng.8b02503>.
- [84] Y. Zhao, L.-Z. Fang, Y.-Q. Kang, L. Wang, Y.-N. Zhou, X.-Y. Liu, T. Li, Y.-X. Li, Z. Liang, Z.-X. Zhang, B.-H. Li, *Rare Met.* **2021**, *40*, 1431, <https://doi.org/10.1007/s12598-020-01587-y>.
- [85] G. Granata, F. Pagnanelli, E. Moscardini, Z. Takacova, T. Havlik, L. Toro, *J. Power Sources* **2012**, *212*, 205, <https://doi.org/10.1016/j.jpowsour.2012.04.016>.
- [86] P. Li, S. Luo, G. Hao, K. Sun, Q. Liu, M. Møller, D. Wang, P. Kær Kristensen, L. Gurevich, L. R. Jensen, L. Wang, X. He, *J. Hazard. Mater.* **2025**, *481*, 136553, <https://doi.org/10.1016/j.jhazmat.2024.136553>.
- [87] Y. Shi, G. Chen, Z. Chen, *Green Chem.* **2018**, *20*, 851, <https://doi.org/10.1039/c7gc02831h>.
- [88] M. S. Whittingham, *Chem. Rev.* **2004**, *104*, 4271.
- [89] Y. Yao, Z. Xue, C. Li, J. Li, J. He, X. Zhang, Y. Xiang, *Energy Storage Mater.* **2024**, *71*, 103666, <https://doi.org/10.1016/j.ensm.2024.103666>.
- [90] J. Wang, J. Ma, K. Jia, Z. Liang, G. Ji, Y. Zhao, B. Li, G. Zhou, H.-M. Cheng, *ACS Energy Lett.* **2022**, *7*, 2816, <https://doi.org/10.1021/acsenergylett.2c01539>.
- [91] A. J. Merryweather, C. Schnedermann, Q. Jacquet, C. P. Grey, A. Rao, *Nature* **2021**, *594*, 522, <https://doi.org/10.1038/s41586-021-03584-2>.
- [92] H. J. Kim, Y. Park, Y. Kwon, J. Shin, Y.-H. Kim, H.-S. Ahn, R. Yazami, J. W. Choi, *Energy Environ. Sci.* **2020**, *13*, 286, <https://doi.org/10.1039/c9ee02964h>.
- [93] X. Yang, C. Wang, P. Yan, T. Jiao, J. Hao, Y. Jiang, F. Ren, W. Zhang, J. Zheng, Y. Cheng, X. Wang, W. Yang, J. Zhu, S. Pan, M. Lin, L. Zeng, Z. Gong, J. Li, Y. Yang, *Adv. Energy Mater.* **2022**, *12*, 2200197, <https://doi.org/10.1002/aenm.202200197>.
- [94] S. Li, K. Li, J. Zheng, Q. Zhang, B. Wei, X. Lu, *J. Phys. Chem. Lett.* **2019**, *10*, 7537, <https://doi.org/10.1021/acs.jpclett.9b02711>.
- [95] Y. Yan, S. Weng, A. Fu, H. Zhang, J. Chen, Q. Zheng, B. Zhang, S. Zhou, H. Yan, C.-W. Wang, Y. Tang, H. Luo, B.-W. Mao, J. Zheng, X. Wang, Y. Qiao, Y. Yang, S.-G. Sun, *ACS Energy Lett.* **2022**, *7*, 2677, <https://doi.org/10.1021/acsenergylett.2c01433>.
- [96] Y. Zhang, X. Tan, L. Song, D. Mao, Z. Fan, S. Su, P. Zhang, J. Xie, Z. Lu, W. Chu, *Mater. Today Energy* **2023**, *34*, 101313, <https://doi.org/10.1016/j.mtener.2023.101313>.
- [97] H. Nie, L. Xu, D. Song, J. Song, X. Shi, X. Wang, L. Zhang, Z. Yuan, *Green Chem.* **2015**, *17*, 1276, <https://doi.org/10.1039/c4gc01951b>.
- [98] X. Mu, K. Huang, G. Zhu, Y. Li, C. Liu, X. Hui, M. Sui, P. Yan, *Nano Energy* **2023**, *112*, 108465, <https://doi.org/10.1016/j.nanoen.2023.108465>.
- [99] L. Kong, Z. Li, W. Zhu, C. R. Ratwani, N. Fernando, S. Karunaratne, A. M. Abdelkader, A. R. Kamali, Z. Shi, *J. Colloid Interface Sci.* **2023**, *640*, 1080, <https://doi.org/10.1016/j.jcis.2023.03.021>.
- [100] S.-D. Zhang, J. Wang, M.-Y. Qi, S.-J. Guo, H. Jin, H. Ji, Y.-R. Lu, T.-S. Chan, A.-M. Cao, *ACS Energy Lett.* **2024**, *9*, 4976, <https://doi.org/10.1021/acsenergylett.4c02219>.
- [101] J. Wang, K. Jia, J. Ma, Z. Liang, Z. Zhuang, Y. Zhao, B. Li, G. Zhou, H.-M. Cheng, *Nat. Sustain.* **2023**, *6*, 797, <https://doi.org/10.1038/s41893-023-01094-9>.
- [102] H. Lei, Z. Zeng, J. Li, X. Cui, B. Wang, Y. Shi, W. Sun, X. Ji, Y. Yang, P. Ge, *Adv. Funct. Mater.* **2024**, *34*, 2416085, <https://doi.org/10.1002/adfm.202402325>.
- [103] H. Lei, X. Cui, Z. Zeng, C. Zhu, W. Sun, Y. Yang, P. Ge, *Angew. Chem., Int. Ed.* **2025**, *64*, 202414918, <https://doi.org/10.1002/anie.202414918>.
- [104] Z. Liu, H. Li, M. Han, L. Fang, Z. Fu, H. Zhang, G. Wang, Y. Zhang, *Adv. Energy Mater.* **2023**, *13*, 2302058, <https://doi.org/10.1002/aenm.202302058>.
- [105] Z. Yang, C. Xing, L. Chen, S. Tao, Y. Zhang, G. Wang, P. Yang, J. Zhou, C. Zhang, J. Chen, L. Fei, *Adv. Funct. Mater.* **2025**, *35*, 2409737, <https://doi.org/10.1002/adfm.202409737>.
- [106] S. Zhao, W. Zhang, G. Li, H. Zhu, J. Huang, W. He, *Resour. Conserv. Recycl.* **2020**, *162*, 105019, <https://doi.org/10.1016/j.resconrec.2020.105019>.
- [107] Y. Liu, H. Yu, Y. Wang, D. Tang, W. Qiu, W. Li, J. Li, *Waste Manage.* **2022**, *143*, 186, <https://doi.org/10.1016/j.wasman.2022.02.024>.
- [108] J. Wang, Q. Zhang, J. Sheng, Z. Liang, J. Ma, Y. Chen, G. Zhou, H.-M. Cheng, *Natl. Sci. Rev.* **2022**, *9*, nwac097, <https://doi.org/10.1093/nsr/nwac097>.
- [109] M. K. Tran, M.-T. F. Rodrigues, K. Kato, G. Babu, P. M. Ajayan, *Nat. Energy* **2019**, *4*, 339, <https://doi.org/10.1038/s41560-019-0368-4>.
- [110] Z. Fei, Y. Su, Q. Meng, P. Dong, Y. Zhang, *Energy Storage Mater.* **2023**, *60*, 102833, <https://doi.org/10.1016/j.ensm.2023.102833>.
- [111] J. Yang, W. Wang, H. Yang, D. Wang, *Green Chem.* **2020**, *22*, 6489, <https://doi.org/10.1039/d0gc02662j>.
- [112] H. Yang, B. Deng, X. Jing, W. Li, D. Wang, *Waste Manage.* **2021**, *129*, 85, <https://doi.org/10.1016/j.wasman.2021.04.052>.
- [113] G. Gao, Y. Zhu, S. Di, J. Zhao, C. Liu, S. Wang, L. Li, *Acta Mater.* **2024**, *273*, 119969, <https://doi.org/10.1016/j.actamat.2024.119969>.
- [114] X. Zhao, Z. Fei, J. Yan, Q. Meng, P. Dong, *J. Energy Storage* **2024**, *83*, 110344, <https://doi.org/10.1016/j.est.2023.110344>.

- [115] Z. Fei, Y. Zhang, Q. Meng, P. Dong, Y. Li, J. Fei, H. Qi, J. Yan, *J. Hazard. Mater.* **2022**, *432*, 128664, <https://doi.org/10.1016/j.jhazmat.2022.128664>.
- [116] M. Xu, C. Wu, L. Ye, Y. Zhang, C. Zhang, J. Hu, R. Tan, D. Gu, X. Wang, O. Fontaine, C. Zhan, L. Zhuang, X. Ai, J. Qian, *Adv. Energy Mater.* **2024**, *14*, <https://doi.org/10.1002/aenm.202401197>.
- [117] T. Yang, Y. Lu, L. Li, D. Ge, H. Yang, W. Leng, H. Zhou, X. Han, N. Schmidt, M. Ellis, Z. Li, *Adv. Sustainable Syst.* **2020**, *4*, 1900088, <https://doi.org/10.1002/adsu.201900088>.
- [118] L. Zhang, Z. Xu, Z. He, *ACS Sustainable Chem. Eng.* **2020**, *8*, 11596, <https://doi.org/10.1021/acssuschemeng.0c02854>.
- [119] Y.-C. Yin, C. Li, X. Hu, D. Zuo, L. Yang, L. Zhou, J. Yang, J. Wan, *ACS Energy Lett.* **2023**, *8*, 3005, <https://doi.org/10.1021/acsenergylett.3c00635>.
- [120] R. Liu, W. Yin, Y. Chen, B. Zhong, G. Wang, Y. Liu, Y. Song, Z. Wu, L. Yang, X. Guo, *Indust. Eng. Chem. Res.* **2020**, *59*, 17911, <https://doi.org/10.1021/acs.iecr.0c03490>.
- [121] X. Lou, P. Yan, B. Jiao, Q. Li, P. Xu, L. Wang, L. Zhang, M. Cao, G. Wang, Z. Chen, Q. Zhang, J. Chen, *Nat. Commun.* **2024**, *15*, 2730, <https://doi.org/10.1038/s41467-024-47024-x>.
- [122] N. Chen, J. Qi, X. Du, Y. Wang, W. Zhang, Y. Wang, Y. Lu, S. Wang, *RSC Adv.* **2016**, *6*, 103541, <https://doi.org/10.1039/c6ra23483f>.
- [123] C. Huang, H. Lv, Z. Yang, C. Lian, J. Du, G. Liu, W. Tang, Z. Xu, Z. Chi, H. Liu, H. Huang, W. Zhang, *J. Mater. Chem. A* **2022**, *10*, 3359, <https://doi.org/10.1039/d1ta08046f>.
- [124] C. Yang, Z. Jin, X. Zhang, X. Zheng, X. He, *ChemElectroChem* **2022**, *9*, 202101494, <https://doi.org/10.1002/celec.202101494>.
- [125] L. Liu, M. Li, L. Chu, B. Jiang, R. Lin, X. Zhu, G. Cao, *Prog. Mater. Sci.* **2020**, *111*, 100655, <https://doi.org/10.1016/j.pmatsci.2020.100655>.
- [126] W. Li, E. M. Erickson, A. Manthiram, *Nat. Energy* **2020**, *5*, 26, <https://doi.org/10.1038/s41560-019-0513-0>.
- [127] J. Sun, X. Cao, H. Yang, P. He, M. A. Dato, J. Cabana, H. Zhou, *Angew. Chem., Int. Ed.* **2022**, *61*, 202207225, <https://doi.org/10.1002/anie.202207225>.
- [128] T. Liu, L. Yu, J. Lu, T. Zhou, X. Huang, Z. Cai, A. Dai, J. Gim, Y. Ren, X. Xiao, M. V. Holt, Y. S. Chu, I. Arslan, J. Wen, K. Amine, *Nat. Commun.* **2021**, *12*, 6024, <https://doi.org/10.1038/s41467-021-26290-z>.
- [129] L. Wang, T. Liu, T. Wu, J. Lu, *Nature* **2022**, *611*, 61, <https://doi.org/10.1038/s41586-022-05238-3>.
- [130] Y. Bi, J. Tao, Y. Wu, L. Li, Y. Xu, E. Hu, B. Wu, J. Hu, C. Wang, J.-G. Zhang, Y. Qi, J. Xiao, *Science* **2020**, *370*, 1313.
- [131] J. Zheng, Y. Ye, T. Liu, Y. Xiao, C. Wang, F. Wang, F. Pan, *Acc. Chem. Res.* **2019**, *52*, 2201, <https://doi.org/10.1021/acs.accounts.9b00033>.
- [132] M. Li, J. Lu, *Science* **2020**, *367*, 979.
- [133] K. Nansai, K. Nakajima, S. Kagawa, Y. Kondo, S. Suh, Y. Shigetomi, Y. Oshita, *Environ. Sci. Technol.* **2014**, *48*, 1391, <https://doi.org/10.1021/es4033452>.
- [134] H.-X. Wei, L.-B. Tang, Y.-D. Huang, Z.-Y. Wang, Y.-H. Luo, Z.-J. He, C. Yan, J. Mao, K.-H. Dai, J.-C. Zheng, *Mater. Today* **2021**, *51*, 365, <https://doi.org/10.1016/j.mattod.2021.09.013>.
- [135] G. Liang, V. K. Peterson, K. W. See, Z. Guo, W. K. Pang, *J. Mater. Chem. A* **2020**, *8*, 15373, <https://doi.org/10.1039/d0ta02812f>.
- [136] W. Liu, P. Oh, X. Liu, M.-J. Lee, W. Cho, S. Chae, Y. Kim, J. Cho, *Angew. Chem., Int. Ed.* **2015**, *54*, 4440, <https://doi.org/10.1002/anie.201409262>.
- [137] Y. Han, S. Heng, Y. Wang, Q. Qu, H. Zheng, *ACS Energy Lett.* **2020**, *5*, 2421, <https://doi.org/10.1021/acsenergylett.0c01032>.
- [138] J. Li, L. Hu, H. Zhou, L. Wang, B. Zhai, S. Yang, P. Meng, R. Hu, *J. Mater. Sci.: Mater. Electron.* **2018**, *29*, 17661, <https://doi.org/10.1007/s10854-018-9870-x>.
- [139] M. Fan, X. Chang, Y.-J. Guo, W.-P. Chen, Y.-X. Yin, X. Yang, Q. Meng, L.-J. Wan, Y.-G. Guo, *Energy Environ. Sci.* **2021**, *14*, 1461, <https://doi.org/10.1039/d0ee03914d>.
- [140] S. Jin, Z.-A. Lu, D. Mu, T. Lin, W. Zhang, Y. Zhang, D. Chen, R. Li, C. Dai, *Adv. Funct. Mater.* **2025**, *35*, 2416085, <https://doi.org/10.1002/adfm.202416085>.
- [141] Y. Han, Y. You, C. Hou, X. Xiao, Y. Xing, Y. Zhao, *J. Electrochem. Soc.* **2021**, *168*, 040525, <https://doi.org/10.1149/1945-7111/abf4e8>.
- [142] Z. Chi, J. Li, L. Wang, T. Li, Y. Wang, Y. Zhang, S. Tao, M. Zhang, Y. Xiao, Y. Chen, *Green Chem.* **2021**, *23*, 9099, <https://doi.org/10.1039/d1gc03526f>.
- [143] Y. Guo, C. Guo, P. Huang, Q. Han, F. Wang, H. Zhang, H. Liu, Y.-C. Cao, Y. Yao, Y. Huang, *eScience* **2023**, *3*, 100091, <https://doi.org/10.1016/j.esci.2023.100091>.
- [144] B. J. Ross, M. LeResche, D. Liu, J. L. Durham, E. U. Dahl, A. L. Lipson, *ACS Sustainable Chem. Eng.* **2020**, *8*, 12511, <https://doi.org/10.1021/acssuschemeng.0c03424>.
- [145] N. Zheng, H. Ji, J. Wang, M. Zhang, L. Wei, R. Shi, K. Jia, X. Wu, X. Xiao, Z. Zhuang, B. Li, H.-M. Cheng, G. Zhou, *J. Am. Chem. Soc.* **2024**, *146*, 27819, <https://doi.org/10.1021/jacs.4c10107>.
- [146] Y. Shi, G. Chen, F. Liu, X. Yue, Z. Chen, *ACS Energy Lett.* **2018**, *3*, 1683, <https://doi.org/10.1021/acsenergylett.8b00833>.
- [147] W. Kwak, J. Ha, J. Lee, J.-H. Song, S. C. Nam, Y.-T. Kim, J. Choi, *J. Power Sources* **2024**, *617*, 235102, <https://doi.org/10.1016/j.jpowsour.2024.235102>.
- [148] V. Gupta, X. Yu, H. Gao, C. Brooks, W. Li, Z. Chen, *Adv. Energy Mater.* **2023**, *13*, 2203093, <https://doi.org/10.1002/aenm.202203093>.
- [149] Y. Guo, X. Liao, P. Huang, P. Lou, Y. Su, X. Hong, Q. Han, R. Yu, Y.-C. Cao, S. Chen, *Energy Storage Mater.* **2021**, *43*, 348, <https://doi.org/10.1016/j.jensm.2021.09.016>.
- [150] P. Xu, Z. Yang, X. Yu, J. Holoubek, H. Gao, M. Li, G. Cai, I. Bloom, H. Liu, Y. Chen, K. An, K. Z. Pupek, P. Liu, Z. Chen, *ACS Sustainable Chem. Eng.* **2021**, *9*, 4543, <https://doi.org/10.1021/acssuschemeng.0c09017>.
- [151] X. Yu, S. Yu, Z. Yang, H. Gao, P. Xu, G. Cai, S. Rose, C. Brooks, P. Liu, Z. Chen, *Energy Storage Mater.* **2022**, *51*, 54, <https://doi.org/10.1016/j.jensm.2022.06.017>.
- [152] X. Yu, S. Yu, J. Lin, V. Gupta, H. Gao, W. Li, M. Appleberry, P. Liu, Z. Chen, *Adv. Mater.* **2024**, *36*, 2408463, <https://doi.org/10.1002/adma.202408463>.
- [153] Y. Liu, B. Jiao, X. Guo, S. Li, X. Lou, F. Jiang, X. Weng, M. Cao, J. Chen, Q. Zhang, G. Wang, J. Di, P. Xu, *Energy Storage Mater.* **2024**, *72*, 103684, <https://doi.org/10.1016/j.jensm.2024.103684>.
- [154] K. Jia, J. Wang, Z. Zhuang, Z. Piao, M. Zhang, Z. Liang, G. Ji, J. Ma, H. Ji, W. Yao, G. Zhou, H.-M. Cheng, *J. Am. Chem. Soc.* **2023**, *145*, 7288, <https://doi.org/10.1021/jacs.2c13151>.
- [155] L. Chen, C. Xing, Z. Yang, S. Tao, Y. Zhang, G. Wang, P. Yang, J. Song, J. Chen, L. Fei, *Adv. Funct. Mater.* **2025**, *35*, 2411182, <https://doi.org/10.1002/adfm.202411182>.
- [156] G. Jiang, Y. Zhang, Q. Meng, Y. Zhang, P. Dong, M. Zhang, X. Yang, *ACS Sustainable Chem. Eng.* **2020**, *8*, 18138, <https://doi.org/10.1021/acssuschemeng.0c06514>.
- [157] J. Ma, J. Wang, K. Jia, Z. Liang, G. Ji, Z. Zhuang, G. Zhou, H.-M. Cheng, *J. Am. Chem. Soc.* **2022**, *144*, 20306, <https://doi.org/10.1021/jacs.2c07860>.
- [158] Z. Qin, Z. Wen, Y. Xu, Z. Zheng, M. Bai, N. Zhang, C. Jia, H. B. Wu, G. Chen, *Small* **2022**, *18*, 2106719, <https://doi.org/10.1002/smll.202106719>.
- [159] X. Liu, R. Wang, S. Liu, J. Pu, H. Xie, M. Wu, D. Liu, Y. Li, J. Liu, *Adv. Energy Mater.* **2023**, *13*, 2302987, <https://doi.org/10.1002/aenm.202302987>.
- [160] Z. Qin, Y. Zhang, W. Luo, T. Zhang, T. Wang, L. Ni, H. Wang, N. Zhang, X. Liu, J. Zhou, G. Chen, *Angew. Chem., Int. Ed.* **2023**, *62*, 202218672, <https://doi.org/10.1002/anie.202218672>.
- [161] Z. Qin, T. Zhang, X. Gao, W. Luo, J. Han, B. Lu, J. Zhou, G. Chen, *Adv. Mater.* **2024**, *36*, 2307091, <https://doi.org/10.1002/adma.202307091>.
- [162] C. Xing, H. Da, P. Yang, J. Huang, M. Gan, J. Zhou, Y. Li, H. Zhang, B. Ge, L. Fei, *ACS Nano* **2023**, *17*, 3194, <https://doi.org/10.1021/acsnano.3c00270>.
- [163] H. Ji, J. Wang, H. Qu, J. Li, W. Ji, X. Qiu, Y. Zhu, H. Ren, R. Shi, G. Ji, W. Zhao, G. Zhou, *Adv. Mater.* **2024**, *36*, 2407029, <https://doi.org/10.1002/adma.202407029>.
- [164] K. Jia, Y. He, Z. Piao, Z. Cao, M. Zhang, Y. Zhu, L. Li, Z. Liang, R. V. Kumar, G. Zhou, S. Ding, K. Xi, *Adv. Mater.* **2025**, *37*, 2413753, <https://doi.org/10.1002/adma.202413753>.
- [165] K. Park, J. Yu, J. Coyle, Q. Dai, S. Frisco, M. Zhou, A. Burrell, *ACS Sustainable Chem. Eng.* **2021**, *9*, 8214, <https://doi.org/10.1021/acssuschemeng.1c02133>.
- [166] X. Li, F. Dogan, Y. Lu, C. Antunes, Y. Shi, A. Burrell, C. Ban, *Adv. Sustainable Syst.* **2020**, *4*, 2000073, <https://doi.org/10.1002/adssu.202000073>.
- [167] J. Ma, J. Wang, K. Jia, Z. Liang, G. Ji, H. Ji, Y. Zhu, W. Chen, H.-M. Cheng, G. Zhou, *Nat. Commun.* **2024**, *15*, 1046, <https://doi.org/10.1038/s41467-024-45091-8>.
- [168] H. Wang, X. Geng, L. Hu, J. Wang, Y. Xu, Y. Zhu, Z. Liu, J. Lu, Y. Lin, X. He, *Nat. Commun.* **2024**, *15*, 1634, <https://doi.org/10.1038/s41467-024-45754-6>.
- [169] N. Ogihara, K. Nagaya, H. Yamaguchi, Y. Kondo, Y. Yamada, T. Horiba, T. Baba, N. Ohba, S. Komagata, Y. Aoki, H. Kondo, T. Sasaki, S. Okayama, *Joule* **2024**, *8*, 1364, <https://doi.org/10.1016/j.joule.2024.02.010>.

- [170] A. K. Padhi, K. S. Nanjundaswamy, J. B. Goodenough, *J. Electrochem. Soc.* **1997**, *144*, 1188.
- [171] R. V. Salvatierra, W. Chen, J. M. Tour, *Adv. Energy Sustain. Res.* **2021**, *2*, 2000110, <https://doi.org/10.1002/aesr.202000110>.
- [172] Q. Cheng, X. Zhao, G. Yang, L. Mao, F. Liao, L. Chen, P. He, D. Pan, S. Chen, *Energy Storage Mater.* **2021**, *41*, 842, <https://doi.org/10.1016/j.ensm.2021.07.017>.
- [173] K. Liu, Y. Liu, D. Lin, A. Pei, Y. Cui, *Sci. Adv.* **2018**, *4*, 9820.
- [174] J. Li, Z.-F. Ma, *Chem.* **2019**, *5*, 3, <https://doi.org/10.1016/j.chempr.2018.12.012>.
- [175] H. Bajolle, M. Lagadic, N. Louvet, *Energy Res. Soc. Sci.* **2022**, *93*, 102850, <https://doi.org/10.1016/j.erss.2022.102850>.
- [176] H. Wang, H. Xu, Z. Zhang, Q. Wang, C. Jin, C. Wu, C. Xu, J. Hao, L. Sun, Z. Du, Y. Li, J. Sun, X. Feng, *eTransportation* **2022**, *13*, 100190, <https://doi.org/10.1016/j.etran.2022.100190>.
- [177] H. M. Barkholtz, Y. Preger, S. Ivanov, J. Langendorf, L. Torres-Castro, J. Lamb, B. Chalamala, S. R. Ferreira, *J. Power Sources* **2019**, *435*, 226777, <https://doi.org/10.1016/j.jpowsour.2019.226777>.
- [178] J. Wang, X. Sun, *Energy Environ. Sci.* **2015**, *8*, 1110, <https://doi.org/10.1039/c4ee04016c>.
- [179] W. A. Ślawiński, H. Y. Playford, S. Hull, S. T. Norberg, S. G. Eriksson, T. Gustafsson, K. Edström, W. R. Brant, *Chem. Mater.* **2019**, *31*, 5024, <https://doi.org/10.1021/acs.chemmater.9b00552>.
- [180] W. Zhang, H.-C. Yu, L. Wu, H. Liu, A. Abdellahi, B. Qiu, J. Bai, B. Orvananos, F. C. Strobridge, X. Zhou, Z. Liu, G. Ceder, Y. Zhu, K. Thornton, C. P. Grey, F. Wang, *Sci. Adv.* **2018**, *4*, 2608.
- [181] G. Ji, J. Wang, Z. Liang, K. Jia, J. Ma, Z. Zhuang, G. Zhou, H.-M. Cheng, *Nat. Commun.* **2023**, *14*, 584, <https://doi.org/10.1038/s41467-023-36197-6>.
- [182] J. Lim, Y. Li, D. H. Alsem, H. So, S. C. Lee, P. Bai, D. A. Cogswell, X. Liu, N. Jin, Y.-S. Yu, N. J. Salmon, D. A. Shapiro, M. Z. Bazant, T. Tylyszczak, W. C. Chueh, *Science* **2016**, *353*, 566.
- [183] J. Hu, H. Zeng, X. Chen, Z. Wang, H. B. Wang, R. Wang, L. Wu, Q. Huang, L. Kong, J. Zheng, Y. Xiao, W. Zhang, F. Pan, *J. Phys. Chem. Lett.* **2019**, *10*, 4794, <https://doi.org/10.1021/acs.jpclett.9b01557>.
- [184] J. Chen, Q. Li, J. Song, D. Song, L. Zhang, X. Shi, *Green Chem.* **2016**, *18*, 2500, <https://doi.org/10.1039/c5gc02650d>.
- [185] B. Wang, Y. Yin, H. Deng, G. Li, H. Zhu, W. He, *Chem. Eng. J.* **2024**, *497*, 154922, <https://doi.org/10.1016/j.cej.2024.154922>.
- [186] Z. Zeng, P. Xu, J. Li, C. Yi, W. Zhao, W. Sun, X. Ji, Y. Yang, P. Ge, *Adv. Funct. Mater.* **2024**, *34*, 2308671, <https://doi.org/10.1002/adfm.202308671>.
- [187] X. Li, M. Wang, Q. Zhou, M. Ge, M. Zhang, W. Liu, Z. Shi, H. Yue, H. Zhang, Y. Yin, S.-T. Yang, *ACS Mater. Lett.* **2024**, *6*, 640, <https://doi.org/10.1021/acsmaterialslett.3c01161>.
- [188] X. Li, Q. Zhou, X. Zhang, M. Ge, H. Zhang, Y. Yin, S.-T. Yang, *ACS Sustainable Chem. Eng.* **2023**, *11*, 14457, <https://doi.org/10.1021/acssuschemeng.3c03232>
- [189] Z. Zeng, H. Lei, J. Li, B. Wang, S. Lei, X. Ji, W. Sun, Y. Yang, P. Ge, *Chem. Eng. J.* **2024**, *499*, 155616, <https://doi.org/10.1016/j.cej.2024.155616>.
- [190] D. Tang, G. Ji, J. Wang, Z. Liang, W. Chen, H. Ji, J. Ma, S. Liu, Z. Zhuang, G. Zhou, *Adv. Mater.* **2024**, *36*, 2309722, <https://doi.org/10.1002/adma.202309722>.
- [191] Y. Cao, J. Li, D. Tang, F. Zhou, M. Yuan, Y. Zhu, C. Feng, R. Shi, X. Wei, B. Wang, Y. Song, H.-M. Cheng, G. Zhou, *Adv. Mater.* **2024**, *36*, 2414048, <https://doi.org/10.1002/adma.202414048>.
- [192] C. Feng, Y. Cao, L. Song, B. Zhao, Q. Yang, Y. Zhang, X. Wei, G. Zhou, Y. Song, *Angew. Chem., Int. Ed.* **2025**, *64*, 202418198, <https://doi.org/10.1002/anie.202418198>.
- [193] K. Jia, J. Ma, J. Wang, Z. Liang, G. Ji, Z. Piao, R. Gao, Y. Zhu, Z. Zhuang, G. Zhou, H.-M. Cheng, *Adv. Mater.* **2023**, *35*, 2208034, <https://doi.org/10.1002/adma.202208034>.
- [194] Y. Xu, B. Zhang, Z. Ge, H. Wang, N. Hong, X. Xiao, B. Song, Y. Zhang, Y. Tian, W. Deng, G. Zou, H. Hou, X. Ji, *Chem. Eng. J.* **2023**, *477*, 147201, <https://doi.org/10.1016/j.cej.2023.147201>.
- [195] P. Xu, Q. Dai, H. Gao, H. Liu, M. Zhang, M. Li, Y. Chen, K. An, Y. S. Meng, P. Liu, Y. Li, J. S. Spanberger, L. Gaines, J. Lu, Z. Chen, *Joule* **2020**, *4*, 2609, <https://doi.org/10.1016/j.joule.2020.10.008>.
- [196] J. Sun, Z. Jiang, P. Jia, S. Li, W. Wang, Z. Song, Y. Mao, X. Zhao, B. Zhou, *Waste Manage.* **2023**, *158*, 125, <https://doi.org/10.1016/j.wasman.2023.01.012>.
- [197] X.-X. Zhao, X.-T. Wang, J.-Z. Guo, Z.-Y. Gu, J.-M. Cao, J.-L. Yang, F.-Q. Lu, J.-P. Zhang, X.-L. Wu, *Adv. Mater.* **2024**, *36*, 2308927, <https://doi.org/10.1002/adma.202308927>.
- [198] D. Yang, Z. Fang, Y. Ji, Y. Yang, J. Hou, Z. Zhang, W. Du, X. Qi, Z. Zhu, R. Zhang, P. Hu, L. Qie, Y. Huang, *Angew. Chem., Int. Ed.* **2024**, *63*, 202409929, <https://doi.org/10.1002/anie.202409929>.
- [199] T. Wang, X. Yu, M. Fan, Q. Meng, Y. Xiao, Y.-X. Yin, H. Li, Y.-G. Guo, *Chem. Commun.* **2020**, *56*, 245, <https://doi.org/10.1039/c9cc08155k>.
- [200] M. Fan, Q. Meng, X. Chang, C.-F. Gu, X.-H. Meng, Y.-X. Yin, H. Li, L.-J. Wan, Y.-G. Guo, *Adv. Energy Mater.* **2022**, *12*, 2103630, <https://doi.org/10.1002/aenm.202103630>.
- [201] D. Peng, X. Wang, S. Wang, B. Zhang, X. Lu, W. Hu, J. Zou, P. Li, Y. Wen, J. Zhang, *Green Chem.* **2022**, *24*, 4544, <https://doi.org/10.1039/d2gc01007k>.
- [202] F. Larouche, K. Amouzegar, A. Vijh, G. P. Demopoulos, *J. Power Sources* **2024**, *624*, 235533, <https://doi.org/10.1016/j.jpowsour.2024.235533>.
- [203] X. Zhao, H. Chen, H. Wu, Y. Zhao, J. Luo, *ACS Nano* **2024**, *18*, 21125, <https://doi.org/10.1021/acsnano.4c03221>.
- [204] G. Ji, D. Tang, J. Wang, Z. Liang, H. Ji, J. Ma, Z. Zhuang, S. Liu, G. Zhou, H.-M. Cheng, *Nat. Commun.* **2024**, *15*, 4086, <https://doi.org/10.1038/s41467-024-48181-9>.
- [205] S. Zhou, J. Du, X. Xiong, L. Liu, J. Wang, L. Fu, J. Ye, Y. Chen, Y. Wu, *Green Chem.* **2022**, *24*, 6278, <https://doi.org/10.1039/d2gc01640k>.
- [206] Y. Qiao, H. Zhao, Y. Shen, L. Li, Z. Rao, G. Shao, Y. Lei, *EcoMat* **2023**, *5*, e12321, <https://doi.org/10.1002/eom.212321>.
- [207] H. Zhang, Y. Yang, D. Ren, L. Wang, X. He, *Energy Storage Mater.* **2021**, *36*, 147, <https://doi.org/10.1016/j.jensm.2020.12.027>.
- [208] S. Natarajan, V. Aravindan, *Adv. Energy Mater.* **2018**, *8*, 1802303, <https://doi.org/10.1002/aenm.201802303>.
- [209] W. Cai, Y.-X. Yao, G.-L. Zhu, C. Yan, L.-L. Jiang, C. He, J.-Q. Huang, Q. Zhang, *Chem. Soc. Rev.* **2020**, *49*, 3806, <https://doi.org/10.1039/c9cs00728h>.
- [210] J. Piątek, S. Afyon, T. M. Budnyak, S. Budnyk, M. H. Sipponen, A. Slabon, *Adv. Energy Mater.* **2021**, *11*, 2003456, <https://doi.org/10.1002/aenm.202003456>.
- [211] H. Xu, Z. Li, T. Liu, C. Han, C. Guo, H. Zhao, Q. Li, J. Lu, K. Amine, X. Qiu, *Angew. Chem., Int. Ed.* **2022**, *61*, 202202894, <https://doi.org/10.1002/anie.202202894>.
- [212] Y. Zhang, N. Song, J. He, R. Chen, X. Li, *Nano Lett.* **2019**, *19*, 512, <https://doi.org/10.1021/acs.nanolett.8b04410>.
- [213] H. Ji, J. Wang, J. Ma, H.-M. Cheng, G. Zhou, *Chem. Soc. Rev.* **2023**, *52*, 8194, <https://doi.org/10.1039/d3cs00254c>.
- [214] Z. Xu, X. Shi, Z. Zhuang, Z. Wang, S. Sun, K. Li, T.-Y. Zhang, *Research* **2021**, *2021*, 176, <https://doi.org/10.34133/2021/9842391>.
- [215] T. Liu, L. Lin, X. Bi, L. Tian, K. Yang, J. Liu, M. Li, Z. Chen, J. Lu, K. Amine, K. Xu, F. Pan, *Nat. Nanotechnol.* **2019**, *14*, 50, <https://doi.org/10.1038/s41565-018-0284-y>.
- [216] G. Wang, M. Yu, X. Feng, *Chem. Soc. Rev.* **2021**, *50*, 2388, <https://doi.org/10.1039/d0cs00187b>.
- [217] S. S. Zhang, L. Ma, J. L. Allen, J. A. Read, *J. Electrochem. Soc.* **2021**, *168*, 040519, <https://doi.org/10.1149/1945-7111/abf40c>.
- [218] Y. Lei, D. Han, J. Dong, L. Qin, X. Li, D. Zhai, B. Li, Y. Wu, F. Kang, *Energy Storage Mater.* **2020**, *24*, 319, <https://doi.org/10.1016/j.jensm.2019.07.043>.
- [219] H. Yu, H. Dai, Y. Zhu, H. Hu, R. Zhao, B. Wu, D. Chen, J. Power Sources **2021**, *481*, 229159, <https://doi.org/10.1016/j.jpowsour.2020.229159>.
- [220] C. Yi, Y. Yang, T. Zhang, X. Wu, W. Sun, L. Yi, *J. Clean. Prod.* **2020**, *277*, 123585, <https://doi.org/10.1016/j.jclepro.2020.123585>.
- [221] Y. Gao, C. Wang, J. Zhang, Q. Jing, B. Ma, Y. Chen, W. Zhang, *ACS Sustainable Chem. Eng.* **2020**, *8*, 9447, <https://doi.org/10.1021/acssuschemeng.0c02321>.
- [222] D. Liu, X. Qu, B. Zhang, J. Zhao, H. Xie, H. Yin, *ACS Sustainable Chem. Eng.* **2022**, *10*, 5739, <https://doi.org/10.1021/acssuschemeng.1c07852>.
- [223] R. Li, S. Zeng, L. Wang, X. Yu, H. Zeng, W. Liu, D. Fu, X. Liu, *J. Alloys Compd.* **2024**, *993*, 174691, <https://doi.org/10.1016/j.jallcom.2024.174691>.
- [224] G. Liu, L. Ma, X. Xi, Z. Nie, *Waste Manage.* **2024**, *178*, 105, <https://doi.org/10.1016/j.wasman.2024.02.023>.
- [225] G. Shi, Y. Cui, J. Wang, J. Cheng, S. Zhang, X. Shao, X. Chen, B. Xin, *J. Alloys Compd.* **2024**, *1009*, 176927, <https://doi.org/10.1016/j.jallcom.2024.176927>.
- [226] Y. Lai, X. Zhu, J. Li, Q. Gou, M. Li, A. Xia, Y. Huang, X. Zhu, Q. Liao, *Chem. Eng. J.* **2023**, *457*, 141196, <https://doi.org/10.1016/j.cej.2022.141196>.
- [227] M. Bhar, S. Ghosh, S. Krishnamurthy, K. Yalamanchili, S. K. Martha, *ACS Sustainable Chem. Eng.* **2022**, *10*, 7515, <https://doi.org/10.1021/acssuschemeng.2c00554>.
- [228] H. Wang, Y. Huang, C. Huang, X. Wang, K. Wang, H. Chen, S. Liu, Y. Wu, K. Xu, W. Li, *Electrochim. Acta* **2019**, *313*, 423, <https://doi.org/10.1016/j.electacta.2019.05.050>.

- [229] D. Yang, Y. Yang, H. Du, Y. Ji, M. Ma, Y. Pan, X. Qi, Q. Sun, K. Shi, L. Qie, *Green Energy Environ.* **2024**, *9*, 1027, <https://doi.org/10.1016/j.gee.2022.11.003>.
- [230] Z. Yuan, Y. Dong, Z. Zeng, W. Zhao, B. Wang, H. Lei, W. Sun, X. Ji, Y. Yang, P. Ge, *Chem. Eng. J.* **2024**, *491*, 151948, <https://doi.org/10.1016/j.cej.2024.151948>.
- [231] W. Chen, R. V. Salvatierra, J. T. Li, C. Kittrell, J. L. Beckham, K. M. Wyss, N. La, P. E. Savas, C. Ge, P. A. Advincula, P. Scotland, L. Eddy, B. Deng, Z. Yuan, J. M. Tour, *Adv. Mater.* **2023**, *35*, 2207303, <https://doi.org/10.1002/adma.202207303>.
- [232] M. Shan, S. Xu, Y. Cao, B. Han, X. Zhu, T. Zhang, C. Dang, J. Zhu, Q. Zhou, Z. Xue, Y. Xu, Q. Zhu, M. S. Islam, B. H. Yin, X. Chang, C. Cao, G. Xu, M. Zhu, *Adv. Funct. Mater.* **2024**, *34*, 2411834, <https://doi.org/10.1002/adfm.202411834>.
- [233] W. Fan, J. Zhang, R. Ma, Y. Chen, C. Wang, *J. Electroanal. Chem.* **2022**, *908*, 116087, <https://doi.org/10.1016/j.jelechem.2022.116087>.
- [234] H. Zhang, Y. Ji, Y. Yao, L. Qie, Z. Cheng, Z. Ma, X. Qian, R. Yang, C. Li, Y. Guo, Y. Yuan, H. Xiao, H. Yang, J. Ma, J. Lu, Y. Huang, *Energy Environ. Sci.* **2023**, *16*, 2561, <https://doi.org/10.1039/d2ee03910a>.
- [235] S. Yang, G. Yang, M. Lan, J. Zou, X. Zhang, F. Lai, D. Xiang, H. Wang, K. Liu, Q. Li, *Small* **2024**, *20*, 2305785, <https://doi.org/10.1002/smll.202305785>.
- [236] H. Gong, H. Xiao, L. Ye, X. Ou, *Waste Manage.* **2023**, *171*, 292, <https://doi.org/10.1016/j.wasman.2023.08.046>.
- [237] J. Wei, X. Chu, X.-Y. Sun, K. Xu, H.-X. Deng, J. Chen, Z. Wei, M. Lei, *InfoMat* **2019**, *1*, 338, <https://doi.org/10.1002/inf2.12028>.
- [238] K. K. Yang, Z. Wu, F. H. Arnold, *Nat. Methods* **2019**, *16*, 687, <https://doi.org/10.1038/s41592-019-0496-6>.
- [239] T. Zhou, Z. Song, K. Sundmacher, *Engineering* **2019**, *5*, 1017, <https://doi.org/10.1016/j.eng.2019.02.011>.
- [240] S. Tao, H. Liu, C. Sun, H. Ji, G. Ji, Z. Han, R. Gao, J. Ma, R. Ma, Y. Chen, S. Fu, Y. Wang, Y. Sun, Y. Rong, X. Zhang, G. Zhou, H. Sun, *Nat. Commun.* **2023**, *14*, 8032, <https://doi.org/10.1038/s41467-023-43883-y>.
- [241] A. Ran, Z. Liang, S. Chen, M. Cheng, C. Sun, F. Ma, K. Wang, B. Li, G. Zhou, X. Zhang, F. Kang, G. Wei, *Acs Energy Lett.* **2022**, *7*, 3817, <https://doi.org/10.1021/acsenergylett.2c01898>.
- [242] X. Lai, C. Deng, J. Li, Z. Zhu, X. Han, Y. Zheng, *IEEE Trans. Veh. Technol.* **2021**, *70*, 1246, <https://doi.org/10.1109/tvt.2021.3055068>.
- [243] X. Lai, C. Deng, X. Tang, F. Gao, X. Han, Y. Zheng, *J. Clean. Prod.* **2022**, *339*, 130786, <https://doi.org/10.1016/j.jclepro.2022.130786>.
- [244] S. Zhu, C. Hu, Y. Xu, Y. Jin, J. Shui, *J. Energy Chem.* **2020**, *46*, 208, <https://doi.org/10.1016/j.jec.2019.11.007>.
- [245] Z. Zhou, A. Ran, S. Chen, X. Zhang, G. Wei, B. Li, F. Kang, X. Zhou, H. Sun, *J. Energy Storage* **2020**, *31*, 101739, <https://doi.org/10.1016/j.est.2020.101739>.
- [246] A. Ran, M. Cheng, S. Chen, Z. Liang, Z. Zhou, G. Zhou, F. Kang, X. Zhang, B. Li, G. Wei, *Energy Environ. Mater.* **2023**, *6*, e12386, <https://doi.org/10.1002/eem.212386>.
- [247] Y. Lu, C.-Z. Zhao, J.-Q. Huang, Q. Zhang, *Joule* **2022**, *6*, 1172, <https://doi.org/10.1016/j.joule.2022.05.005>.
- [248] T. Li, Z. Zhou, A. Thelen, D. A. Howey, C. Hu, *Cell Rep. Phys. Sci.* **2024**, *5*, 101891, <https://doi.org/10.1016/j.xcrp.2024.101891>.
- [249] B. Jiang, W. E. Gent, F. Mohr, S. Das, M. D. Berliner, M. Forsuelo, H. Zhao, P. M. Attia, A. Grover, P. K. Herring, M. Z. Bazant, S. J. Harris, S. Ermon, W. C. Chueh, R. D. Braatz, *Joule* **2021**, *5*, 3187, <https://doi.org/10.1016/j.joule.2021.10.010>.
- [250] B.-R. Chen, C. M. Walker, S. Kim, M. R. Kunz, T. R. Tanim, E. J. Dufek, *Joule* **2022**, *6*, 2776, <https://doi.org/10.1016/j.joule.2022.10.016>.
- [251] Y. Zhang, Q. Tang, Y. Zhang, J. Wang, U. Stimming, A. A. Lee, *Nat. Commun.* **2020**, *11*, 1706, <https://doi.org/10.1038/s41467-020-15235-7>.
- [252] H. Yu, H. Dai, G. Tian, B. Wu, Y. Xie, Y. Zhu, T. Zhang, A. M. Fathollahi-Fard, Q. He, H. Tang, *Renewable Sustainable Energy Rev.* **2021**, *135*, 110129, <https://doi.org/10.1016/j.rser.2020.110129>.
- [253] A. Weng, E. Dufek, A. Stefanopoulou, *Joule* **2023**, *7*, 837, <https://doi.org/10.1016/j.joule.2023.04.002>.
- [254] I. C. Dikmen, T. Karadag, *IEEE Access* **2022**, *10*, 6496, <https://doi.org/10.1109/access.2022.3143040>.
- [255] P. Zhong, B. Deng, T. He, Z. L. C. Gerbrand, *Joule* **2024**, *8*, 1837.
- [256] W. H. Chen, G. Foo, S. Kara, M. Pagnucco, *Robot. Comput. Integr. Manuf.* **2021**, *68*, 102056, <https://doi.org/10.1016/j.rcim.2020.102056>.
- [257] J. Liu, Z. Zhou, D. T. Pham, W. Xu, C. Ji, Q. Liu, *Robot. Comput. Integr. Manuf.* **2020**, *61*, 101829, <https://doi.org/10.1016/j.rcim.2019.101829>.
- [258] A. Realyvásquez-Vargas, K. Cecilia Arredondo-Soto, J. Luis García-Alcaraz, B. Yail Márquez-Lobato, J. Cruz-García, *Robot. Comput. Integr. Manuf.* **2019**, *57*, 315, <https://doi.org/10.1016/j.rcim.2018.12.015>.
- [259] K. Wegener, W. H. Chen, F. Dietrich, K. Dröder, S. Kara, *Procedia CIRP* **2015**, *29*, 716, <https://doi.org/10.1016/j.procir.2015.02.051>.
- [260] H. Poschmann, H. Brüggemann, D. Goldmann, *Procedia CIRP* **2021**, *98*, 282, <https://doi.org/10.1016/j.procir.2021.01.104>.
- [261] S. E. Zaatar, Y. Wang, Y. Hu, W. Li, *J. Intell. Manuf.* **2022**, *33*, 1503, <https://doi.org/10.1007/s10845-021-01743-w>.
- [262] Y. Zhou, Y. Peng, W. Li, D. T. Pham, *Robot. Comput. Integr. Manuf.* **2022**, *77*, 102370, <https://doi.org/10.1016/j.rcim.2022.102370>.
- [263] C. Lv, X. Zhou, L. Zhong, C. Yan, M. Srinivasan, Z. W. Seh, C. Liu, H. Pan, S. Li, Y. Wen, Q. Yan, *Adv. Mater.* **2022**, *34*, 2101474, <https://doi.org/10.1002/adma.202101474>.
- [264] Z. Zhu, J. Qiu, L. Wang, G. Cao, X. He, J. Wang, H. Zhang, *J. Electrochem.* **2022**, *1*, <https://doi.org/10.13208/j.electrochem.2219003>.
- [265] F. I. F. F. O. A. A. IFF, *Intelligente Demontage Von Elektronik für Remanufacturing Und Recycling (Projekt iDEAR)*, <https://www.ifffraunhofer.de/de/geschaeftsbereiche/idear.html> (accessed: August, 2025).
- [266] Redway, *Circu Li-Ion's Smart Devices Can Analyze Valuable Spent Batteries to Rescue Them from Shredders*, <https://www.redwaybattery.com/circu-li-ons-smart-devices-can-analyze-valuable-spent-batteries-to-rescue-them-from-shredders/> (accessed: August, 2025).
- [267] B. Recycling, <https://www.brnpu.com.cn/technological-innovation?tp=41> (accessed: August, 2025).
- [268] J. Pryshlakivsky, C. Searcy, *J. Clean. Prod.* **2013**, *57*, 115, <https://doi.org/10.1016/j.jclepro.2013.05.038>.
- [269] F. Wu, L. Li, L. Crandon, Y. Cao, F. Cheng, A. Hicks, E. Y. Zeng, J. You, *J. Clean. Prod.* **2022**, *339*, 130697, <https://doi.org/10.1016/j.jclepro.2022.130697>.
- [270] F. Marinelli, J. D. Faraldo-Gómez, *Biophys. J.* **2015**, *108*, 158a, <https://doi.org/10.1016/j.bpj.2014.11.873>.
- [271] M. Alipanah, D. Reed, V. Thompson, Y. Fujita, H. Jin, *J. Clean. Prod.* **2023**, *382*, 135274, <https://doi.org/10.1016/j.jclepro.2022.135274>.
- [272] CAS, *Lithium Ion Battery Recycling*, [https://www.cas.org/resources/cas-insights/lithium-ion-battery-recycling#:~:text=%E2%88%BC{text=Today%2C%20only%2020%25%20of%20the,8%20million%20tons%20of%20waste}](https://www.cas.org/resources/cas-insights/lithium-ion-battery-recycling#:~:text=%E2%88%BC{text=Today%2C%20only%2020%25%20of%20the,8%20million%20tons%20of%20waste) (accessed: August, 2025).
- [273] H. Ritchie, *Tracking Global Data on Electric Vehicles*, <https://ourworldindata.org/electric-car-sales> (accessed: March, 2025).
- [274] Rock-to-Metal Ratios of Mined Materials, <https://ourworldindata.org/grapher/rock-to-metal-ratio> (accessed: March, 2025).
- [275] X. Duan, W. Zhu, Z. Ruan, M. Xie, J. Chen, X. Ren, *Energies* **2022**, *15*, 1611, <https://doi.org/10.3390/en15051611>.
- [276] IEA, *Outlook for Key Energy Transition Minerals-Lithium*, <https://www.iea.org/reports/lithium#dashboard> (accessed: May, 2024).
- [277] IEA, *Outlook for Key Energy Transition Minerals-Nickel*, <https://www.iea.org/reports/nickel#dashboard> (accessed: May, 2024).
- [278] IEA, *Outlook for Key Energy Transition Minerals-Cobalt*, <https://www.iea.org/reports/cobalt#dashboard> (accessed: May, 2024).
- [279] Z. Li, H. Yi, W. Ding, H. Ren, Y. Du, M. Shang, W. Zhao, H. Chen, L. Zhou, H. Lin, Q. Zhao, F. Pan, *Adv. Funct. Mater.* **2024**, *34*, 2312837, <https://doi.org/10.1002/adfm.202312837>.
- [280] C. Lin, J. Li, Z.-W. Yin, W. Huang, Q. Zhao, Q. Weng, Q. Liu, J. Sun, G. Chen, F. Pan, *Adv. Mater.* **2024**, *36*, 2307404, <https://doi.org/10.1002/adma.202307404>.
- [281] W. Ai, B. Wu, E. Martínez-Pañeda, *J. Power Sources* **2022**, *544*, 231805, <https://doi.org/10.1016/j.jpowsour.2022.231805>.
- [282] Z. Liu, Y. Zeng, J. Tan, H. Wang, Y. Zhu, X. Geng, P. Guttmann, X. Hou, Y. Yang, Y. Xu, P. Cloetens, D. Zhou, Y. Wei, J. Lu, J. Li, B. Liu, M. Winter, R. Kostecki, Y. Lin, X. He, *Nat. Nanotechnol.* **2024**, *19*, 1821, <https://doi.org/10.1038/s41565-024-01773-4>.
- [283] Y. Liu, X. Wang, Q. Li, T. Yan, X. Lou, C. Zhang, M. Cao, L. Zhang, T.-K. Sham, Q. Zhang, L. He, J. Chen, *Adv. Funct. Mater.* **2023**, *33*, <https://doi.org/10.1002/adfm.202210283>.
- [284] C. Wang, X. Wang, R. Zhang, T. Lei, K. Kisslinger, H. L. Xin, *Nat. Mater.* **2023**, *22*, 235, <https://doi.org/10.1038/s41563-022-01461-5>.
- [285] R. Lin, S.-M. Bak, Y. Shin, R. Zhang, C. Wang, K. Kisslinger, M. Ge, X. Huang, Z. Shadike, A. Pattammattel, H. Yan, Y. Chu, J. Wu, W. Yang, M. S. Whittingham, H. L. Xin, X.-Q. Yang, *Nat. Commun.* **2021**, *12*, 2530, <https://doi.org/10.1038/s41565-021-22635-w>.
- [286] F. Lin, I. M. Markus, D. Nordlund, T.-C. Weng, M. D. Asta, H. L. Xin, M. M. Doeff, *Nat. Commun.* **2014**, *5*, 3529, <https://doi.org/10.1038/ncomms4529>.

- [287] X. Fan, C. Tan, Y. Li, Z. Chen, Y. Li, Y. Huang, Q. Pan, F. Zheng, H. Wang, Q. Li, *J. Hazard. Mater.* **2021**, *410*, 124610, <https://doi.org/10.1016/j.jhazmat.2020.124610>.
- [288] N. Šimić, A. Jodlbauer, M. Oberaigner, M. Nachtnebel, S. Mitsche, H. M. R. Wilkening, G. Kothleitner, W. Grogger, D. Knez, I. Hanzu, *Adv. Energy Mater.* **2024**, *14*, 2304381, <https://doi.org/10.1002/aenm.202304381>.
- [289] Y. Guo, Y. Li, K. Qiu, Y. Li, W. Yuan, C. Li, X. Rui, L. Shi, Y. Hou, S. Liu, D. Ren, T. Tan, G. Zhu, L. Lu, S. Xu, B. Deng, X. Liu, M. Ouyang, *Energy Environ. Sci.* **2025**, *18*, 264, <https://doi.org/10.1039/d4ee03021d>.
- [290] J. Zhou, C. Xing, J. Huang, Y. Zhang, G. Li, L. Chen, S. Tao, Z. Yang, G. Wang, L. Fei, *Adv. Energy Mater.* **2024**, *14*, 2302761, <https://doi.org/10.1002/aenm.202302761>.

Manuscript received: July 16, 2025

Revised manuscript received: September 7, 2025

Version of record online: